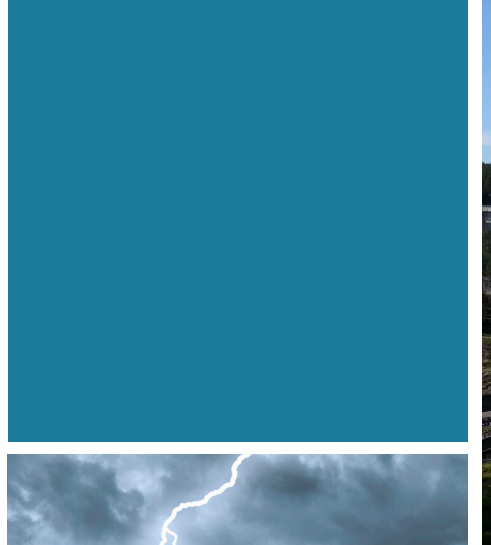
ANALYSIS OF LOAD AND RESPONSE ON LARGE HYDROPOWER DRAFT TUBE STRUCTURES

REPORT 2019:567















Analysis of load and response on large hydropower draft tube structures

ROGHAYEH ABBASIVERKI LAMIS AHMED ERIK NORDSTRÖM

Foreword

This report was written as a part of the project Analysis of load and response on large hydropower draft tube structures. The project was carried out by Roghayeh Abbasiverki, KTH, Lamis Ahmed, KTH and Erik Nordström Sweco/KTH.

The aim of this project was to clarify which loads and load distributions other than fast filling that internal walls in draft tubes are exposed to and if that could explain the cracking that has been identified. One aim is also to demonstrate the behavior of a cracked and repaired draft tube construction, to give guidance regarding when and how action should be taken for a damaged construction.

The reference group of SVC structural engineering has been following this project and consists of Anders Ansell (KTH), Carl-Oscar Nilsson (Uniper), Daniel Eriksson (KTH/SWECO), Erik Nordström (KTH/SWECO), Fredrik Johansson (KTH/SWECO), Håkan Bond (WSP), Lars-Elof Bryne (Vattenfall), Magnus Svensson (Fortum), Manouchehr Hassanzadeh (SWECO/LTH), Marcus Hautakoski (VRF), Marie Westberg-Wilde (KTH/ÅF), Martin Hansson (Statkraft), Martin Rosenqvist (LTH/Vattenfall), Mats Persson (Vattenfall), Mats Stenmark (Norconsult), Rikard Hellgren (KTH/WSP), Robert Lundström (Skellefteå kraft), Tobias Gasch (KTH/Vattenfall) and Tomas Ekström (ÅF). A preliminary version of the report was reviewed by Gunnar Hellström (LTU) and Mårten Janz (ÅF).

This project was part of Swedish Hydropower Center, SVC. The organizations that sponsored this project were Falu Energi & Vatten, Fortum Generation, Holmen Energi, Jämtkraft, Jönköping Energi, Karlstads Energi, Mälarenergi, Norconsult, Skellefteå Kraft, Sollefteåforsens, Statkraft Sverige, Svenska Kraftnät, Sweco Infrastructure, SveMin, Umeå Energi, Uniper, Vattenfall Research and Development, Vattenfall Vattenkraft, WSP Samhällsbyggnad and ÅF Industry.

May 2019,

Lennart Kjellman, Energiforsk

Reported here are the results and conclusions from a project in a research program run by Energiforsk. The author / authors are responsible for the content and publication which does not mean that Energiforsk has taken a position.



Sammanfattning

I en reaktionsturbin är löphjulskammarens utlopp sammankopplad med en diffusor som kallas sugrör. Stora vattenkraftsaggregat med stor effekt och stor drivvattenföring kräver också stora dimensioner på vattenvägen. I vissa storskaliga anläggningar är spännvidden på sugröret tvärs strömningsriktingen så stor att det behövs en stödjande mellanvägg i sugrörets förlängning. Inom den svenska vattenkraften finns flera fall där skador och sprickor har rapporterats framförallt i kontakten mellan sugrörstaket och den stödjande mellanväggen. Troligast är att sprickbildningen vanligen uppkommit vid för snabb återfyllning efter att sugrörets tömt för t.ex. inspektion och därigenom skapat en lyftkraft på taket större än fogens kraftöverförande förmåga. Det finns dock fortfarande oklarheter angående om det finns något långtidsscenario som skulle kunna ge fortsatt sprickpropagering under något driftsfall.

Vattenfall vattenkraft har gjort en installation med tryck- och töjningsgivare i en av sina anläggningar med en mellanvägg i sugröret och ett tomt utrymme mellan takets översida och berget. Målet med projektet är att skapa en bättre förståelse för beteendet hos taket och väggen under olika driftsfall genom att utvärdera mätningarna från sugröret och undersöka om det finns lastfall som kan ge upphov till propagerande uppsprickning. Därför har, i föreliggande projekt, mätningarna analyserats för att studera olika driftsfall och deras påverkan på de tryck som uppstår på sugrörets mellanvägg och tak samt strukturens respons. En förenklad numerisk modell av sugröret har skapats för att demonstrera responsen vid olika belastningar och för jämförelse med mätningarna.

Mätningarna från ett års drift av aggregatet indikerade att det kördes över hela effektregistret och med periodvis många start och stopp. Tre huvudmönster för drift var dock normal drift (körning dagtid, stillestånd nattetid), kontinuerlig drift utan stopp och relativt snabba start-/stopptillfällen under för- eller eftermiddag. Analys av tryckmätningarna indikerar att strömningen i den raka diffusorn är turbulent och möjligen påverkade av virvelrep som bildas under löphjulet. Därav är trycket på höger sida av väggen högre än på vänster sida.

Kvaliteten på töjningsmätningarna visade sig vara av otillfredsställande kvalitet och det finns brister i dokumentationen från installationen. Det har gett frågetecken kring möjligheterna att få tillförlitliga resultat i utvärderingen. I vilket fall har en utvärdering gjorts. Utvärderingen av töjningsmätningarna gav högre töjningsvärden längre uppströms på mellanväggen och taket. Dessutom var töjningarna större på takets undersida än på väggen. Plötsliga fluktuationer under kontinuerlig drift och vid start/stop-sekvenser är de driftsfall som skulle kunna ge skador på strukturen på lång sikt. Resultaten från den numeriska modellen indikerar höga dragspänningar i uppströmsdelen av den raka diffusorn i kontakten mellan taket och mellanväggen på samma ställe som där det finns en spricka i den verkliga konstruktionen.



Summary

In a reaction turbine, the runner outlet is connected to a diffuser which is called the draft tube. Large hydropower units with large effect and large discharge normally require large dimensions on the waterways. In some large-scale facilities, the total width of the draft tube is so large there is a need for a supporting centre wall in the draft tube. In the Swedish hydropower business, there are several cases where damages or cracks have been reported in the contact between the roof and the supporting centre wall. The most likely reason for cracking between wall and roof is when refilling the draft tube after it has been drained for inspection. A too quick refilling will give an upwards lifting force on the roof that can be larger than the capacity in the joint. There are still uncertainties regarding the risk for a long-term scenario where any operational pattern could give continued crack propagation.

Vattenfall Hydropower has made an installation with pressure and strain sensors in one of their facilities with a centre wall supported draft tube and a cavity between the roof and the rock cavern. The aim of the project is to get a better understanding on the behaviour of the roof and centre wall during different operational events by evaluating measurements from the draft tube and investigating possible load cases that can create continued crack propagation during operation. In this regard, in this project, the measurements are analysed to discover the different operational patterns and the corresponding effect on applied pressure on draft tube central wall and roof and structure response. A simplified finite element model of the draft tube is demonstrated and the response from the structure due to extracted load patterns is compared with the measurements.

One-year measurements of the unit operation indicated that unit operates over the whole range with many start/stops. Three major types of operation were: normal operation (working in daytime and downtime at night), continuous operation with no stop and start-stop events with sharp start/stop in the morning and afternoon. The analysis of pressure measurements indicated that the fluid motion in the straight diffuser is turbulent and possibly influenced by vortex formation under the runner. Therefore, the pressure on the right side of the central wall was higher than on the left side.

The quality of the strain measurements showed to be of insufficient quality and lack of information regarding the set-up. This has given questions on the possibility to get reliable results in the evaluation. Nevertheless, an evaluation has been performed. The evaluation of strain measurements demonstrated higher strain values at the upstream side of the central wall and roof. Moreover, the strain on underside of the roof was higher than on the central wall. Sudden fluctuation during continuous operation and sequence of start/stop were the cases that in long-term may cause damage to the structure due to fatigue problems. The results from finite element model indicated high tensile strength at the upstream side of the straight diffuser, in contact between the roof and the central wall where a crack has been detected in the real structure.



List of content

1	Intro	oduction	7
	1.1	Background	9
	1.2	Principal of draft tube	11
	1.3	Crack on draft tubes central wall	12
2	Mea	surements	13
	2.1	Monitoring set-up	13
	2.2	Pressure and strain data interpretation	16
3	Unit	operation measurements	18
	3.1	Normal operation	18
	3.2	Continuous operation	21
	3.3	Start and stop events	22
4	Press	sure measurements	23
	4.1	Normal operation	29
	4.2	Continuous operation	35
	4.3	Fast Start and stop events	40
5	Strai	n measurements	44
	5.1	Normal operation	47
	5.2	Continuous operation with no stop	56
	5.3	Start and stop events	61
6	Finite	e element model	68
	6.1	FE modelling	68
	6.2	Load	69
	6.3	Structure response	70
7	Conc	clusions	73
	7.1	Discussions	73
	7.2	General conclusions and future work	76
8	Refe	rences	78



1 Introduction

The majority of the electricity production in Sweden relies on hydropower and nuclear power. Up to 50% of the electricity is produced now by hydroelectric plants where flowing water creates energy that can be captured and turned into electricity. Most of the Swedish hydropower resources were developed during the 1950s and 1960s and today a need for refurbishment is growing. Furthermore, Energy market deregulation and arrivals of new energy sources, such as solar and wind turbines, make it also attractive to improve the turbines and other related components over a wide range of operating conditions.

Today, the most commonly used turbines, on a worldwide basis, are the Pelton, Francis, Propeller, Kaplan, and Kinetic turbines. In a hydraulic turbine, the water is directed to the turbine from the headwater via the penstock and then discharged into the tailwater, as illustrated in Figure 1.1. Inside the turbine, the energy of waters is converted into mechanical energy of the rotating shaft via the runner. The shaft rotates the rotor of the generator, where the mechanical energy is finally transformed into electricity and supplied to customers. The difference is that in all turbines, except Pelton, the runner is rotating inside the water and interacting with all of its blades simultaneously. This permits the runner to utilize all components of the water energy, i.e. both pressure energy and kinetic energy. In Pelton turbines, however, the runner rotates in the free air, allowing only some of the buckets to interact with the water. Hence, a Pelton turbine is also only capable of utilizing the kinetic part of the water energy. Thus, the Pelton turbine is categorized into impulse turbine while the other is reaction turbines (Marjavaara, 2006).

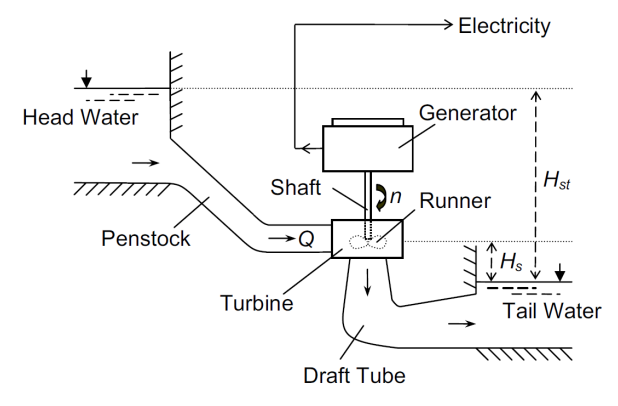


Figure 1.1: A representative sketch of a reaction turbine (Marjavaara, 2006).

In a reaction turbine, water leaves the runner with remaining kinetic energy and possibly some potential energy. To recover as much of this energy as possible, the runner outlet is connected to a diffuser: the draft tube. The draft tube converts the dynamic pressure (kinetic energy) into a static pressure (see Figure 1.2). Due to losses, not all energy is recovered, which is why the total pressure (the solid line) is decreasing through the diffuser in the figure. Since the conditions at the outlet of the draft tube determine the level (1) of the static pressure, the pressure level (2)



must be reduced at the inlet of the draft tube. Thus, the draft tube creates an extra 'draft' after the runner, or more correctly, the draft tube enables the utilisation of the available head in the flow.

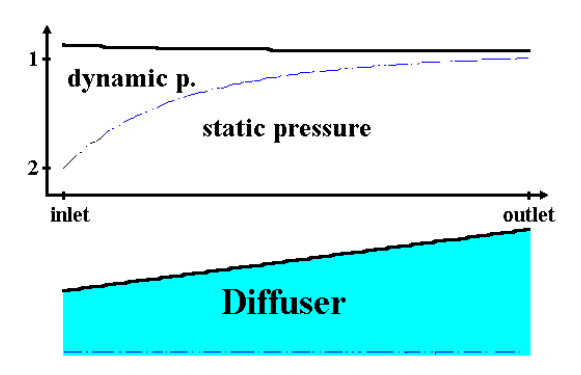


Figure 1.2: The change in the relationship between dynamic and static pressure along a diffuser. The solid line indicates the total pressure that decreases slightly due to losses (Andersson, 2009).

Inspection of some of the large-scale Swedish draft tubes indicated crack propagation in the contact between draft tube central wall and roof in the most upstream part of the wall. There are still some uncertainties regarding the reason for the cracks or more specifically if there are any long-term scenarios that could give continued crack propagation. One of the probable major reasons for the first initiation of the crack is too fast filling of the draft tube after it has been completely drained for inspection. Especially in facilities with an empty space between the draft tube roof and the rock, there is a risk for uplift pressure on the roof before it has been equalised through drainage holes in the draft tube roof.

Inspection of cracks, with the naked eye, is a challenge in getting useful information due to limitations in light and difficulties in getting into the close, hand distance from the cracks. It is also very difficult to see the structural impact from the cracks and thereby also suggesting repair methods for the crack. Lack of input regarding the actual load situation also limits the design of a reinforcement measure for a cracked draft tube wall-roof-contact. The access to the draft tube is commonly limited, especially for single units where the disruption of production is avoided due to economic reasons.

Vattenfall Hydropower has made an installation with pressure and strain sensors in one of their facilities with a centre wall supported draft tube with a crack initiated in the contract between the wall and the roof. Vattenfall has given this project within the Swedish Hydropower Centre (SVC) the possibility to evaluate the data from a longer period of measurements.

The objective with the project is to get a better understanding on the behaviour of the roof and centre wall during different operational events by evaluating measurements from the draft tube. The goal is to define loads and response of a cracked, but not repaired, draft tube with a supporting centre wall. The purpose is to give input to the design on how and when measures should be taken on the damaged structure. The goal is also to clarify if there are any load cases apart from quick refill of the draft tube after drainage that can create continued crack propagation during operation.



1.1 BACKGROUND

Different types of draft tube and their specifications are presented in Table 1.1 and a schematic diagram is shown in Figure 1.3 (Abbas & Kumar, 2015). Elbow draft tubes are widely used since they require less excavation. They consist of a cylindrical cone, an elbow and a straight diffuser. For a draft tube with outlet width larger than 10 to 12 m, central wall (piers) is usually necessary (Andersson et.al, 2008). Figure 1.4 shows a schematic view of typical Swedish draft tubes with the central wall where also there is an empty space between the draft tube roof and the rock tunnel above, which is filled with water during operation.

Table 1.1: Different types of draft tubes and specifications (1973, Abbas & Kumar, 2015)

	Straight conical	Moody/ bellmouth	Elbow
Year of development	1840s	1920s	1940s
Runner size	Small and medium-size runner (up to 2.5m)	Medium size runner (up to 5m)	Large size runner (up to 10 m)
Inlet-outlet area ratios for the same length	Less	High	High
Pressure recovery at non-optimal operating conditions	High	Reduce	Relatively high
Vertical height	More	Less	Less

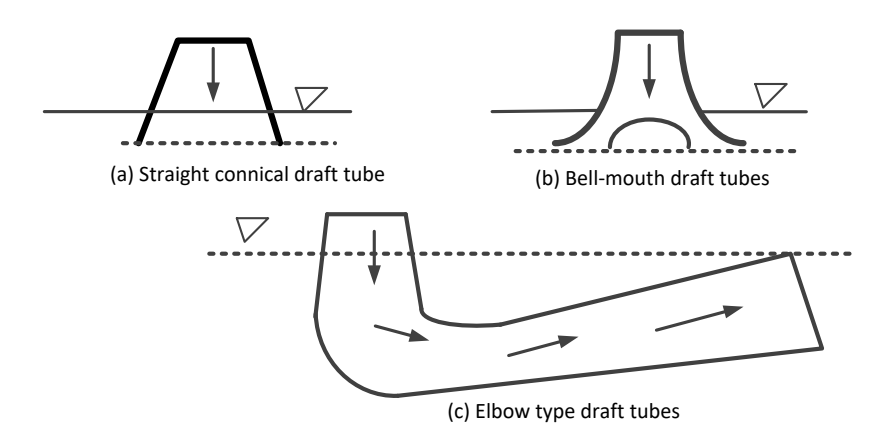


Figure 1.3: Schematic diagram of different types of draft tubes (Abbas & Kumar, 2015)



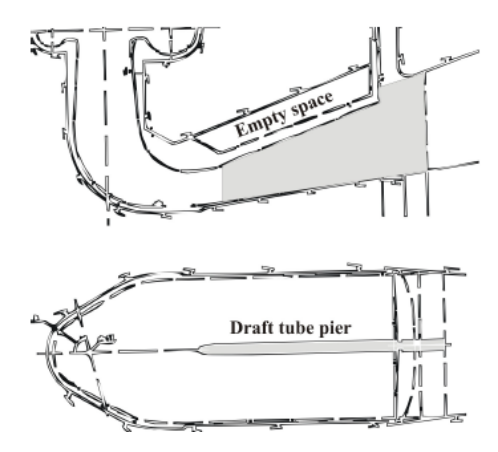


Figure 1.4: Elbow draft tube with the central wall (Andersson et.al, 2008)

High flow rates in large dimensions cause the fluid motion in curved draft tubes to be highly turbulent. The outflow from the runner can have more or less swirl depending on the operating condition, and this will affect the performance of the draft tube. At optimal operating conditions this swirl suppresses the boundary layer thickness in the draft tube cone and causes it to operate with full flow across the entire cross-section. Hence, separation is delayed, and the draft tube performance is increased. The larger amount of swirl, a vortex breakdown will be present due to hydraulic instabilities. The vortex core, located underneath the centre of the runner, reduces the cross-sectional area and thereby is also the draft tube performance decreased due to the higher velocities. The presence of a vortex rope will moreover give rise to large pressure fluctuations which can cause structural damage and flow separation (Marjavaara, 2006).

In the cone, which generally is a straight-conical diffuser, the flow decelerates, and the pressure increases. Any occurrence of severe separation will drastically reduce the draft tube performance and cause damaging pressure fluctuations. Most of the pressure recovery is furthermore obtained in this part of the fluid domain. The primary function of the elbow is to turn the flow from the vertical to the horizontal direction with a minimum loss of energy. The elbow has usually a converging cross-section to avoid separation on its inner section due to the centrifugal forces induced to the flow by the elbow curvature. The outflow diffuser also recovers a part of the kinetic energy, but to a smaller extent than the initial cone, as the velocity at the inlet section of the diffuser is considerably reduced. In addition, the flow in the diffuser is influenced by the flow characteristics at the exit of the elbow, (Gubin, 1973; Amiri et.al., 2016).

Experimental and numerical investigation on the draft tube with a central wall indicated that the central wall strongly affects the flow. The flow is distributed between the two channels of the draft tube which creates a pressure difference between both channels. In another word, it creates a force on the central wall. This force may fluctuate with a frequency related to the runner frequency f_r , (Mauri, 2002; Arpe, 2003).



1.2 PRINCIPAL OF DRAFT TUBE

A reaction turbine always runs completely filled with the working fluid. The tube that connects the end of the runner to the tailrace is known as a draft tube and should completely be filled with the working fluid flowing through it. The kinetic energy of the fluid finally discharged into the tailrace is wasted. A draft tube is made divergent so as to reduce the velocity at the outlet to a minimum. Therefore, a draft tube is basically a diffuser and should be designed properly to prevent the flow separation from the wall and to reduce accordingly the loss of energy in the tube (Som &Biswas, 2008).

The role of the draft tube can be described by considering the energetic balance ΔE between sections 1 and II with and without the draft tube (see Figure 1.3):

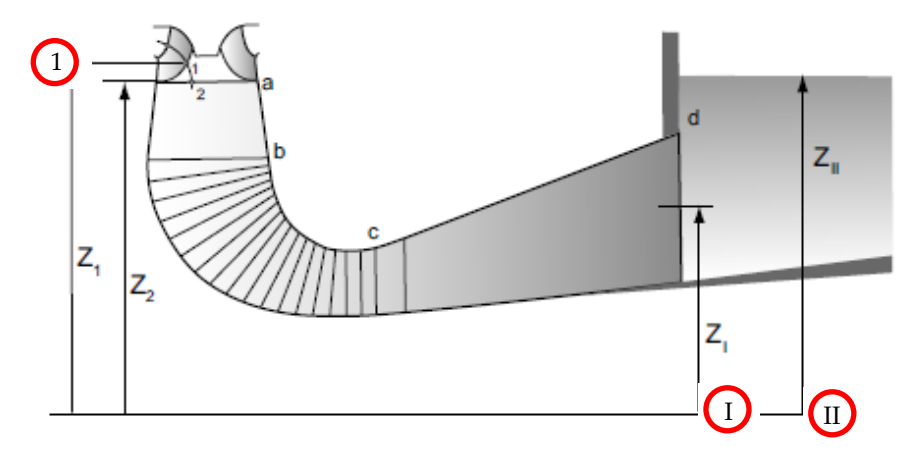


Figure 1.3: Schematic of a draft tube (Mauri, 2002)

$$\Delta E = g\Delta z + \frac{1}{\rho}\Delta p + \frac{1}{2}\Delta c^2 = g(z_1 - z_{II}) + \frac{1}{\rho}(p_1 - p_a) + \frac{c_1^2}{2}$$
(1.1)

where g is the gravitational acceleration, z the geostatic height, p the pressure, c the mean velocity and p_a the atmospheric pressure. The mean velocity at position II is considered negligible (large surface). The energetic balance between sections 1-I and I-II can be written as follows:

$$gz_1 + \frac{p_1}{\rho} + \frac{c_1^2}{2} = gz_I + \frac{p_I}{\rho} + \frac{c_I^2}{2} + \Delta E_{loss_{1-I}}$$
 (1.2)

$$gz_I + \frac{p_I}{\rho} + \frac{c_I^2}{2} = gz_{II} + \frac{p_a}{\rho} + \Delta E_{loss_{I-II}}$$
 (1.3)

where the losses due to the sudden change in the section between I and II can be estimated as $\Delta E_{loss_{I-II}} = (c_I - c_{II})^2 / 2 = c_I^2 / 2$. Without the draft tube $p_1 = pa$ so that Equation (1.1) becomes:



$$\Delta E_{without} = g\left(z_1 - z_{II}\right) + \frac{c_1^2}{2} \tag{1.4}$$

$$\Delta E_{with} = \frac{c_I^2}{2} + \Delta E_{loss_{1-I}}$$
(1.5)

The energetic gain due to the diffuser is, therefore:

$$\Delta E_{without} - \Delta E_{with} = g(z_1 - z_{II}) + \frac{c_1^2 - c_I^2}{2} - \Delta E_{loss_{1-I}}$$
(1.6)

The draft tube allows the recovery of a part of the kinetic energy between runner outlet and free surface and the level difference.

1.3 CRACK ON DRAFT TUBES CENTRAL WALL

Several hydropower units in Sweden have a draft tube with the central wall. For one major facility cracks on the central wall of draft tubes were detected at first part of the wall, between roof and wall, see **Figure 1.6**. To fix the problem, concrete was injected through the cracks and a support wall was constructed as an extension of the wall up to the rock. Finally, a failure of the most upstream part of the wall occurred with ruptured reinforcement and parts of the wall came loose but remained in position.

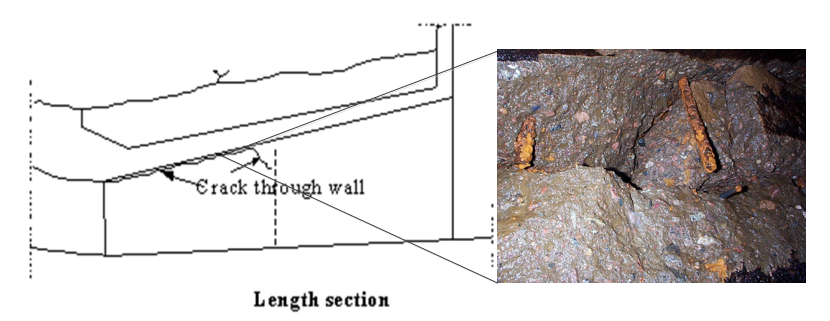


Figure 1.6: Example of failed contact between central wall and roof

To find out the reasons for the continued crack propagation, model tests were performed at the Hydraulic Machinery Laboratory of Vattenfall Research and Development, Älvkarleby, Sweden (Andersson et.al, 2008). An adjustable draft tube central wall with several pressure holes was used to estimate the load acting on the central wall. The results indicated a significant difference in pressure between both channels due to an uneven flow. At part load the pressure was considerably higher on one side of the central wall, the pressure difference was about 1.5-3 *kPa*. The pressure difference decreases with increased flow and change high-pressure side at full load. The tests did not indicate any operating point that would cause direct failure of the wall, but possible fatigue problems.



2 Measurements

In one of the Vattenfall facilities with a large, centre wall supported (pier), draft tube, a long-term measurement of pressures and strains on the centre wall and roof have been performed. The monitoring was performed during the period May 2010 to February 2011. This chapter contains a compilation of measurements set-up and calculations. In the first section descriptions of the sensor positions for the draft tube are given, followed by a section that demonstrates the calculation of the pressure from the acquired data. The results from these calculations are used for finite element model, see Chapter6.

2.1 MONITORING SET-UP

A description of the system is done in a Vattenfall report (Holmström, 2010) but a general description of the set-up can be seen in **Figure 2.1** and **Figure 2.2**. To measure the pressure difference across the central wall, a total of four pressure sensors were placed. The sensors were mounted on each side of the central wall with distances of 4 meters from the upstream end of the wall and at the same distance from the draft tube gate and at the centre of the wall. To measure the differential pressure across the draft tube roof, mainly during filling from an empty draft tube, a hole was drilled through the ceiling about 6.5 meters from the upstream end of the wall. All boreholes were sealed with joint foam to prevent pressure equalization in the measurement points.

As illustrated in **Figure 2.1**, the position of the sensors is P1 at upstream/left side of the wall, P2 at downstream/left side of the wall, P3 at upstream/right side of the wall, P4 at downstream/right side of the wall and P5 at roof/right side of draft tube. It should be noted that sensors P1 and P3 unfortunately failed during the monitoring campaign.

To measure the concrete structure's response to variations in the water pressure, 10 strain gauges have been placed in the right section of the draft tube, central wall and roof of the draft tube. Four strain gauges were mounted on the central wall, as well as six sensors in the roof to follow any deformation of the draft tube structure under load. To measure the change of crack width in the crack between the roof and central wall, a crack-mouth opening gauge was mounted. This gauge failed directly after filling the draft tube. The strain gauges on the central wall located along the draft tube from upstream to downstream are denominated as H1, H3, H10 and H2, respectively, see Figure 2.1. The strain gauges on the roof and along the draft tube from upstream to downstream are denominated as H4, H6, H8 and H9, respectively, see Figure 2.2. Two strain gauges have also been placed on the roof and across the draft tube, H5 and H7 but the former failed from the beginning. The strain gauges were installed on a dog bone shape plate with three different lengths: 300 mm, 160 mm and 132 mm for stain gauges H1-H4, H5-H8 and H9-H10, respectively. The direction of dog bones plates has been shown in Figures 2.1 and 2.2.



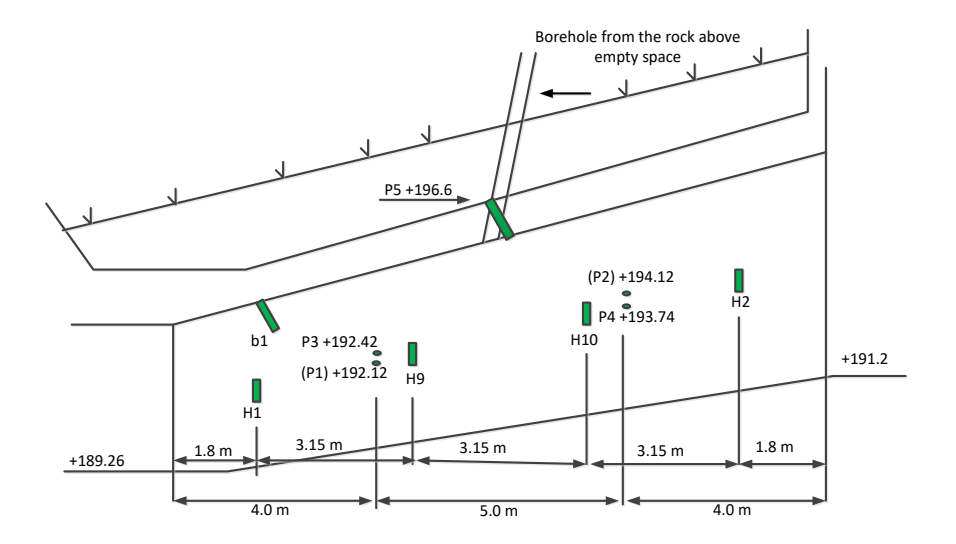


Figure 2.1: Sensor position in right-hand draft tube central wall and roof (H: strain gauges, P: pressure sensors and b1: crack-opening meter) (Holmström, 2010).

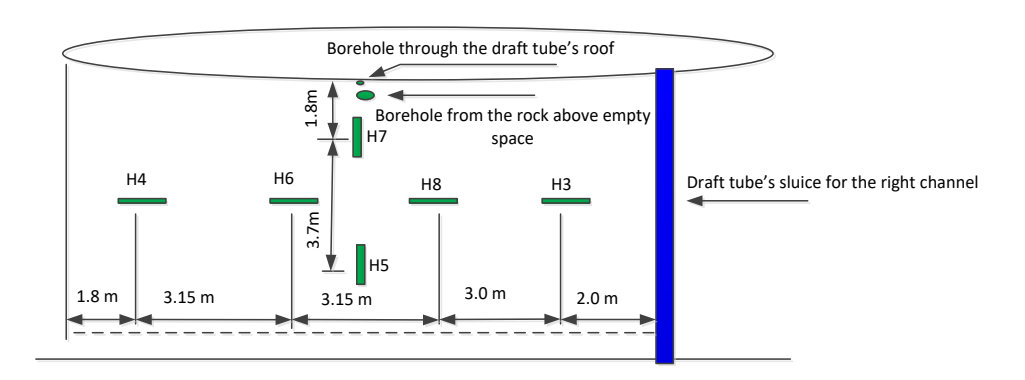


Figure 2.2: Sensor position on the right-hand side of the draft tube roof (H: strain gauges) (Holmström, 2010).

Tables 2.1 and **2.3** shows measurements during filling the draft tube. It should be noted that downstream level was +212.96 masl (metres above sea level) during filling the draft tube. During this period the signal from the different sensors was read manually using a Fluke multimeter. As seen in these Tables, sensors had an offset error (before filling draft tube) which has been normalized to zero in **Tables 2.2** and **2.4**.



Table 2.1: Readings on multimeters (Holmström, 2010) (in Swedish)

	Före fyllning	Nivå = uk sugrörstak	Nivå = uk sugrörstakl	Nivå = NVY
Nivå vid fyllning	20:30 2010-04- 28	21:45 2010-04- 28	23:00 2010-04- 28	08:00 2010-04- 29
P 1 +192.12 möh	0.988 V	1.472 V	1.485 V	2.620 V
P 2 +194.12 möh	0.985 V	1.364 V	1.377 V	2.554 V
P 3 +192.43 möh	0.986 V	1.447 V	1.460 V	2.595 V
P 4 +193.74 möh	0.983 V	1.340 V	1.353 V	2.483 V
P 5 +196.60 möh	0.988 V	1.120 V	1.153 V	2.270 V

Table 2.2: Recalculated values normalized to zero meters of waterpressure before filling (Holmström, 2010) (in Swedish)

	Före fyllning	Nivå = uk sugrörstak	Nivå = uk sugrörstak	Nivå = NVY
Nivå vid fyllning	20:30 2010-04- 28	21:45 2010-04- 28	23:00 2010-04- 28	08:00 2010-04- 29
P 1 +192.12 möh	0 mvp	6.18 mvp	6.35 mvp	20.84 mvp
P 2 +194.12 möh	0 mvp	4.84 mvp	5.00 mvp	19.43 mvp
P 3 +192.43 möh	0 mvp	5.89 mvp	6.05 mvp	20.54 mvp
P 4 +193.74 möh	0 mvp	4.56 mvp	4.72 mvp	19.15 mvp
P 5 +196.60 möh	0 mvp	1.69 mvp	2.11 mvp	16.36 mvp

Table 2.3: Readings on multimeters (Holmström, 2010) (in Swedish)

	Före fyllning	Nivå = uk sugrörstak	Nivå = uk sugrörstakl	Nivå = NVY
Nivå vid fyllning	20:30 2010-04- 28	21:45 2010-04- 28	23:00 2010-04- 28	08:00 2010-04- 29
H 1 +192.12 möh	-1.178 V	-	-1.087 V	-1.056 V
H 2 +193.53 möh	0.034 V	-	0.059 V	0.082 V
H 3 +192.42 möh	-0.712 V	-	-0.707 V	-0.691 V
H 4 +193.81 möh	-1.153 V	-	-1.150 V	-1.142 V
H 5 +196.60 möh	-1.172 V	-	-1.166 V	-1.186 V
H 6 +196.60 möh	-1.174 V	-	-1.166 V	-1.126 V
H 7 +196.60 möh	-1.009 V	-	-0.943 V	-0.877V*
H 8 +196.60 möh	-0.031 V	-	-0.024 V	-0.017V*
H 9 +196.60 möh	-0.766 V	-	-0.691 V	-0.671 V
H10 +196.60 möh	-0.544 V	-	-0.544 V	-0.557 V

^{*}Estimated values due to lack of input



Table 2.4: The voltages normalized to 0 V before filling (Holmström, 2010)

	Före fyllning	Nivå = uk sugrörstak	Nivå = uk sugrörstak	Nivå = NVY
Nivå vid fyllning	20:30 2010-04- 28	21:45 2010-04- 28	23:00 2010-04- 28	08:00 2010-04- 29
H 1 +192.12 möh	0 V	-	+0.091 V	
H 2 +193.53 möh	0 V	-	+0.025 V	
H 3 +192.42 möh	0 V	-	+0.005 V	
H 4 +193.81 möh	0 V	-	+0.003 V	
H 5 +196.60 möh	0 V	-	+0.006 V	
H 6 +196.60 möh	0 V	-	+0.008 V	
H 7 +196.60 möh	0 V	-	+0.066 V	
H 8 +196.60 möh	0 V	-	+0.007 V	
H 9 +196.60 möh	0 V	-	+0.075 V	
H10 +196.60 möh	0 V	-	+0.031 V	

2.2 PRESSURE AND STRAIN DATA INTERPRETATION

Pressure sensors measured total/absolute pressure which contains both effects from static and operational pressure. In mathematical form it can be written as:

$$P_{s} + \frac{\rho V^{2}}{2} = P_{0} \tag{2.1}$$

Where $\rho V^2/2$ is called the dynamic pressure, P_s the static pressure, and P_0 the total pressure (Nakayama & Boucher, 1999).

Bernoulli equation is applied to the location of the pressure sensor (point 1) and downstream reading point (point 2), see **Figure 2.3**:

$$\frac{P_1}{\rho g} + \frac{V_1^2}{2g} + Z_1 = \frac{P_2}{\rho g} + \frac{V_2^2}{2g} + Z_2 + h_1$$
(2.2)

Where h_l is head loss due to friction between two points. If we consider small friction loss and also the small value of $V_2^2/2g$, with considering atmospheric pressure at downstream and P_0 as a total pressure at sensor position (point 1), the Bernoulli equation will be:

$$\frac{P_0}{\rho g} + Z_1 = 0 + 0 + Z_2 \tag{2.3}$$

$$P_0 = \left(Z_2 - Z_1\right) \rho g \tag{2.4}$$



For a condition that there is no operation, the sensors show hydrostatic pressure, i.e. the pressure due to elevation difference between sensor position and downstream level.

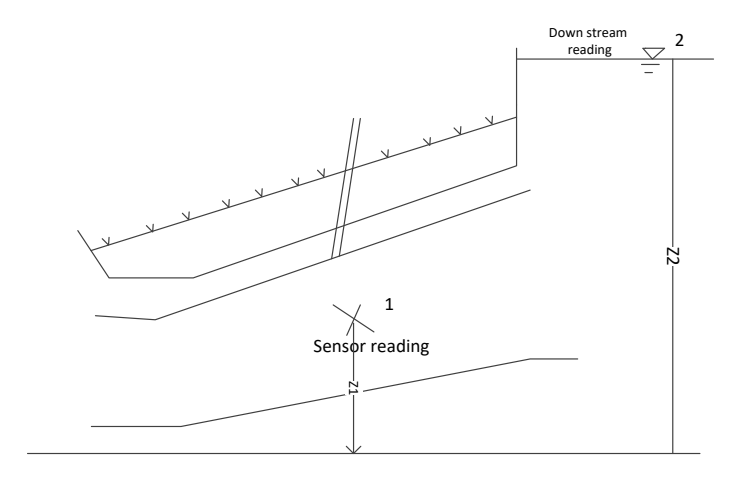


Figure 2.3: Pressure measurement

A linear relationship is used to normalize offset error of readings to zero and converting the voltage to mvp (=10 kPa) according to **Table 2.1-2.2**. **Figure 2.4** shows a linear relationship that used for example for sensor P2.

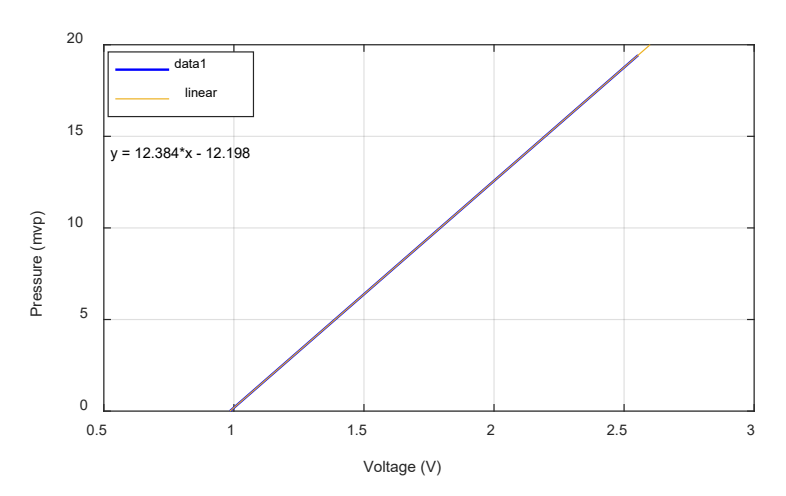


Figure 2.4: A linear relationship used for sensor P2 for converting the voltage to mvp and normalizing offset error

For strain measurement, the zero reading is considered for the case when the draft tube was filled with water (2010-04-29 08:00), see Table 2.3. In this way, the offset error before filling the draft tube and effect for when the draft tube was partly filled is removed. According to the report (Holmström, 2010), 1V was equal to 100 µstrain. For example, for sensor H1, the measurement is corrected as:

$$H1 = (reading + 1.056) \times 0.0001$$
 (2.5)



3 Unit operation measurements

The measurements were divided into two parts; the operation unit measurements and the acquired reading from the sensors and strain gauges. In this chapter, the output effect that was generated from hydropower is presented. In order to see the patterns in the draft tube behaviour regarding load and response, the unit operational conditions have been considered; normal operation, continuous operation and start and stop events.

3.1 NORMAL OPERATION

It is nowadays common to see turbines being operated over the whole range, with many start/stops, instead of continuous close to peak operation as in the former days. Measurement of unit operation for one year indicated that for normal operation the unit production in daytime is almost between 80-130 MW, see Figure 3.1. It should be noted that the capacity of the unit is 150 MW, but it was restricted to operate not more than 130 MW. It can be seen from Figure 3.1 that the unit had been stopped for a certain time during the summer time; i.e. from July 05 at 01:00 to July 12 at 17:00. Figure 3.2 -3.3 show the unit operation and downstream level as moving average for ten months.

As an example, Figure 3.4 shows normal operation with producing the power of almost 120 MW during daytime for one week. It can be seen also that the operation of the unit starts in the morning for almost 17 hours and stops in the evening.



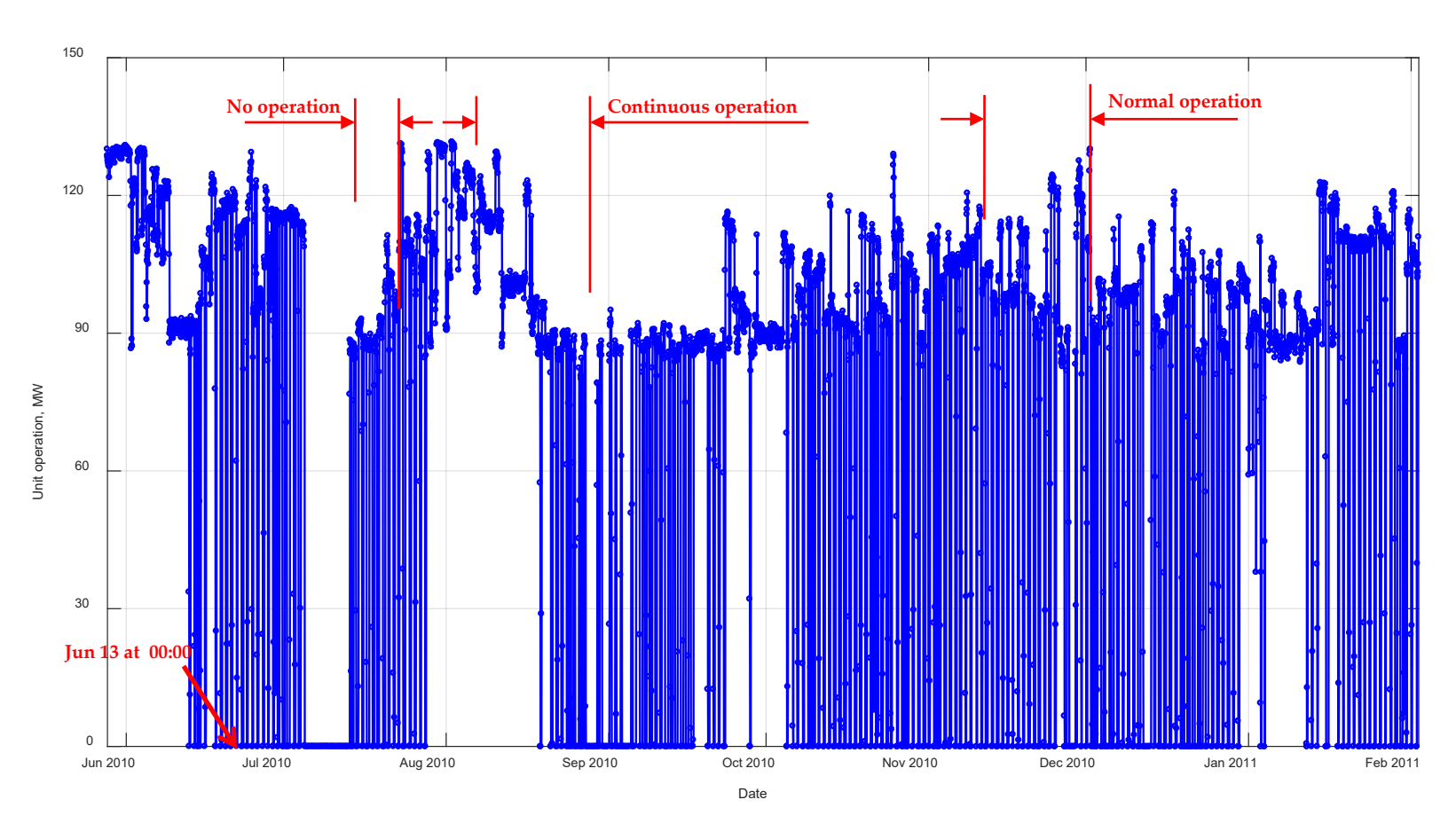


Figure 3.1: Unit operation during one-year measurement



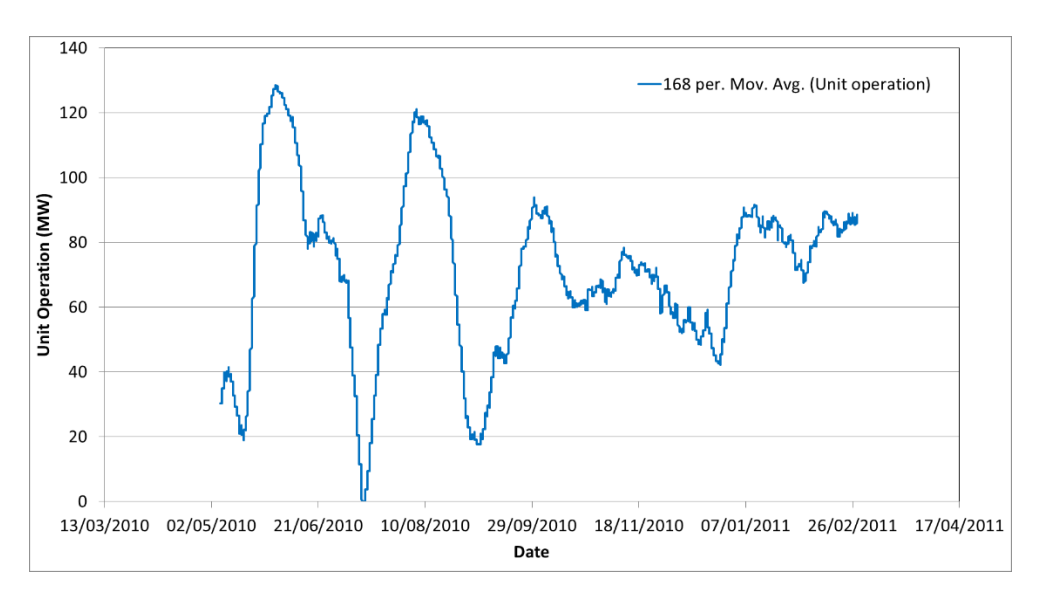


Figure 3.2 Unit operation as moving average for ten months.

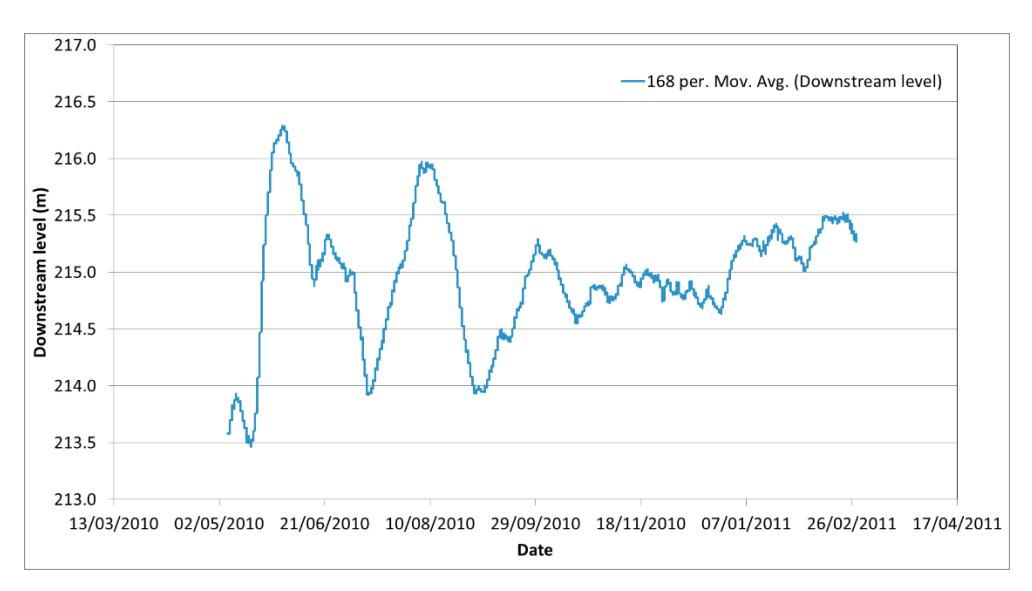


Figure 3.3 Downstream water level as moving average for ten months.



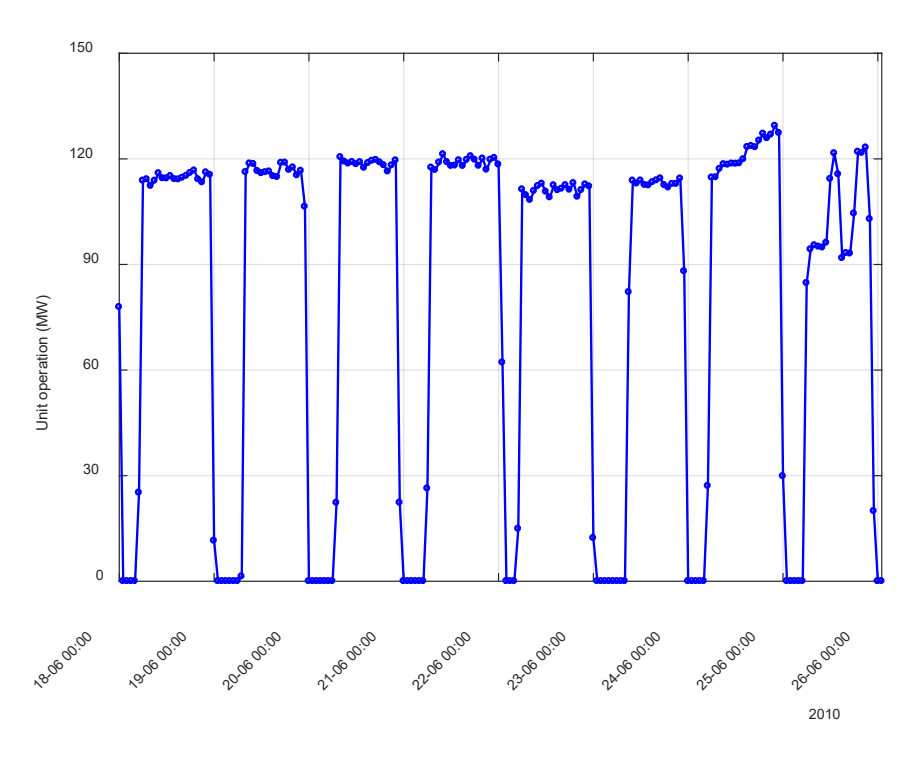


Figure 3.4: Normal operation with producing power almost 120 MW during daytime for one week

3.2 CONTINUOUS OPERATION

For continuous operation, the unit operates between almost 85 to 130 MW during daytime and nighttime, see Figure 3.1. Figure 3.5 indicates a continuous operation for one week in May-June. As seen in this figure, there are almost no major unit operation fluctuations in production.



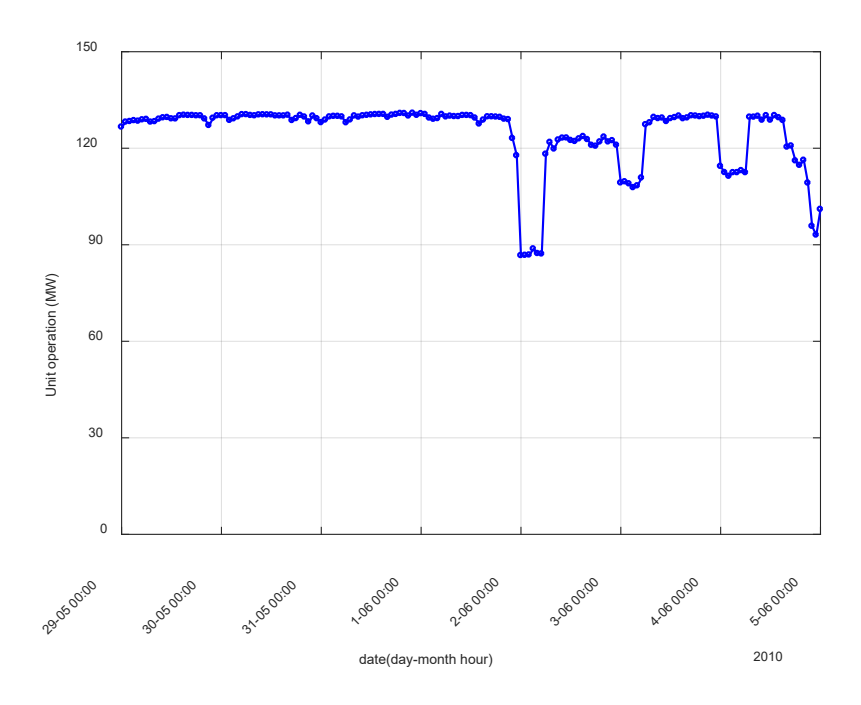


Figure 3.5: Continuous operation with producing power between 90-130 MW for one week

3.3 START AND STOP EVENTS

The sequence of start and stop during the daytime is illustrated in Figure 3.6. It can be seen in this figure that the stop times are commonly during night-time, but also some at day-time. These sharp starts/stops during day-time can be due to some problems in unit operation.

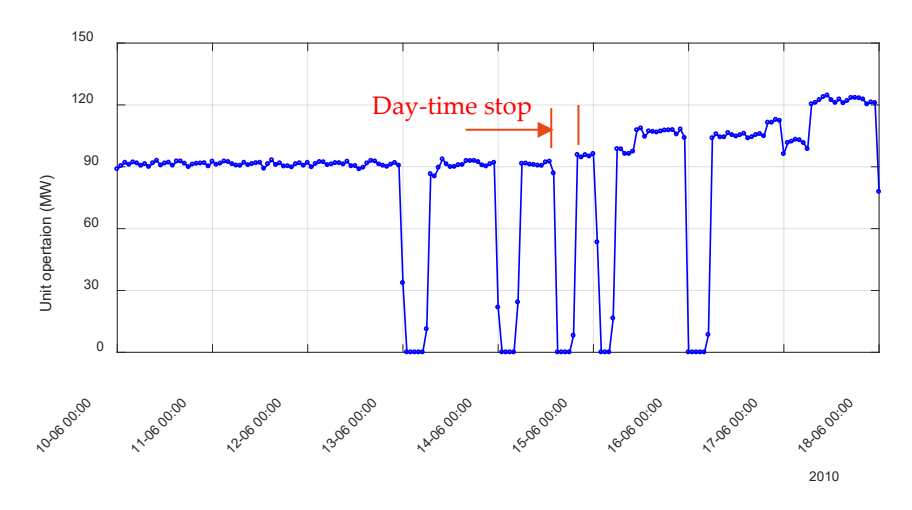


Figure 3.6: Normal and quick start and stops, for one week



4 Pressure measurements

Pressure sensors are installed on the draft tube central wall and roof; to measure the dynamic pressure due to the water which is being finally discharged from the turbine. Depending on the operation unit, the pressure range could be very small. Generally speaking, if the pressure of a system is below or equal to its hydrostatic pressure, the unit is most likely not to operate at all. If the pressure of a system is above its hydrostatic pressure, it operates. The pressure has been measured during one minute for every hour which the mean value of the measurements is considered and presented as a measured pressure for each hour. Furthermore, 15 minutes measurements also have been done for some stop/start-sequences and fluctuations. The sampling frequency is 100 Hz for all measurements.

In this chapter, the pressures measurements have been presented for two weeks, 24 hours, 15 minutes and 1 minute. Table 4.1 shows abbreviations that have been used in this report to describe pressure sensors position.

Table 4.1: Abbreviation for pressure sensors on the central wall and roof of the draft tube (see also Figure 2.1 and 2.2).

Sensor	Location	Abbreviation
P1	upstream/left side of the central wall	P1 (US/L)
P2	downstream/left side of the central wall	P2 (DS/L)
Р3	upstream/right side of the central wall	P3 (US/R)
P4	downstream/right side of the central wall	P4 (DS/R)
P5	roof/right side of the draft tube	P5 (RF/R)

The pressure measurements of all five sensors are shown in Figure 4.1. The pressure measurements from 28^{th} May 2010 to 28^{th} February 2011 were recorded. It can be seen that P1 was no longer working in the early stage of measurements on 13^{th} June at 00:00 when the first stop event occurred, i.e. see Figure 2.1 (a). The cause of such failure may occur due to the connectors were broken, or the cable insulation was damaged because of the fluctuation of the water during the start of the operation unit. Whereas, P3 failed during the stop event of the unit on 10^{th} July at 00:00 but in some periods the reading could be considered for example during 19^{th} to 25^{th} January , see Figure 4.1(c). It can also be seen that P2, P4 and P5 have the same behaviour pattern with minor differences. By excluding P1 and P3, Figure 4.2 shows the minor differences in the measurements of P2, P4 and P5.



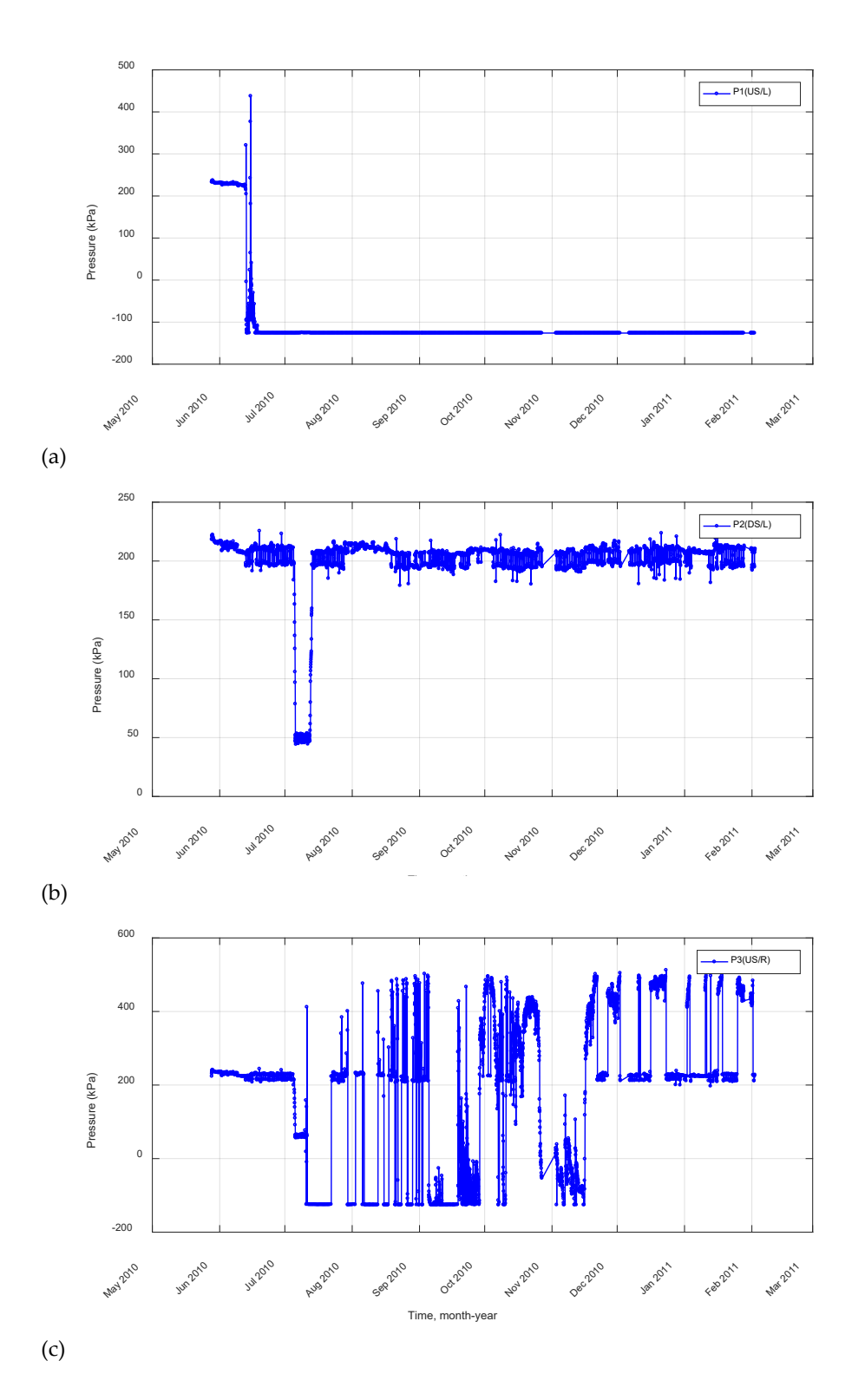
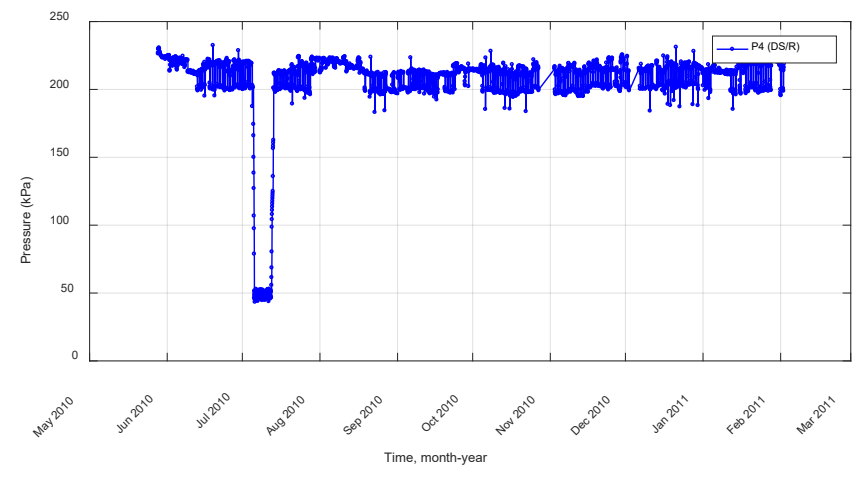
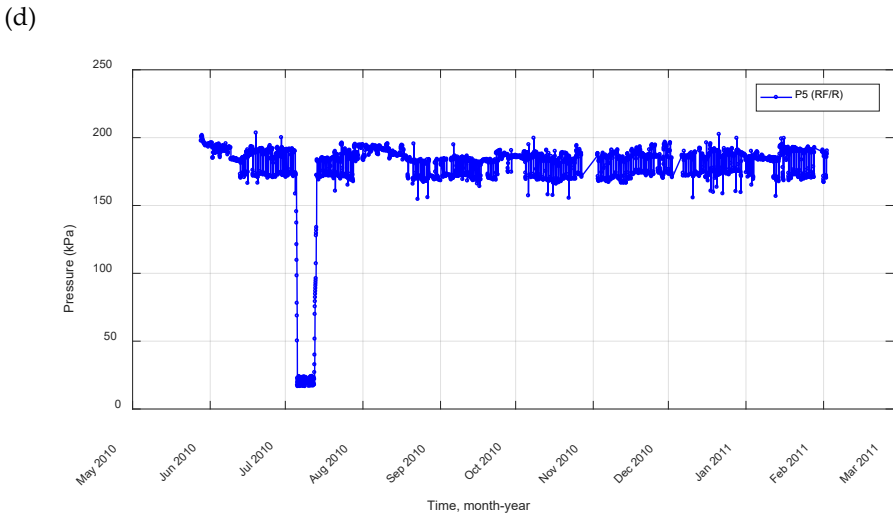


Figure 4.1: Pressure measurement during one year for (a) P1 (US/L), (b) P2 (DS/L), (c) P3 (US/R), (d) P4 (DS/R) and (e) P5 (RF/R).







(Cont.) Figure 4.1: Pressure measurement during one year for (a) P1 (US/L), (b) P2(DS/L), (c) P3 (US/R), (d) P4 (DS/R) and (e) P5 (RF/R).

(e)

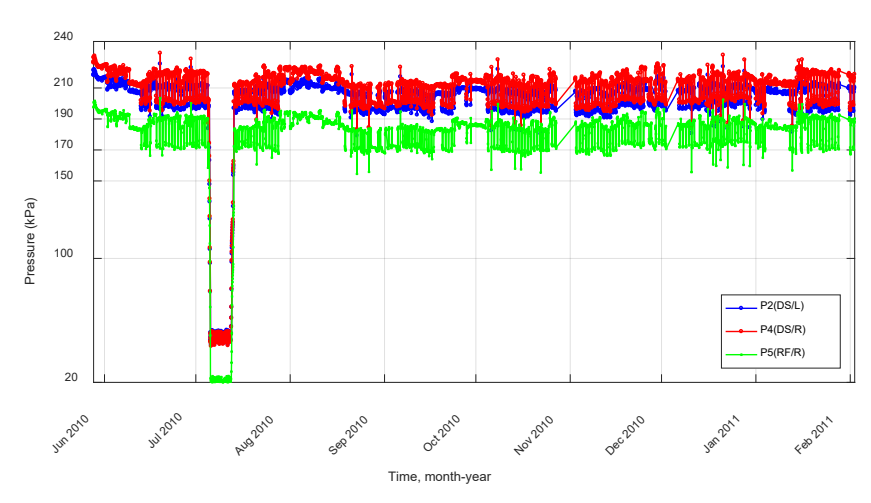


Figure 4.2: Pressure measurement during one year for P2 (DS/L), P4 (DS/R) and P5 (RF/R).



The pressure difference along and across the central wall is also calculated from pressure measurement. The pressure due to elevation difference between sensors is removed to calculate pure pressure difference along the central wall and across the central wall. Equations 4.1 and 4.2 show calculation of pressure difference across the central wall at upstream and downstream of the wall, respectively. Equations 4.3 and 4.4 show calculation of pressure difference along the central wall at right and left the side of the central wall, respectively.

$$\Delta P(ACRS/US) = (P3 + 0.31\rho g) - P1$$
 (4.1)

$$\Delta P(ACRS / DS) = (P4 - 0.38\rho g) - P2$$
 (4.2)

$$\Delta P(ALG/R) = (P3 - 1.31\rho g) - P4$$
 (4.3)

$$\Delta P(ALG/L) = (P1 - 2\rho g) - P2$$
 (4.4)

However, the pressure measurements of five sensors for two weeks form 29th May at 00:00 until 13th June at 00:00 are shown in Figure 4.3. In this period, all five sensors work very well. Also, it can be seen that the measured pressure follows the unit operational pattern.

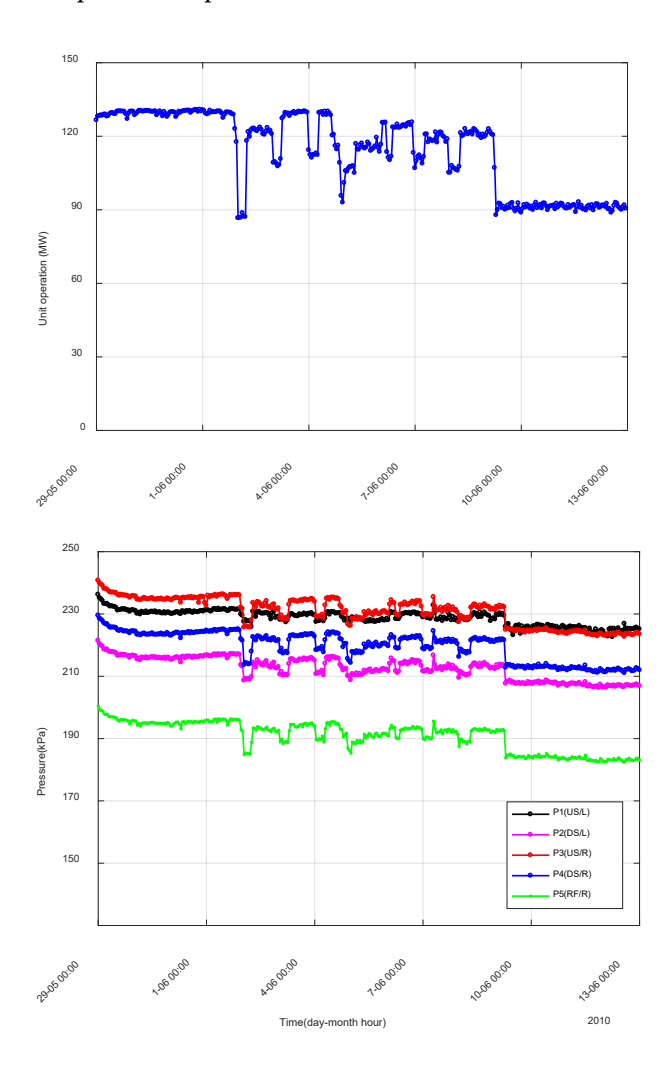


Figure 4.3: The pressure measurement of five sensors from 29th May at 00:00 to 13th June at 00:00.



The variation of the pressure across the central wall at the downstream and upstream sides of the draft tube can be calculated by using Eq. 4.1-4.2 for the same period from 29^{th} May at 00:00 to 13^{th} June at 00:00 and is shown in Figure 4.4 (b). The variation of the pressure along the central wall at right and left sides of the central wall are calculated by using Eq. 4.3-4.4 for the same period and illustrated in Figure 4.4 (c).

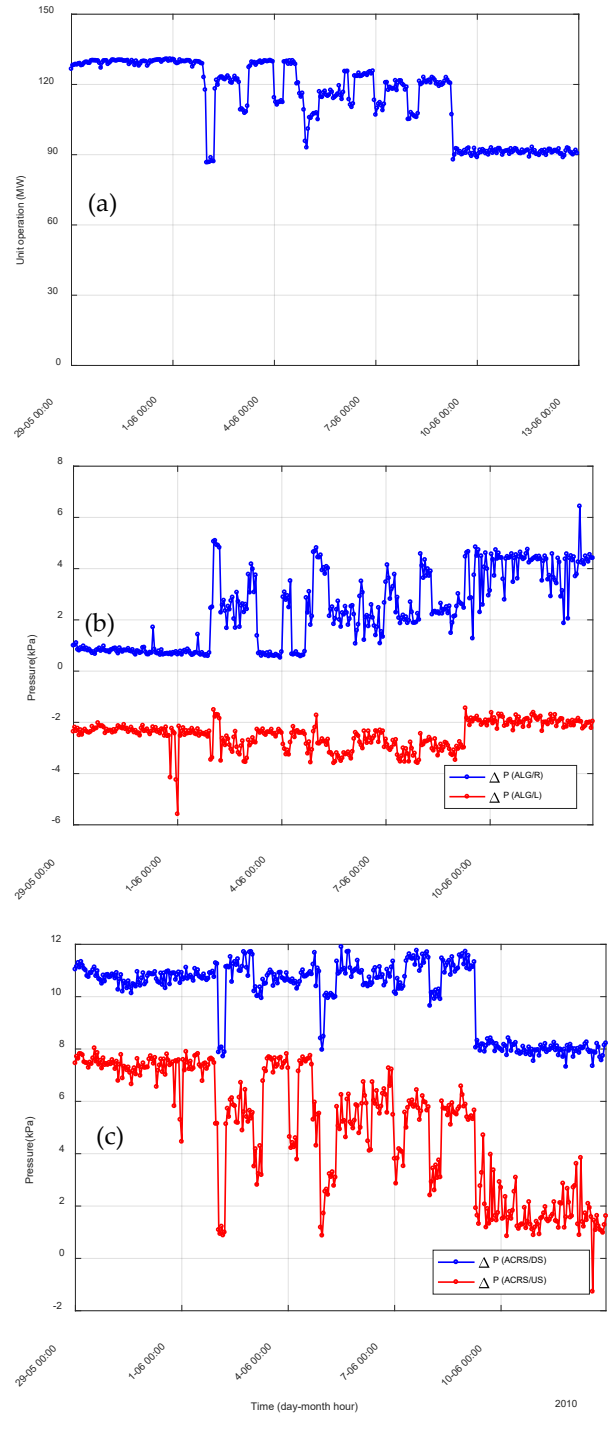


Figure 4.4: The variation of the pressure during (a) unit operation, (b) across and (c) along the central wall for two weeks.



It can be seen in Figure 4.4 that a drop of the output of 40 MW gives a relative increase of the pressure with approximately four kPa on the upstream position, whereas this reduction gives a decrease of the pressure on the right-hand side with approximately six kPa. A higher relative difference in pressure across the wall can be observed in the downstream position due to even lower values on left-hand side downstream.

For one-month measurements, the variation of the pressure of only three sensor P2, P3 and P4 can be achieved by excluding P1 and illustrated in Figure 4.5 (b). Also, the variations of the pressure across the central wall at the downstream side and along the central wall at right side of the central wall are shown in Figure 4.5 (c).

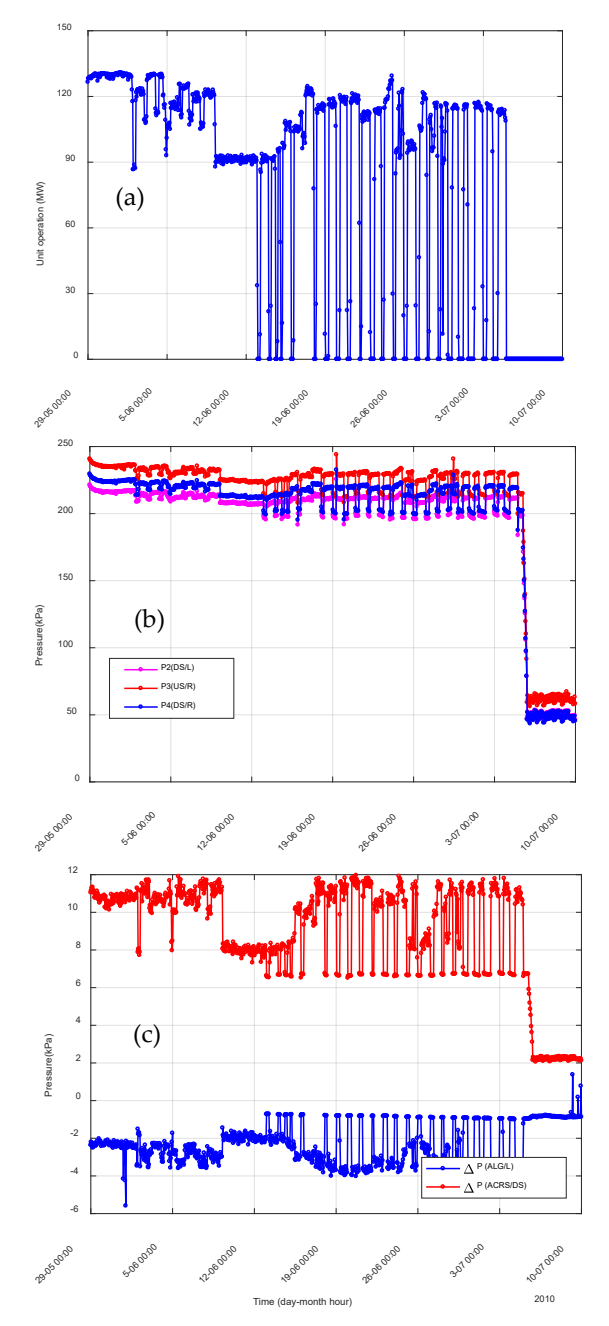


Figure 4.5: The variation of the pressure during (a) unit operation, (b) across and (c) along the central wall during a month.



4.1 NORMAL OPERATION

In this section, the pressure measurement for normal operation by producing the effect of about 120 MW during daytime is described. Figures 4.6 – 4.7 illustrate a variation of measured pressure for one week and 24 hours, respectively. As shown in these figures, pressure on the right side of the central wall (P3 (US/R) and P4 (DS/R)) is higher than the left side of the central wall (P2 (DS/L)). Pressure on the roof is less than for other sensors. It should be noted that when the unit is off, sensors show hydrostatic pressure. As seen from these figures, the maximum pressure during operation is for sensor P3 (US/R) with a value of almost 230 kPa. The minimum pressure during operation is for sensor P5 (RF/R) with a value of 190.5 kPa.

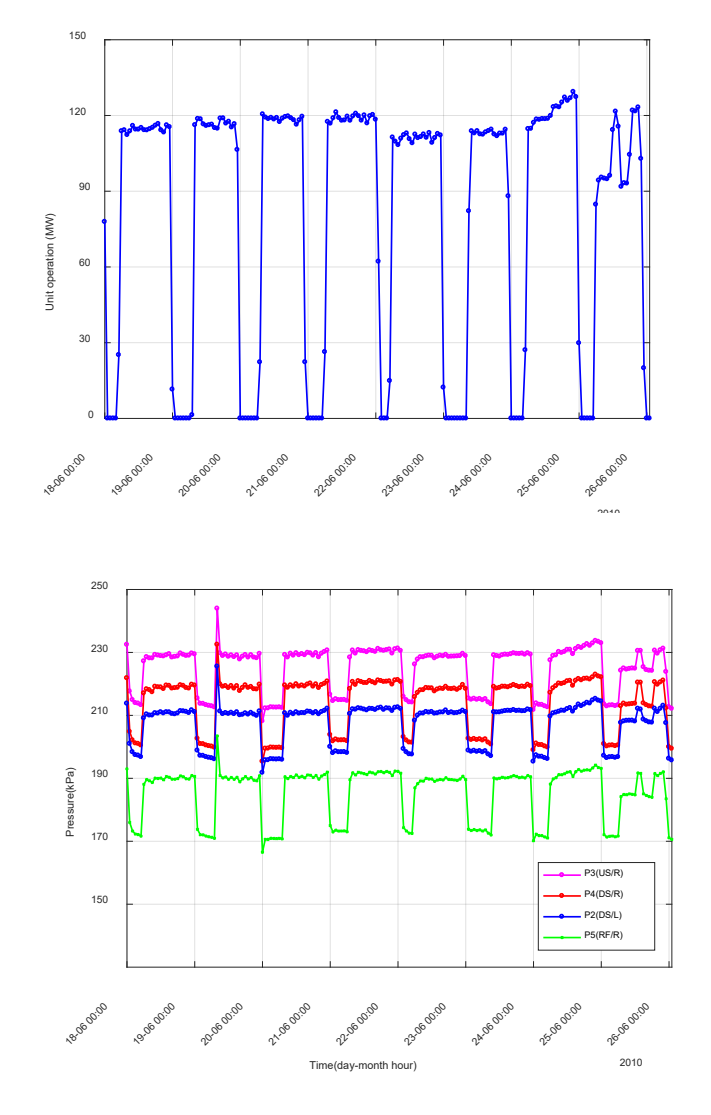


Figure 4.6: Variation of measured pressure in a week for normal operation by producing the power of about 120 MW.



In Figure 4.7 it can be seen there is pressure reduction from daytime (operation of 120 MW) to night-time (no operation) of about 20 kPa in all sensors.

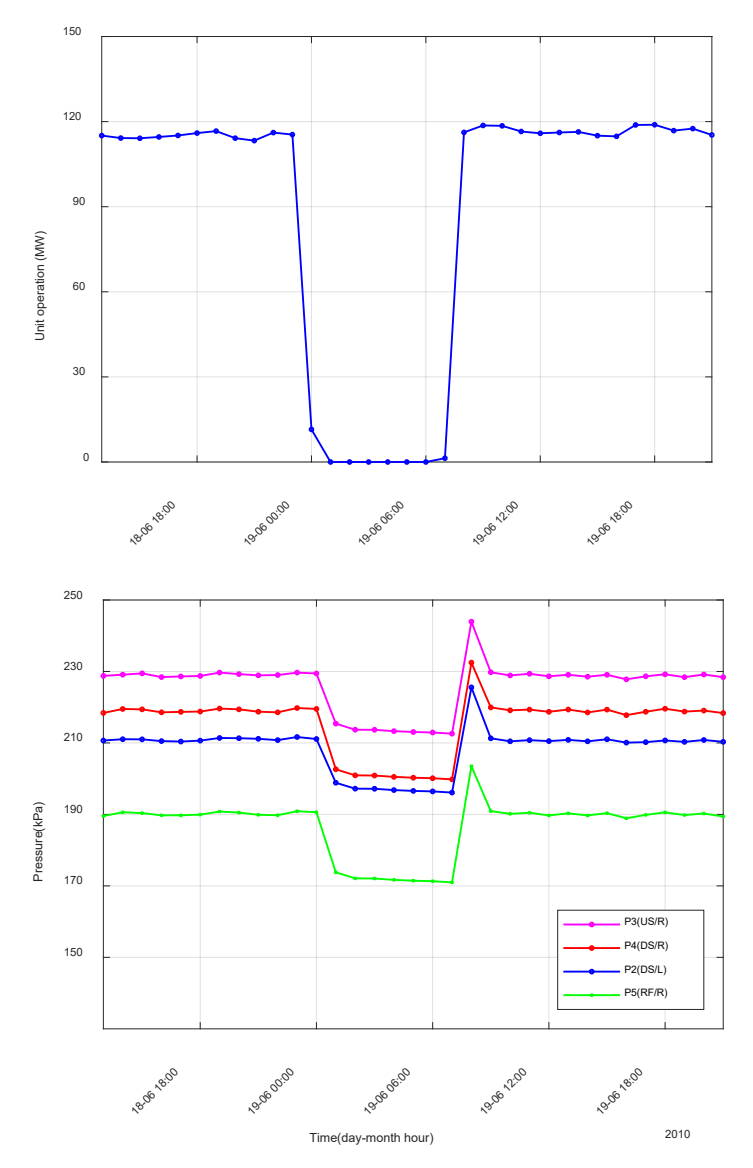


Figure 4.7: Variation of measured pressure in 24 hours for normal operation by producing the effect of about 120 MW.

Figure 4.8 illustrates a variation of pressure across the central wall at the downstream side of the draft tube ($\Delta P(ACRS/DS)$) and along the central wall at right side of the central wall ($\Delta P(ALG/R)$). As seen in this figure during operation of 120 MW the pressure across and along the central wall is almost 11 kPa and -4 kPa, respectively. These values indicate that during operation pressure on the right side of the wall is higher than left side and pressure along the central wall is increasing from upstream to downstream. The figure also highlights that during the reduction of power from 120 MW to 0 MW, pressure across the wall has a reduction of 5 kPa while an increase of 3 kPa for along the wall. Table 4.2



summarises average pressure measurement during daytime and nighttime for the normal operation.

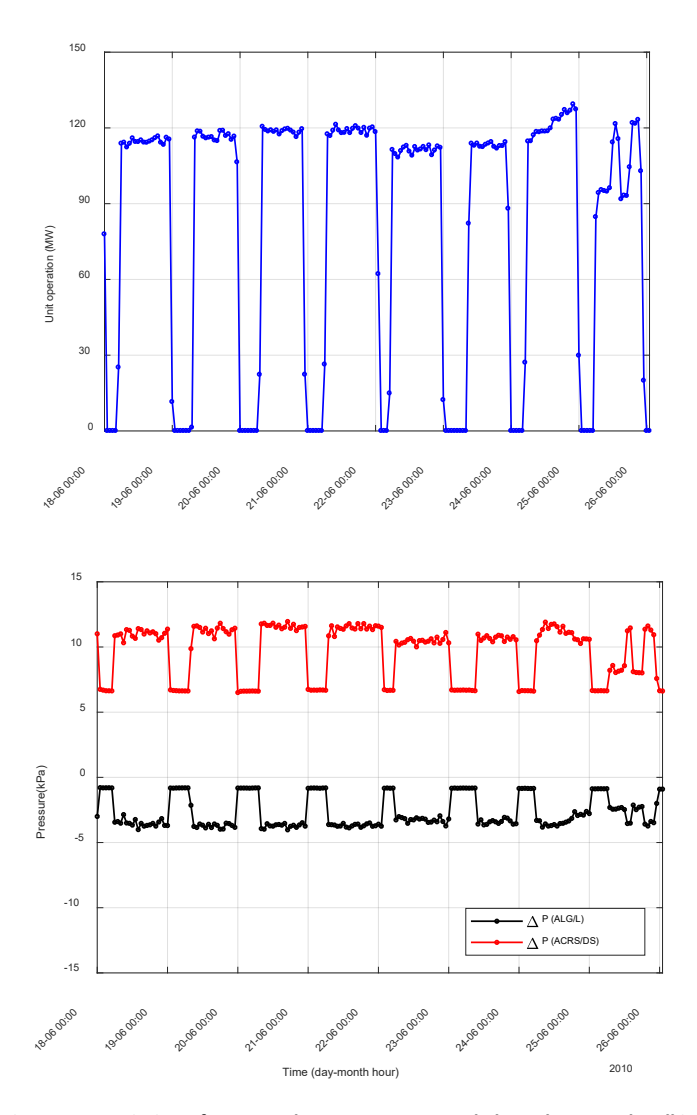


Figure 4.8: Variation of measured pressure across and along the central wall in a week for normal operation by producing the power of about 120 MW.

Table 4.2: Average of pressure measurement for normal operation, unit kPa

	No operation	Operation 120 MW
P2 (DS/L)	197	211
P3 (US/R)	213	229
P4 (DS/R)	201	219
P5 (RF/R)	172	190
$\Delta P(ACRS / DS)$	7	12
$\Delta P(ALG / R)$	-0.8	-3.8



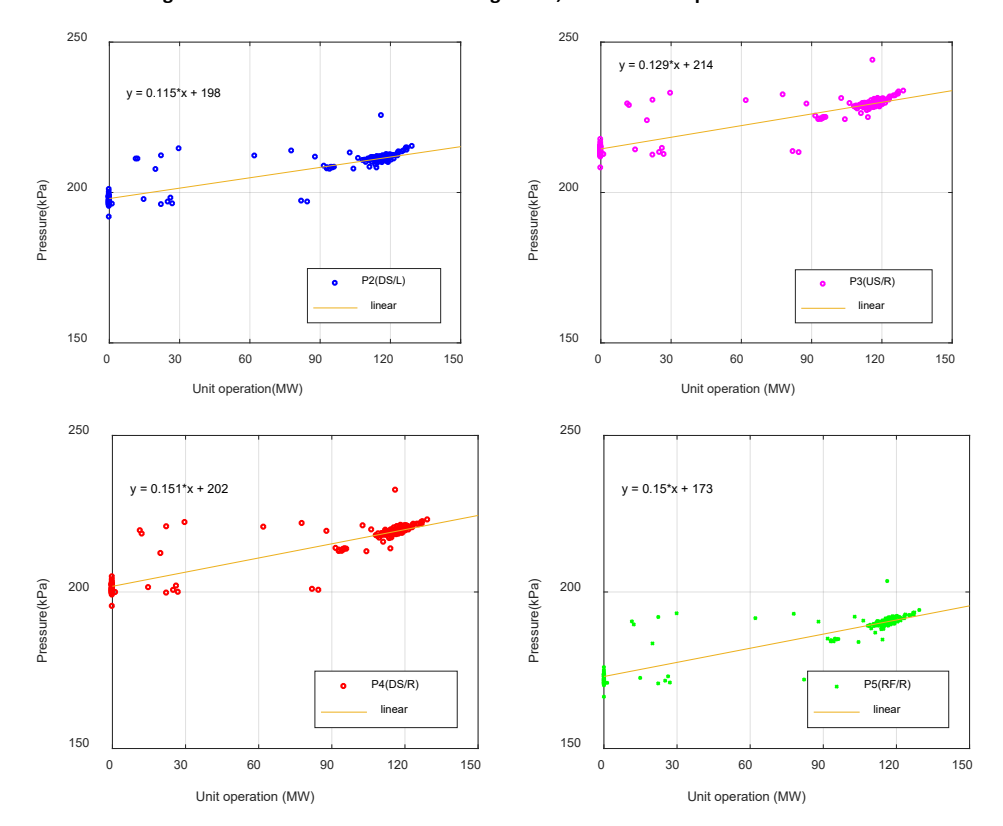
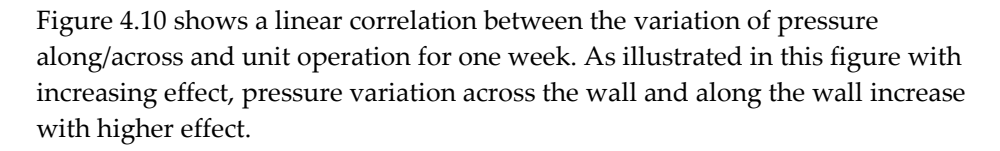


Figure 4.9 illustrates a linear correlation between pressure measurement and unit operation for one week. As seen from this figure for sensors P2-P5 with increasing effect, the measured pressure is increased.

Figure 4.9: Correlation between pressure measurement and unit operation in a week for normal operation by producing the power of about 120 MW during daytime



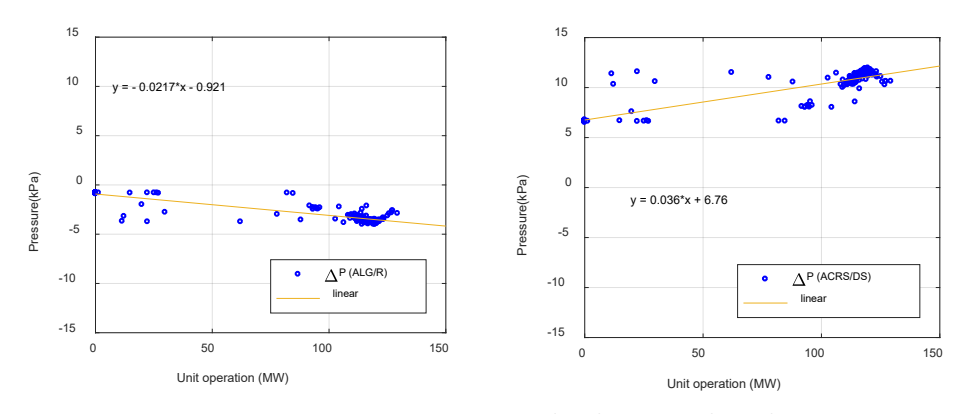


Figure 4.10: Correlation between variation of pressure along (LEFT) and across (RIGHT) the central wall and unit operation in a week for normal operation with producing the power of about 110 MW during daytime

The pressure measurement during a stop (2011-01-19 22:51) and start (2011-01-20 06:49) of the unit from 15 min measurement is described. For 15 min measurement,



during the stop the unit, the reducing effect from 75 MW to 0, at time 22:51 has been shown in Figure 4.11. This measurement should be compared with 1 min measurement at time 23:00 see Table 4.3. As seen in this Figure pressure measured after 15 min is close to the values measured in 1 min at time 23:00. The same goes for the pressure difference along and across the central wall, see Figure 4.12. From the pressure measurements, it is obvious that the changes in total pressure (20-25 kPa the first minutes) from reducing the unit effect is overruling any differential pressures along and across the wall (less than two kPa).

Table 4.3: Average measured pressure at time 22.00 and 23:00 from 1 min reading (unit kPa)

	P3(US/R)	P4(DS/R)	P2(DS/L)	P5(RF/R)	ΔP(ACRS / DS)	$\Delta P(ALG/R)$
75 MW (22:00)	230.7	221.1	213.2	192.6	4.099	-3.493
0 MW (23:00)	216.9	201.9	200.9	176.3	0.2537	-1.161

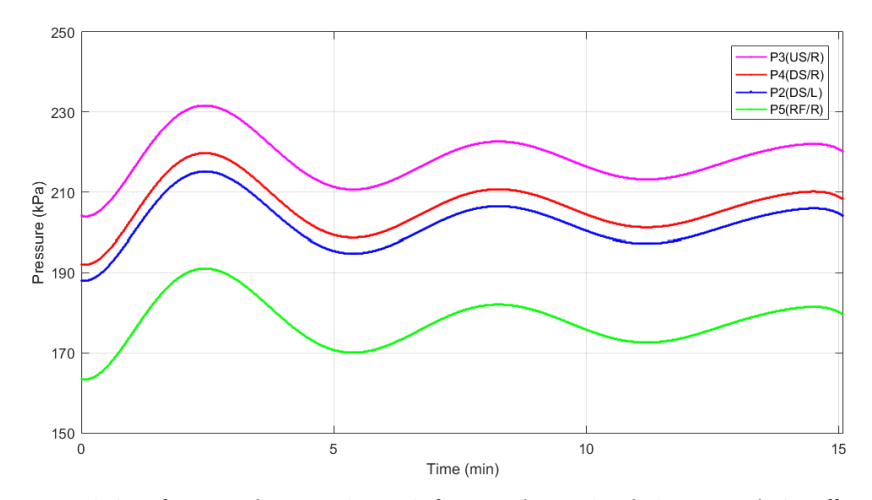


Figure 4.11: Variation of measured pressure in 15 min for normal operation during stop-reducing effect from 75 MW to 0 (2011-01-19 22:51)

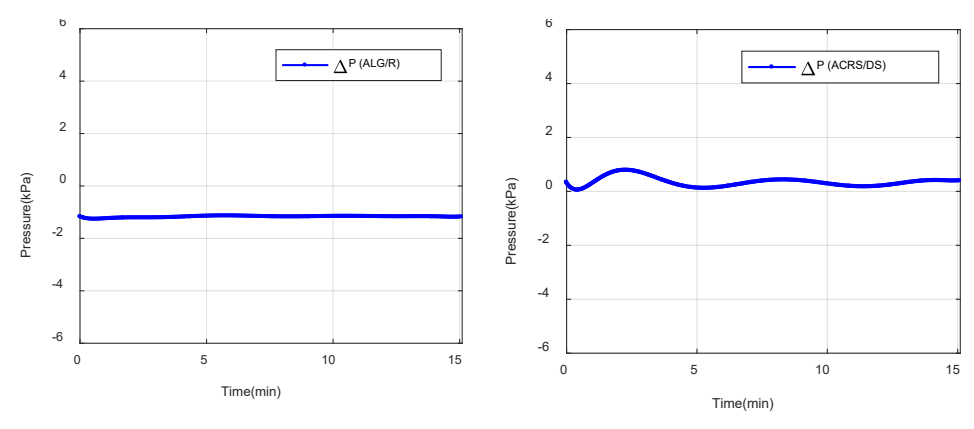


Figure 4.12: Variation of pressure along and across the central wall in 15 min for normal operation during stopreducing effect from 75 MW to 0 (2011-01-19 22:51)



Figure 4.13 illustrates 15 min measurement during a start at time 06:49, increasing effect from 25 MW to 110 MW. This measurement is compared with measured pressure in 1 min at 07:00, see Table 4.4. The comparison indicates that the last peak in pressure measurement of Figure 4.7 is close to the measured pressure at time 07:00 from 1 min reading. The same goes for pressure along and across the central wall, see Figure 4.14. The reason is that in the last 5 min measurement the unit operates with the production of 110 MW. It can be seen that the change in total pressure when increasing the unit operation can be as large as 30-35 kPa and the increase in differential pressures are visible after 5 to 10 minutes, but in the same range as during normal operation.

Table 4.4: Average measured pressure at time 06.00 and 07:00 from 1 min reading (unit kPa)

	P3 (US/R)	P4 (DS/R)	P2 (DS/L)	P5 (RF/R)	ΔP(ACRS / DS)	$\Delta P(ALG/R)$
25 MW (06:00)	212.7	200.8	196.8	172.2	0.1399	-1.149
110 MW (07:00)	228.4	218.7	210.9	190.1	4.017	-3.433

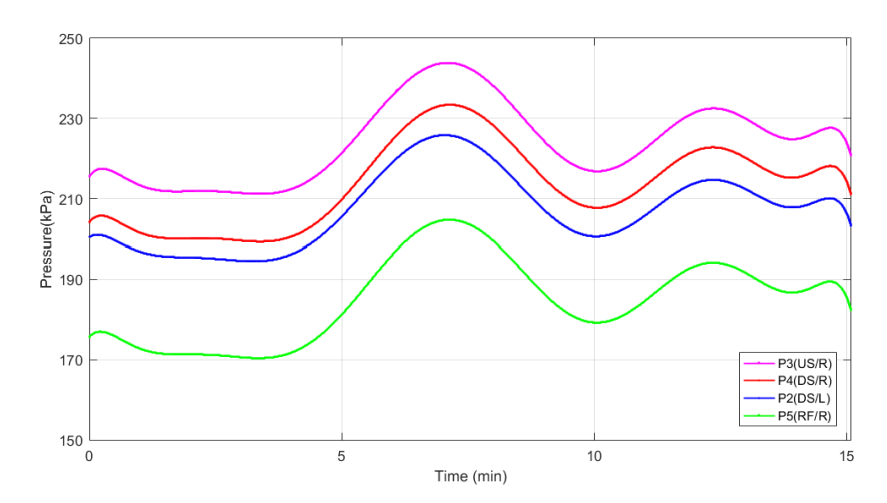


Figure 4.13: Variation of measured pressure in 15 min for normal operation during start-increasing effect from 25 MW to 110 MW (2011-01-20 06:49)



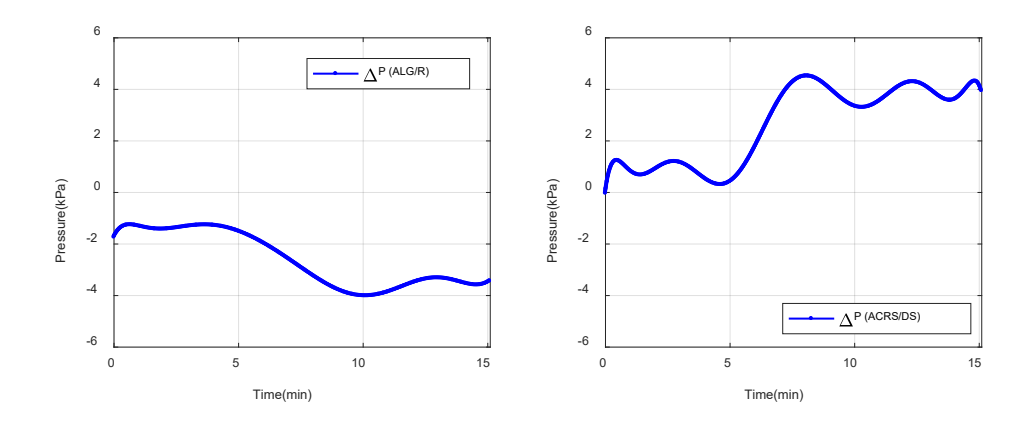


Figure 4.14: Variation of pressure along and across the central wall in 15 min for normal operation during start-increasing effect from 25 MW to 110 MW (2011-01-20 06:49).

4.2 CONTINUOUS OPERATION

In this section, the pressure measurement for continuous operation by producing power between 85-130 MW is described. Figures 4.15 and 4.16 show variation of measured pressure for one week and 24 hours, respectively. As seen from this Figures, pressure measurement follows unit operation pattern. Furthermore, pressure on the right side of the central wall is higher than the left side of the central wall. Pressure on the roof is less than others.



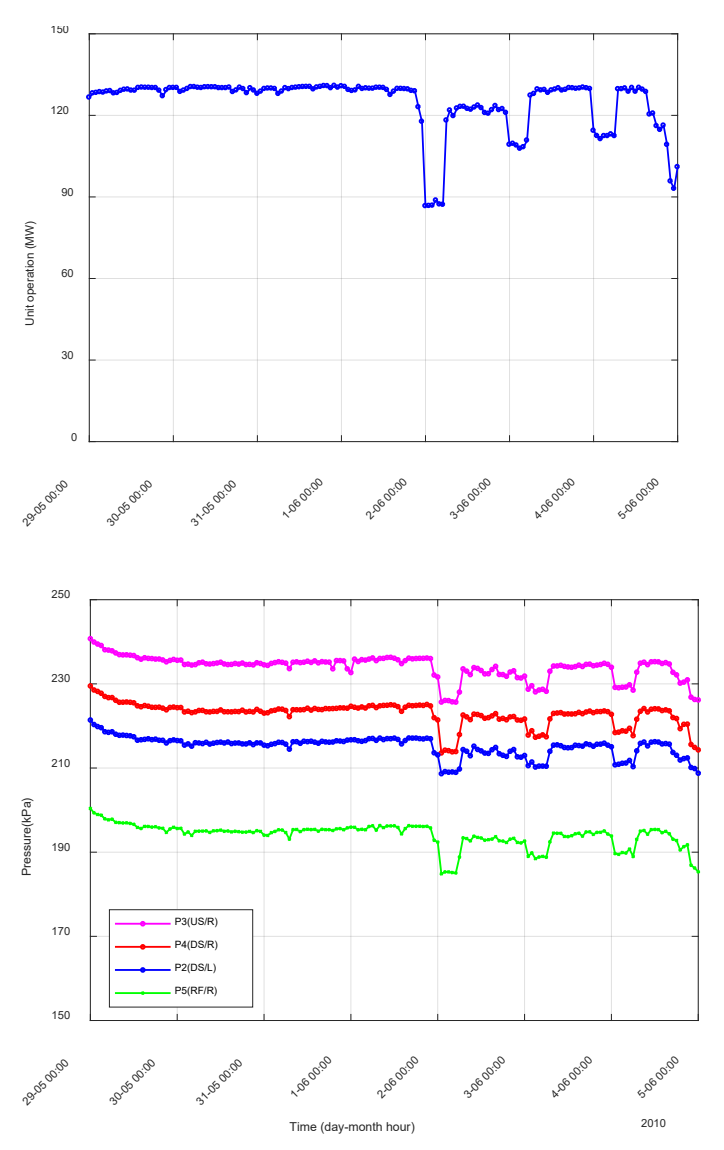


Figure 4.15: Variation of measured pressure in a week for continuous operation with producing power between 85-130 MW (see Table 4.1 for pressure sensor abbreviation).



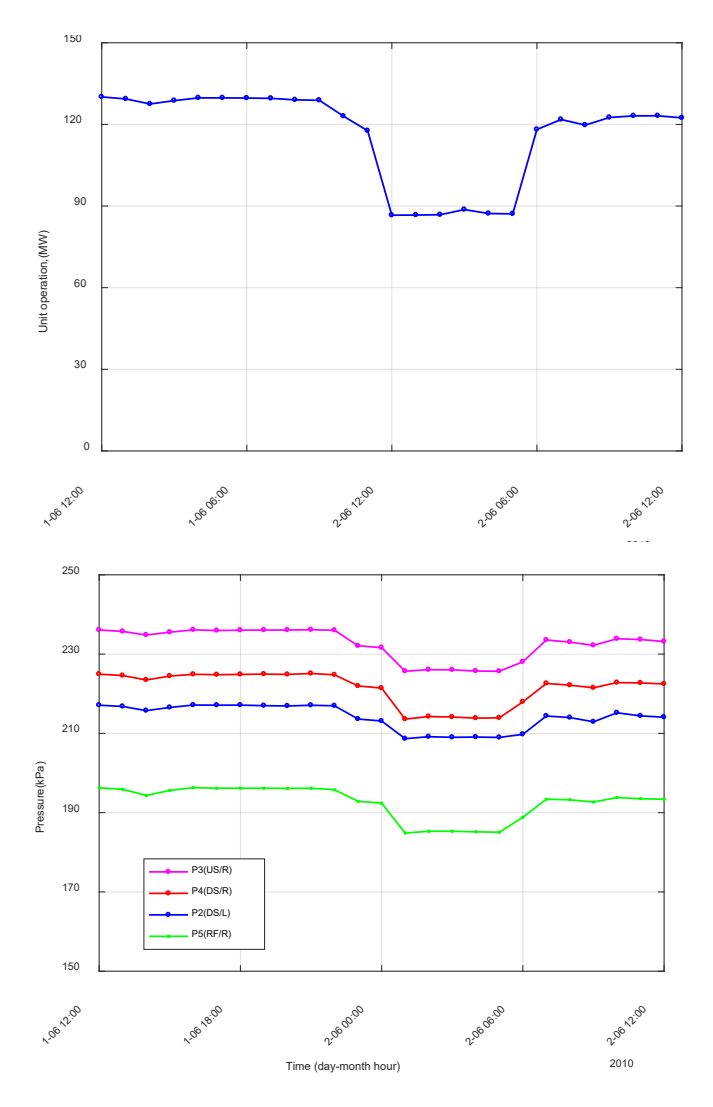


Figure 4.16: Variation of measured pressure in 24 hours for continuous operation with producing power between 85-130 MW

The variations of pressure across the central wall and along the central wall for continuous operation are demonstrated in Figure 4.17. As seen from this figure average pressure measurement across the central wall during 130 MW and 85 MW operations is 10.8 kPa and 8.1 kPa, respectively. Furthermore, average pressure measurement along the central wall during operation of 130 MW and 85 MW is - 2.3 kPa and -1.85 kPa, respectively. The minus sign indicates increasing pressure along the central wall from upstream to downstream (this shows the effect of the draft tube, increasing static pressure along the draft tube).



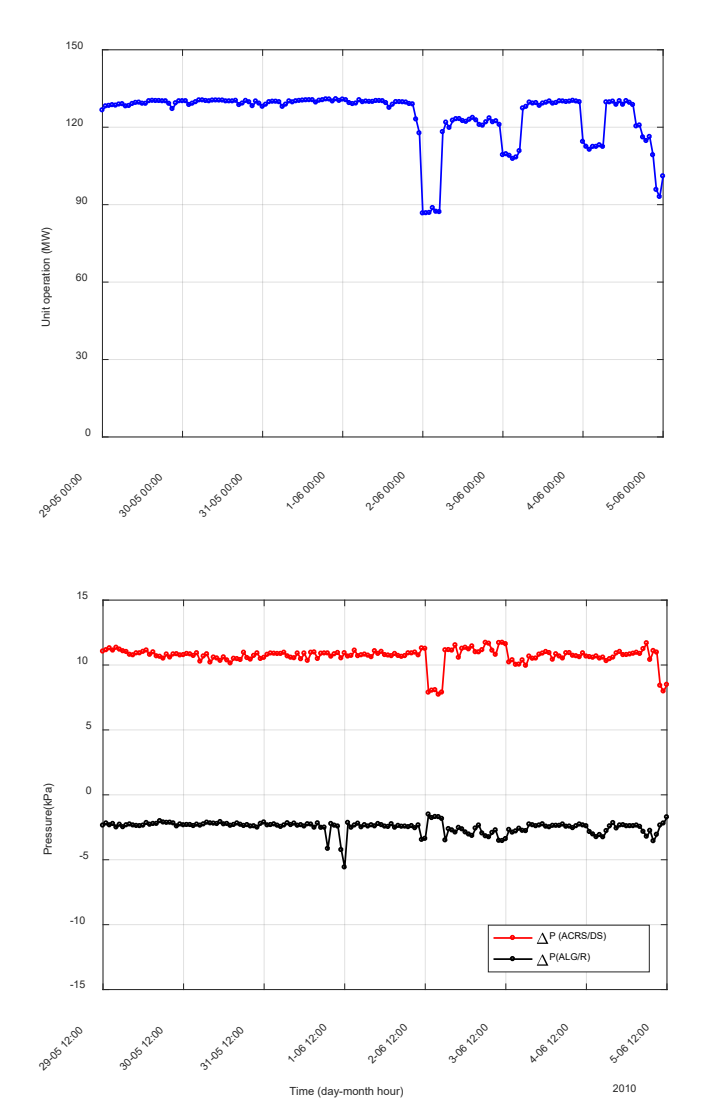


Figure 4.17: Variation of measured pressure across and along the central wall in a week for continuous operation with producing power between 85-130 MW.

However, the average pressure measurement during operation of 130 MW and 80 MW are summarised in Table 4.4.

Table 4.4: Average of pressure measurement for continuous operation, unit kPa

	130 MW	85 MW
P3 (US/R)	226.7	223.45
P4 (DS/R)	216.37	213.46
P2 (DS/L)	209.5	207.45
P5 (RF/R)	187.88	184.94
ΔP(ACRS / DS)	10.8	8.1
$\Delta P(ALG/R)$	-2.3	-1.9



A linear correlation between pressure measurement and unit operation can be found for one-week occasion and shown in Figure 4.18. As seen from this figure for all sensors with increasing the unit operation power, the measured pressure is increased. Figure 4.19 shows the correlation between unit operation and pressure along and across the central wall. It is observed that with the increasing effect the pressure difference across and along the central wall is increased. The behaviour regarding pressures along and across the wall show a good correlation with the unit operation.

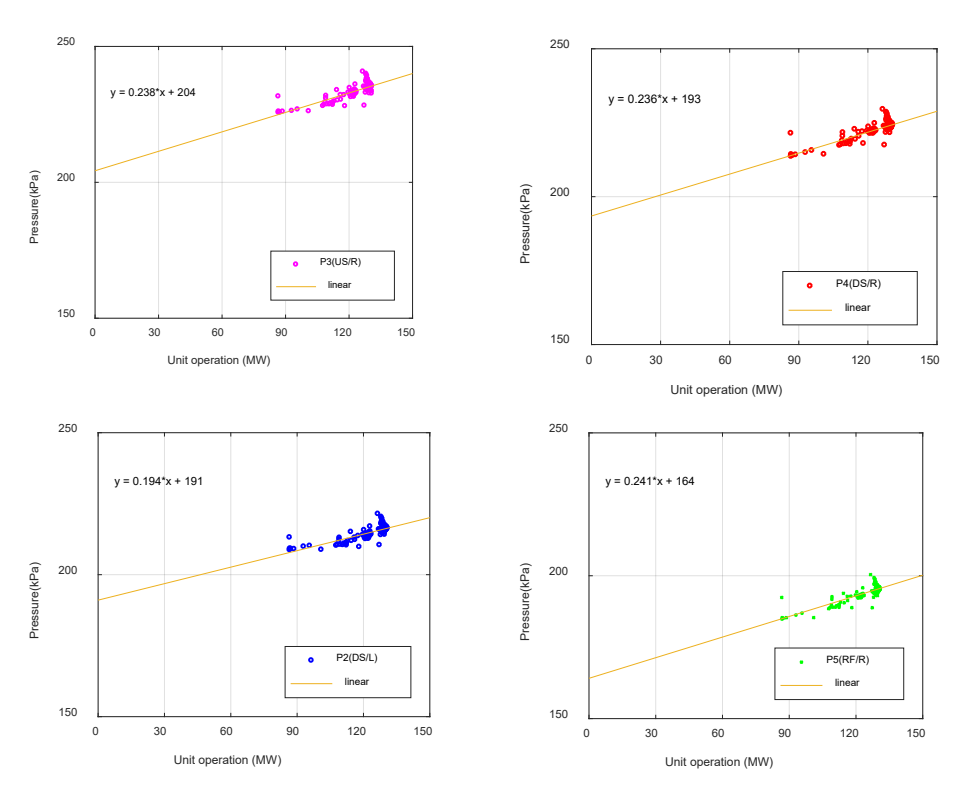


Figure 4.18: Correlation between pressure measurement and unit operation in a week for continuous operation with producing power between 85-130 MW

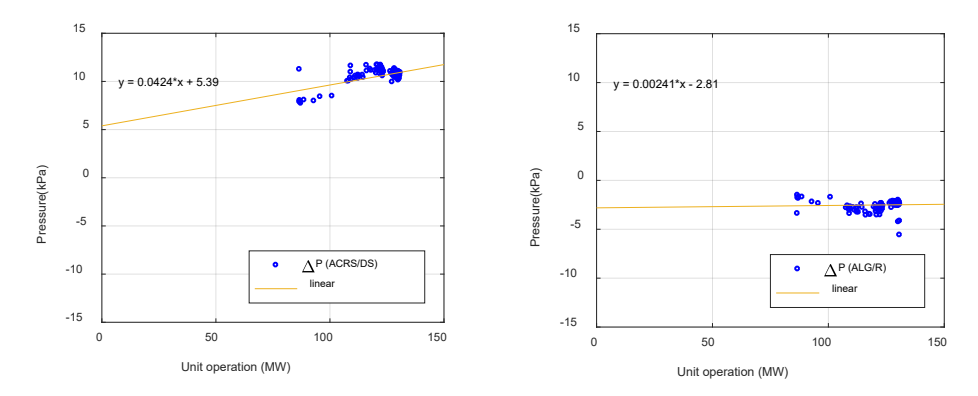


Figure 4.19: Correlation between variation of pressure along/across the central wall and unit operation in a week for week for continuous operation with producing power between 85-130 MW



4.3 FAST START AND STOP EVENTS

The variation of pressure of four sensors during operation with a sharp stop and start was considered in this section and shown in Figure 4.20. As seen from this figure during stopping the unit, pressure goes lower than the hydrostatic pressure (pressure during no operation). For example, the unit was shut down on 14th June from 15:00 to 18:00 for unknown reasons, therefore, the unit operation power dropped from 90 MW to 0 MW. The overall behaviour pattern of the measured pressure is about the same as for the normal operation. The sequence of start and stop in daytime on 14th June is shown in Figure 4.21.

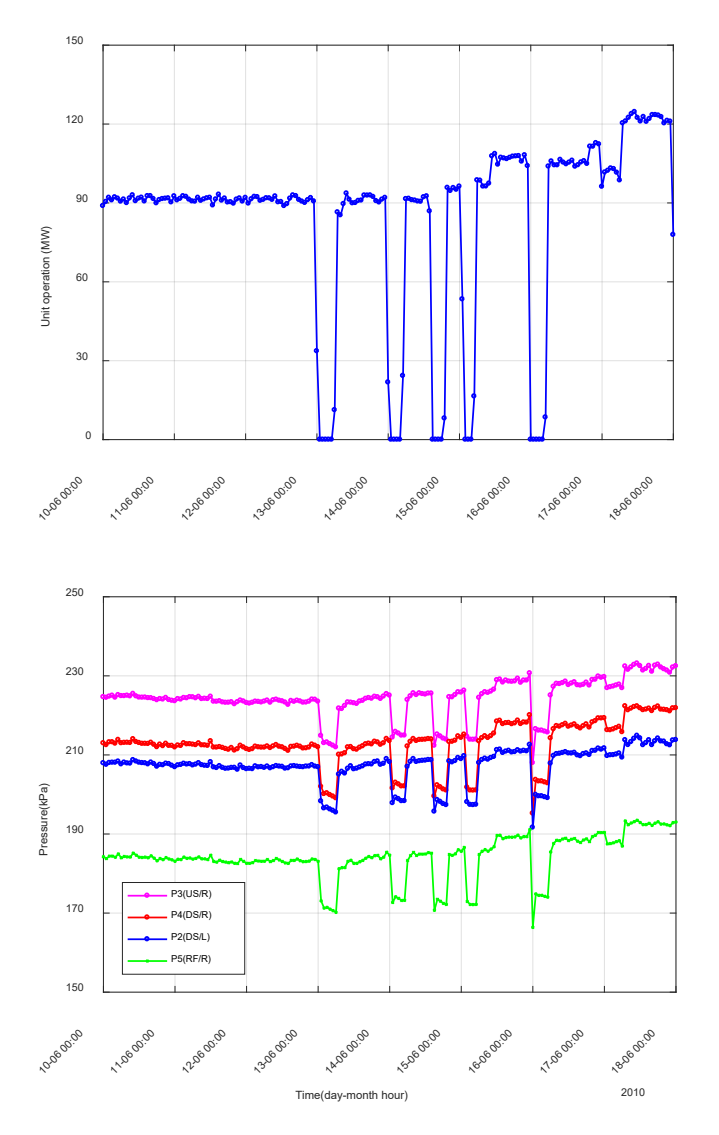


Figure 4.20: Variation of measured pressure in a week for normal and quick start and stops



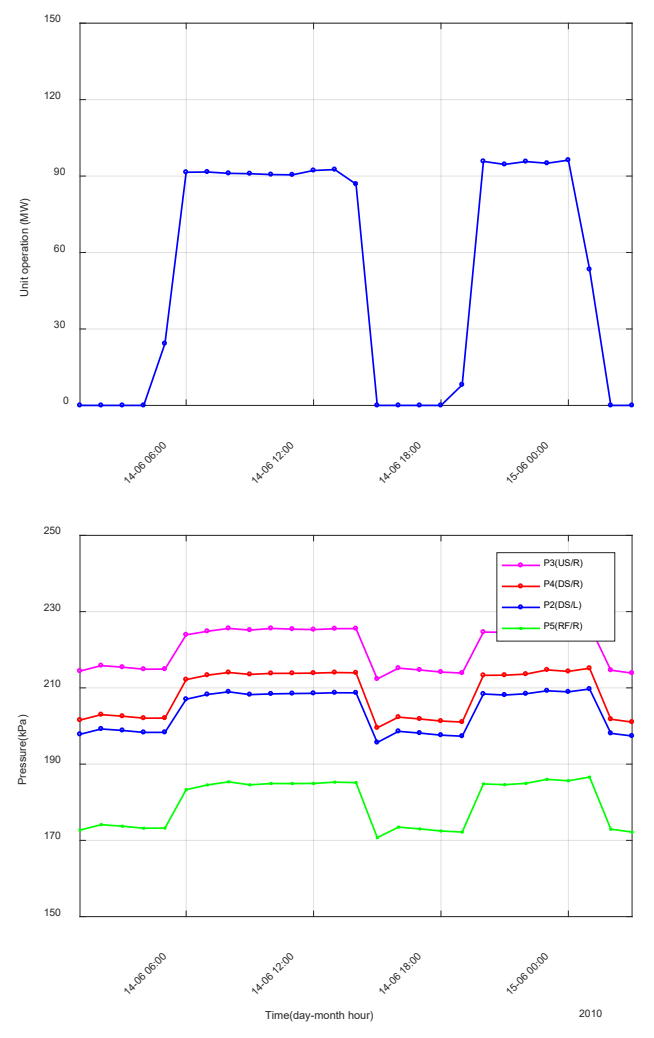


Figure 4.21: Variation of measured pressure in 24 hours for normal and quick start and stops

Variation of pressure across the central wall has been shown in Figure 4.22. The highest pressure difference across the wall is five kPa during operation of 90 MW. **Table 4.5** summarises pressure measurement during a sequence of start/stop.

Table 4.5: Average measured pressure for stop and started event (unit: kPa)

	90 MW (14:00)	0 MW (15:00)
P2 (DS/L)	209	196
P3 (US/R)	226	212
P4 (DS/R)	214	200
P5 (RF/R)	185	170
$\Delta P(ACRS / DS)$	17	4



In the following pressure measurement in 15 min during stopping the unit from 8.68 MW and 19.15 MW is shown. It should be noted that pressure measurement during the starting unit is not shown due to insignificant variation in pressure across the central wall. Figure 4.20 shows a variation of measured pressure in 15 min during stop-reducing effect from 8.68 MW to 0 (2010-12-20 10:16). The variation of pressure across the central wall is almost zero, see Figure 4.21.

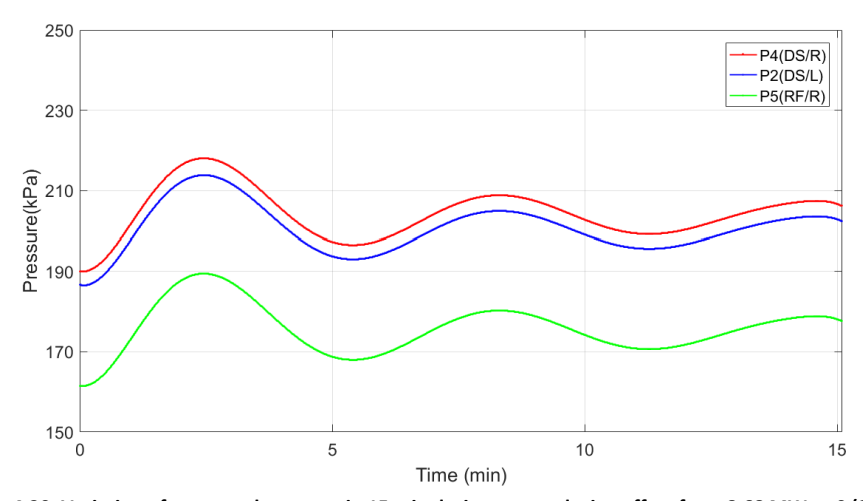


Figure 4.20: Variation of measured pressure in 15 min during stop-reducing effect from 8.68 MW to 0 (2010-12-20 10:16)

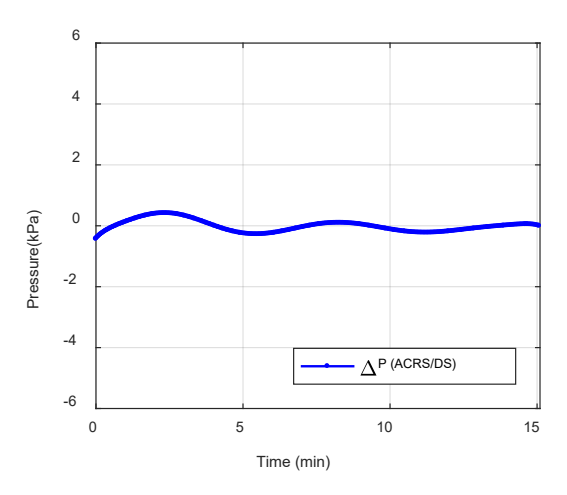


Figure 4.21: Variation of pressure across the central wall in 15 min during stop-reducing effect from 8.68 MW to 0 (2010-12-20 10:16)

Figure 4.22 shows a variation of measured pressure in 15 min during stop-reducing effect from 19.15 MW to 0 (2010-12-20 12:23). It has more pressure fluctuation compared to Figure 4.20. Furthermore, maximum pressure across the central wall is almost four kPa, see Figure 4.23. This must be compared with 1 min measurement which shows almost zero pressure difference.



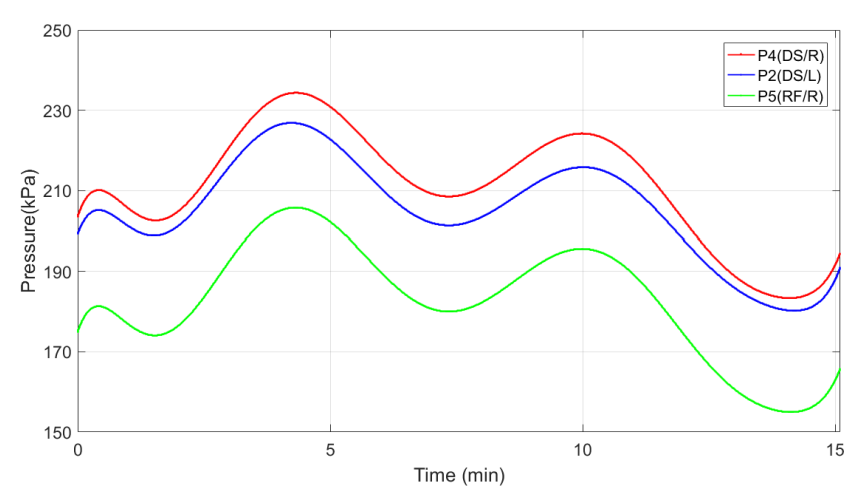


Figure 4.22: Variation of measured pressure in 15 min during stop-reducing effect from 19.15 MW to 0 (2010-12-20 12:23)

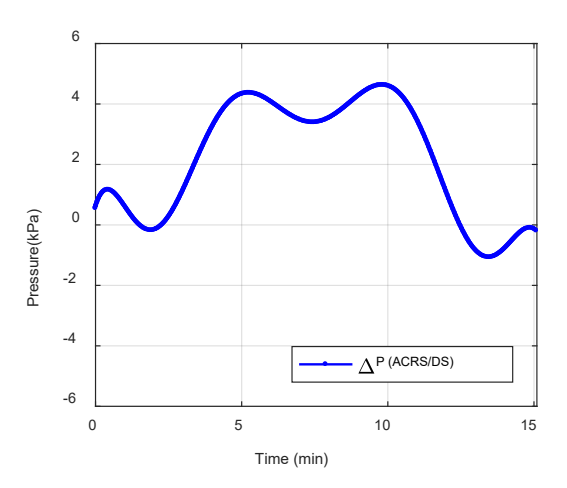


Figure 4.23: Variation of pressure across the central wall in 15 min during stop-reducing effect from 19.15 MW to 0 (2010-12-20 12:23)



5 Strain measurements

In this chapter, the response of the draft tube due to pressure changes induced by the different operational pattern is described. Strain gauges are installed on the draft tubes central wall and roof. The strain has been measured one minute for each hour which means the value of it is considered as a measured strain for each hour.

Furthermore, 15 minutes measurement also has been done for during stop/start and at large fluctuations in operation. In the following, examples of strain measurement corresponding to the operational patterns and pressure measurement are described. **Table 5.1** and **5.2** shows abbreviations that have been used to describe the strain gauges position. See also Figure 2.1 and 2.2 for their position.

Table 5.1: Abbreviations for strain gauges on the right side of the central wall from upstream to downstream (See also Figure 2.1 and 2.2)

Sensor	Location	Abbreviation
H1	Upstream	H1 (US/WL)
Н9	Upstream, after sensor H1	H9 (USb/WL)
H10	Downstream, before sensor H2	H10 (DSb/WL)
H2	Downstream	H2 (DS/WL)

Table 5.2: Abbreviations for strain gauges on the roof /right side of the draft tube

Sensor	Location	Abbreviation
H4	Upstream	H4 (US/RF)
Н6	Upstream, after sensor H4	H6 (USb/RF)
Н8	Downstream, before sensor H9	H8 (DSb/RF)
Н3	Downstream	H3 (DS/RF)
H7	Across the draft tube roof	H7 (ACRS/RF)

Figure 5.1-5.3 illustrates pressure measurements of all ten strain gauges during one year starting from 28 May 2010. The measured strain along the right side of the middle wall in the draft tube is presented in Figure 5.1. Whereas, the measured strain under the roof is presented in Figure 5.2-5.3. It can be seen from these figures that after July the measurement of H1-4 and H6-10 had drifted while H5 was failed from the beginning.

This drift can be because of draining draft tube in July and refilling it. In Figure 5.4, the blue curve shows strain measurement. A best-fit curve with red colour indicates the trend in data. The green curve shows strain measurement after eliminating the trend. Trend removal process has been used for example in signal processing and shock vibration test of concrete to remove rigid body motion of the specimens, see, e.g. Kwan et al. (2002). In Figure 5.5 to 5.7 the corrected strain measurements are shown.



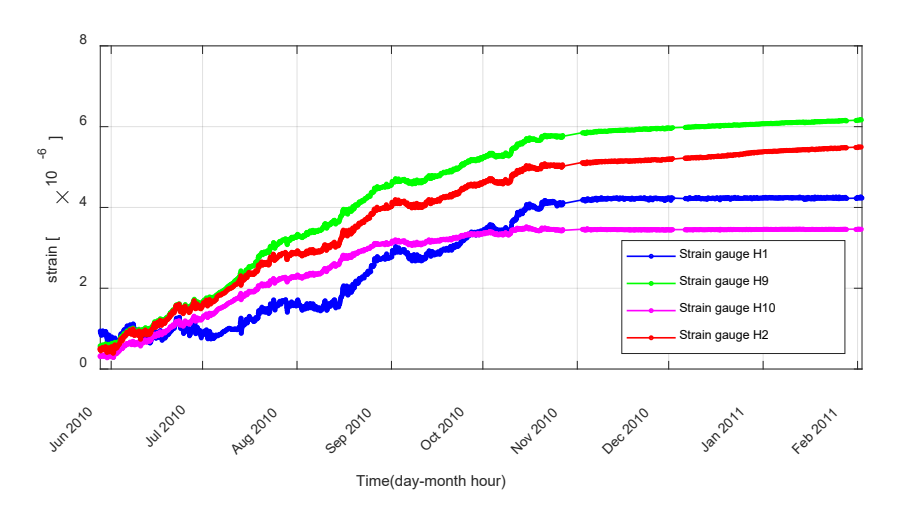


Figure 5.1 Measured strain of H1, H9, H10 and H2 on the right side of the central wall.

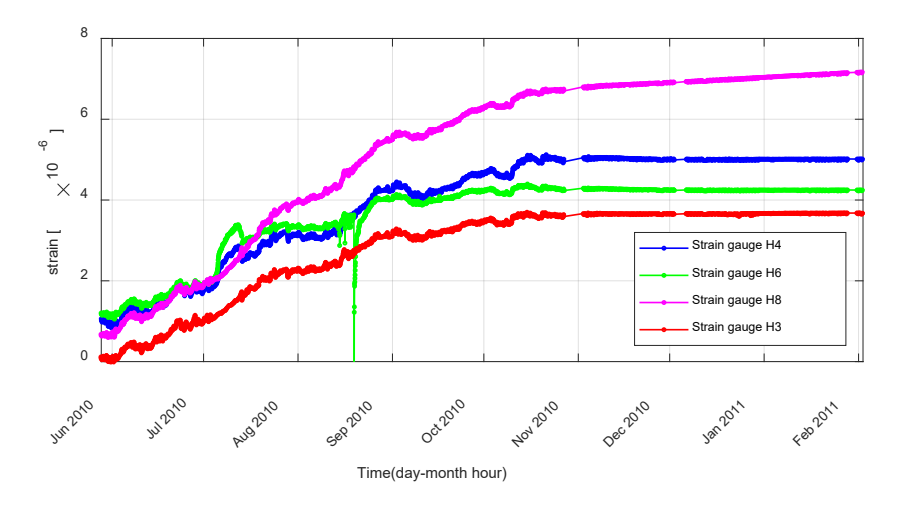


Figure 5.2 Measured strain of H4, H6, H8 and H3 along the roof.



Figure 5.3 Measured strain of H7 and H5, across the roof.



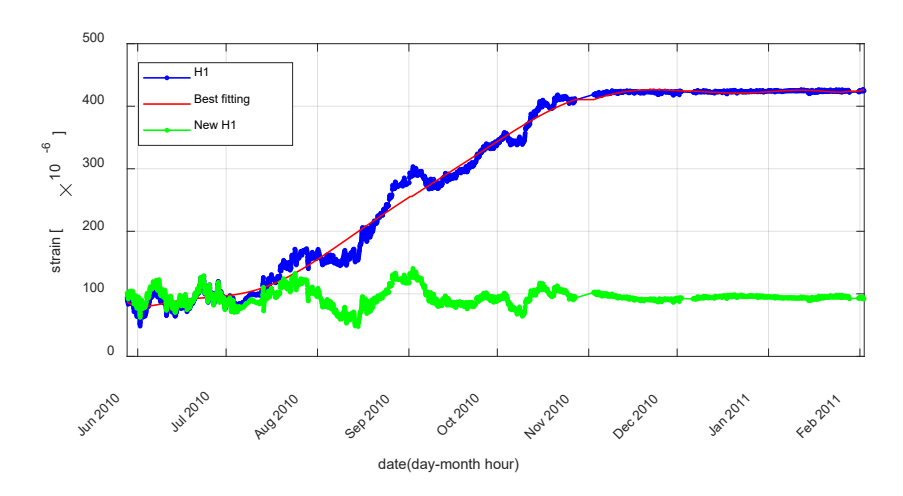


Figure 5.4: Trend removal process from strain measurement

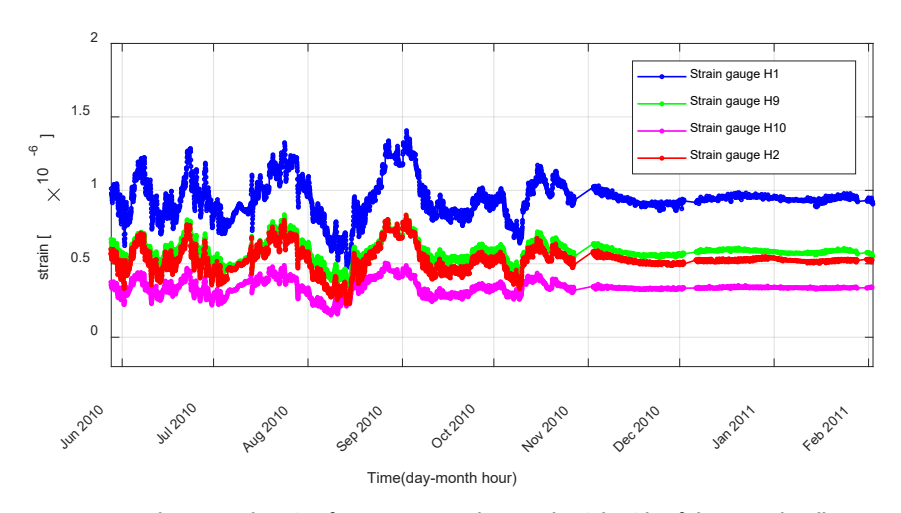


Figure 5.5 Corrected measured strain of H1, H9, H10 and H2 on the right side of the central wall.

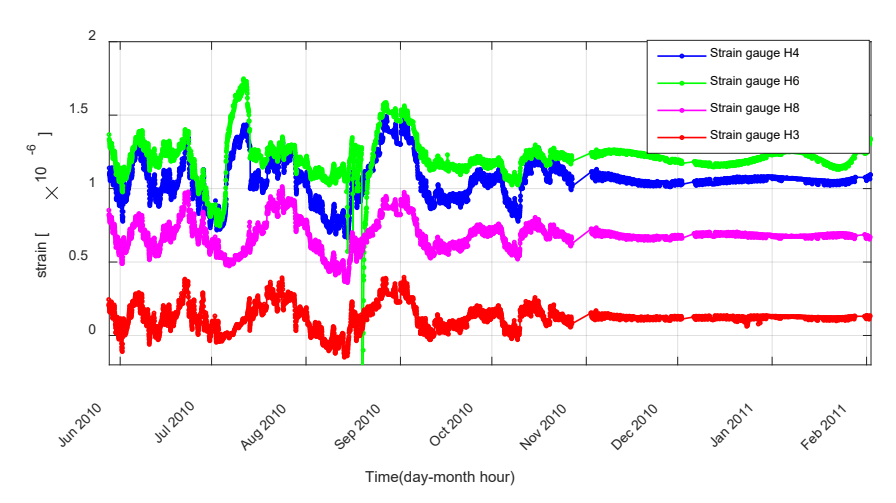


Figure 5.6 Corrected measured strain of H4, H8, H3 and H6 along the roof.



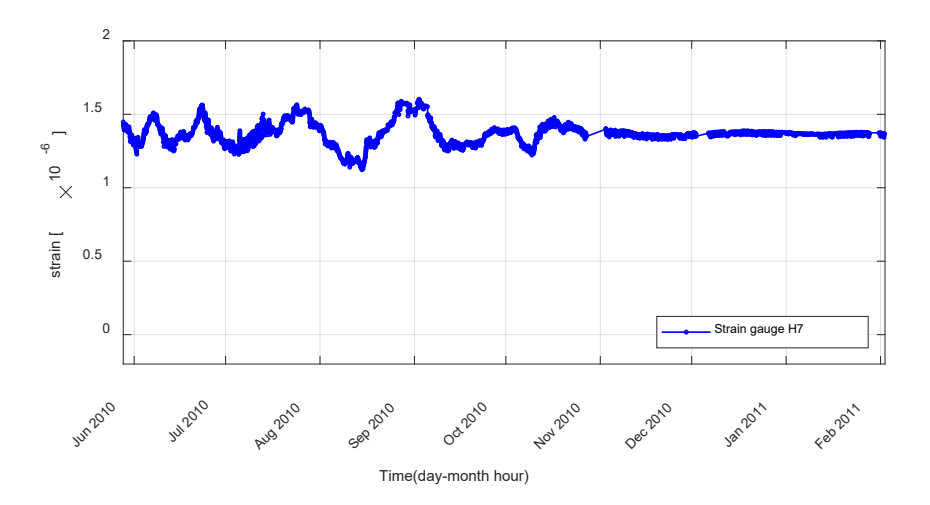
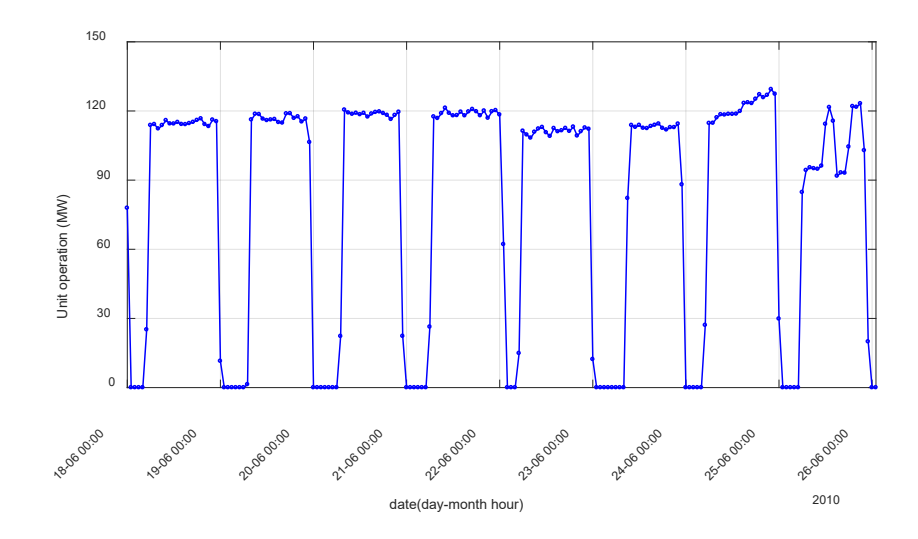


Figure 5.7 Corrected measured strain of H7 without H5, across the roof (see Figure 2.2).

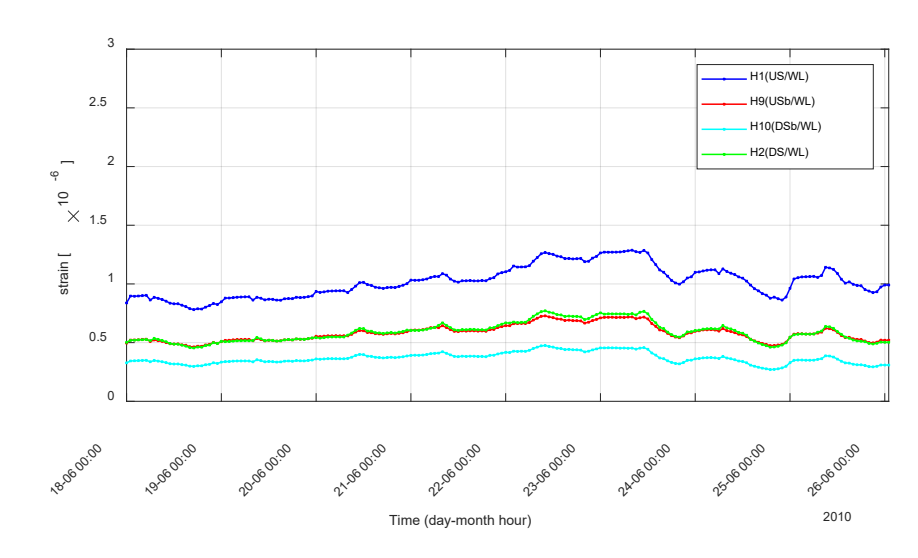
5.1 NORMAL OPERATION

In this section, the strain measurement for normal operation by producing the power of about 110 MW during daytime is described. Figure 5.8 illustrates a variation of measured strain on the wall and roof for one week. Comparison between two figures indicates that the general strain level under the roof is higher than the strain on the wall. The maximum strain on the wall is about 94.55e-6 for sensor H1 at the upstream side of the draft tube, and maximum strain on the roof is about 105.22e-6 for sensor H7 across the draft tube.





(b)



(c)



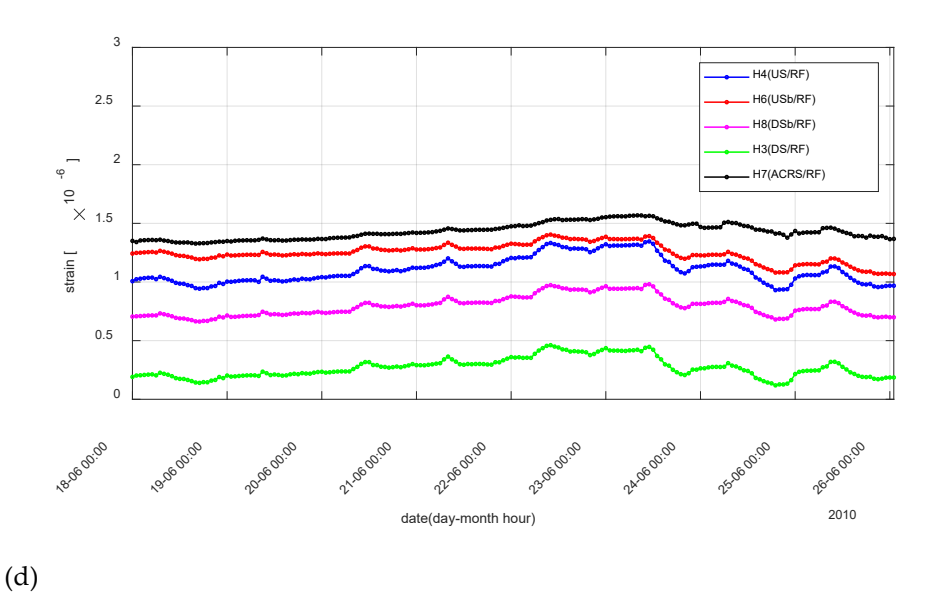
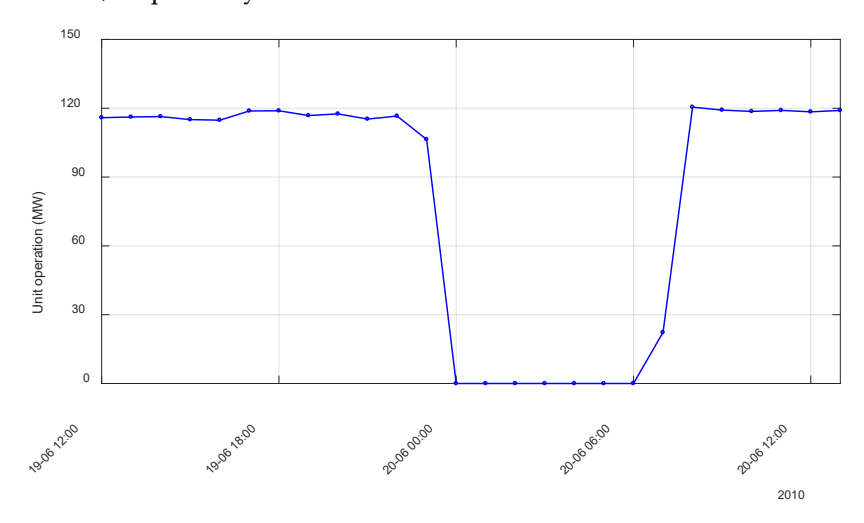


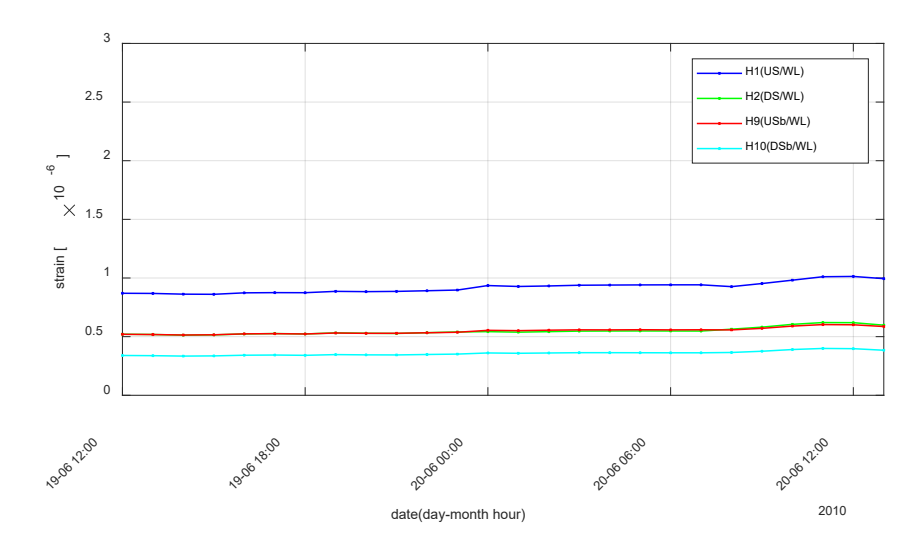
Figure 5.8: Normal operation with producing the power of about 110 MW (a) for one week measured pressures (b) and measured strains on the wall (c) and the roof (d).

Figures above also show drifts in strain measurement during start and stop events. To see these changes, a variation of measured strain on the wall and roof is studied for 24 hours, see Figures 5.9. As seen from these figures, the fluctuations in pressure from changing operation have almost no impact on the strains and no obvious correlation to either pressure or operation. The average measured strain on the wall and roof during daytime and nighttime has been summarized in Tables 5.3 and 5.4, respectively.

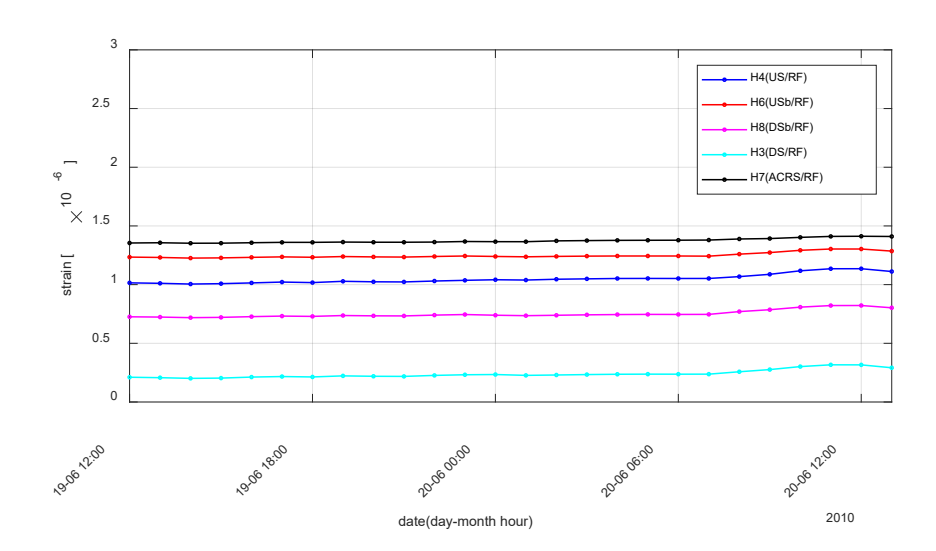


(a)





(b)



(c)

Figure 5.9: Variation of measured strain on (a) the wall and (b) roof in 24 hours for normal operation with producing the power of about 120 MW.

Table 5.3: Average measured strain on the wall during daytime and nighttime for normal operation (µstrain)

	H1 (US/WL)	H9 (USb/WL)	H10 (DSb/WL)	H2 (DS/WL)
0 MW (night time)	0.9418	0.5586	0.3994	0.5477
120 MW (daytime)	1.013	0.6028	0.365	0.6192
120 MW to 0 MW	0.0712	0.0442	0.0344	0.0715



Table 5.4: Average measured strain on the roof during daytime and nighttime for normal operation (μstrain)

	H4 (US/RF)	H6 (USb/RF)	H8 (DSb/RF)	H3 (DS/RF)	H7 (ACRS/RF)
0 MW (night time)	1.052	1.242	0.7464	0.2369	1.38
120 MW (daytime)	1.135	1.303	0.8215	0.3167	1.412
120 MW to 0 MW	0.083	0.061	0.0751	0.0798	0.032

Figures 5.10-5.12 show a correlation between pressure and strain measurement on the roof, central wall and across the wall, respectively. Correlation has been shown for the closest strain sensor to the pressure gages.

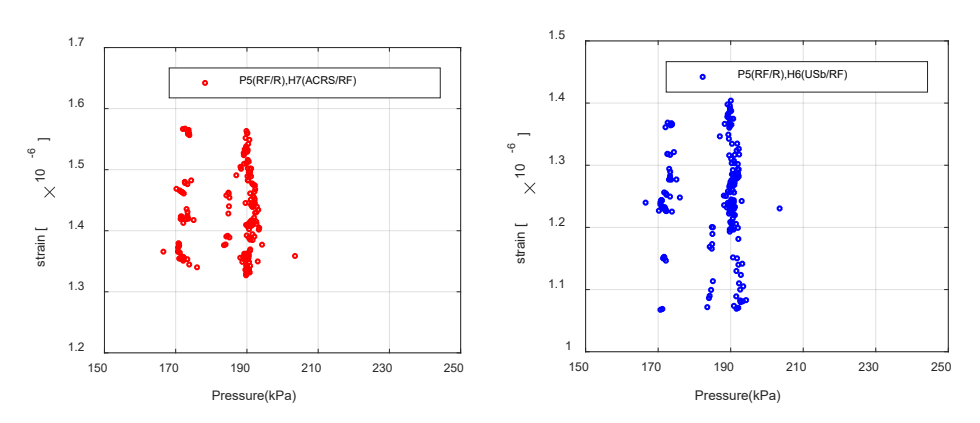


Figure 5.10: Correlation between pressure and strain measurement on the roof for normal operation with production of 110 MW in a week. Y-axis scale is 0.5 µstrain.

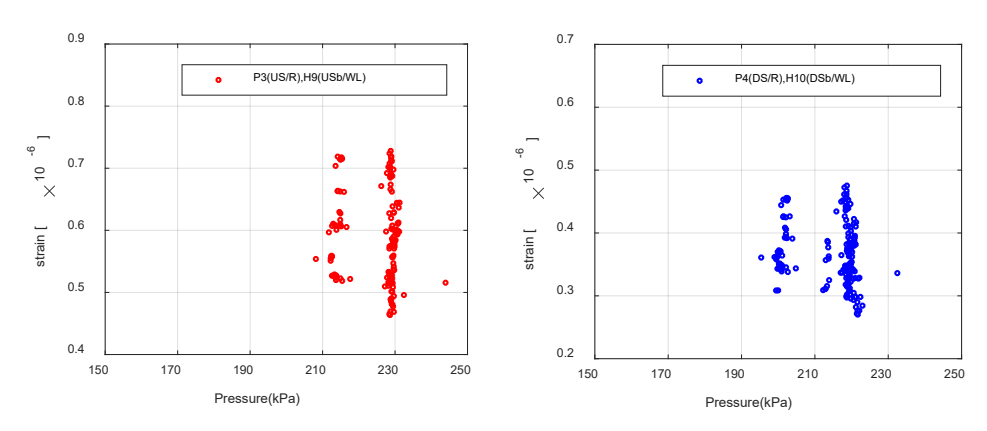


Figure 5.11: Correlation between pressure and strain measurement on the wall for normal operation with production of 110 MW in a week. Y-axis scale is 0.5 µstrain.



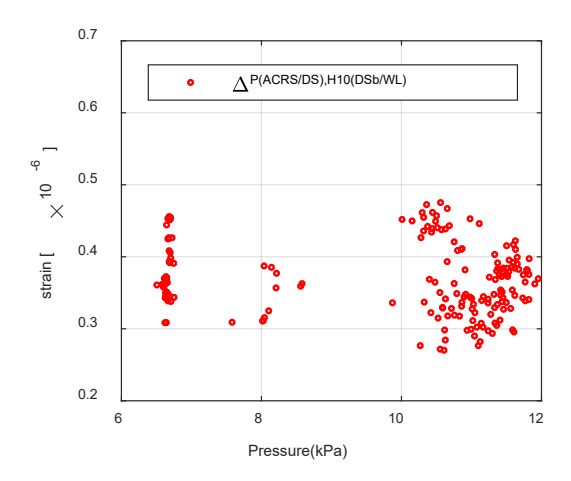


Figure 5.12: Correlation between pressure across the central wall and strain measurement on the wall for normal operation with production of 110 MW in a week. Y-axis scale is 0.5 µstrain.

15 min measurement during the stop the unit, reducing effect from 75 MW to 0, at time 22:51 has been shown in Figures 5.13 and 5.14 for wall and roof, respectively. As seen from the figures, apart from sensor H7 (ACRS/RF), all sensors have small descending behaviour. This measurement is compared with 1 min reading at time 23:00, see Tables 5.5-5.6. Comparison between 15 min readings and 1 min readings indicates that after almost 10 min of reading the strain values convergence to the values from 1 min reading at time 23:00.

Table 5.5: Average measured strain on the wall at time 22.00 and 23:00 from 1 min reading (µstrain)

	H1 (US/WL)	H9 (USb/WL)	H10 (DSb/WL)	H2 (DS/WL)
75 MW (22:00)	0.9388	0.1987	0.3387	0.5291
0 MW (23:00)	0.9627	0.1915	0.34	0.5256

Table 5.6: Average measured strain on the roof at time 22.00 and 23:00 from 1 min reading (μ strain)

	H4 (US/RF)	H6 (USb/RF)	H8 (DSb/RF)	H3 (DS/RF)	H7 (ACRS/RF)
75 MW (22:00)	1.051	1.17	0.6942	0.5156	1.375
0 MW (23:00)	1.03	1.16	0.682	0.5211	1.366



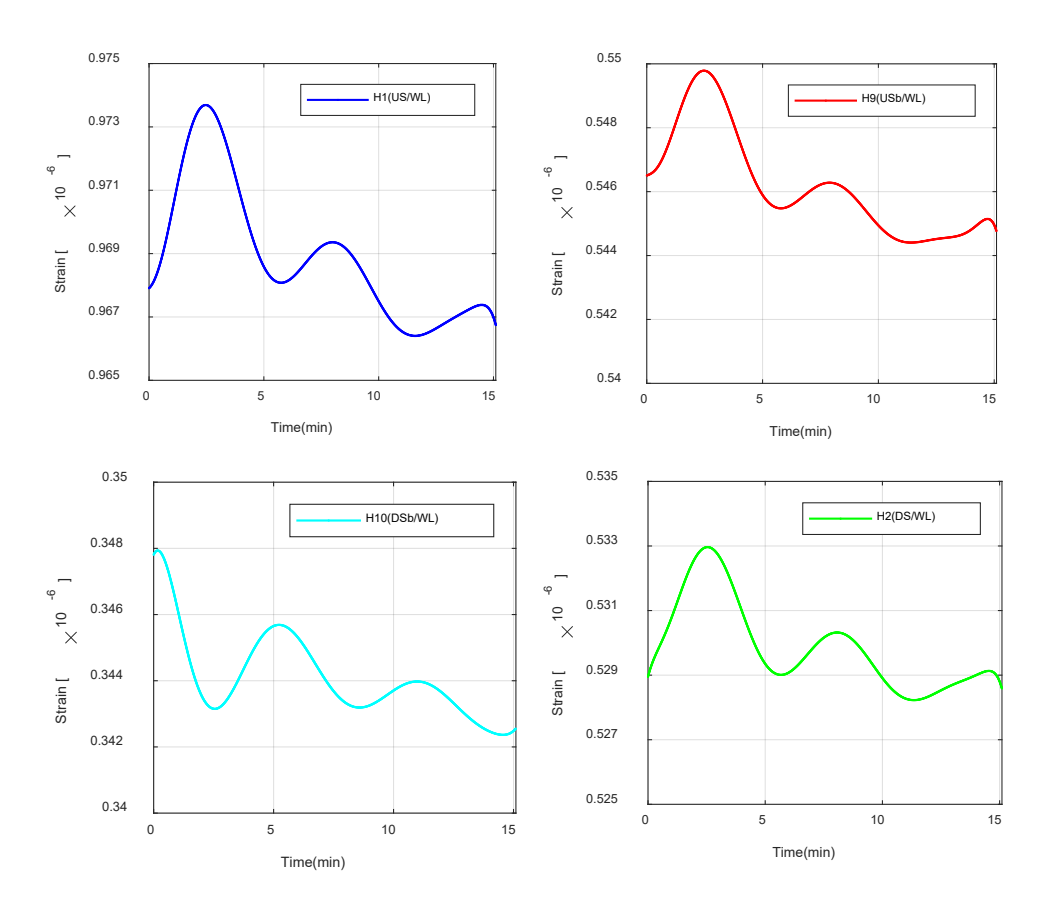


Figure 5.13: Variation of measured strain on the wall in 15 min for normal operation during stop- reducing effect from 75 MW to 0 (2011-01-19 22:51). Y-axis scale is $0.01 \, \mu strain$.



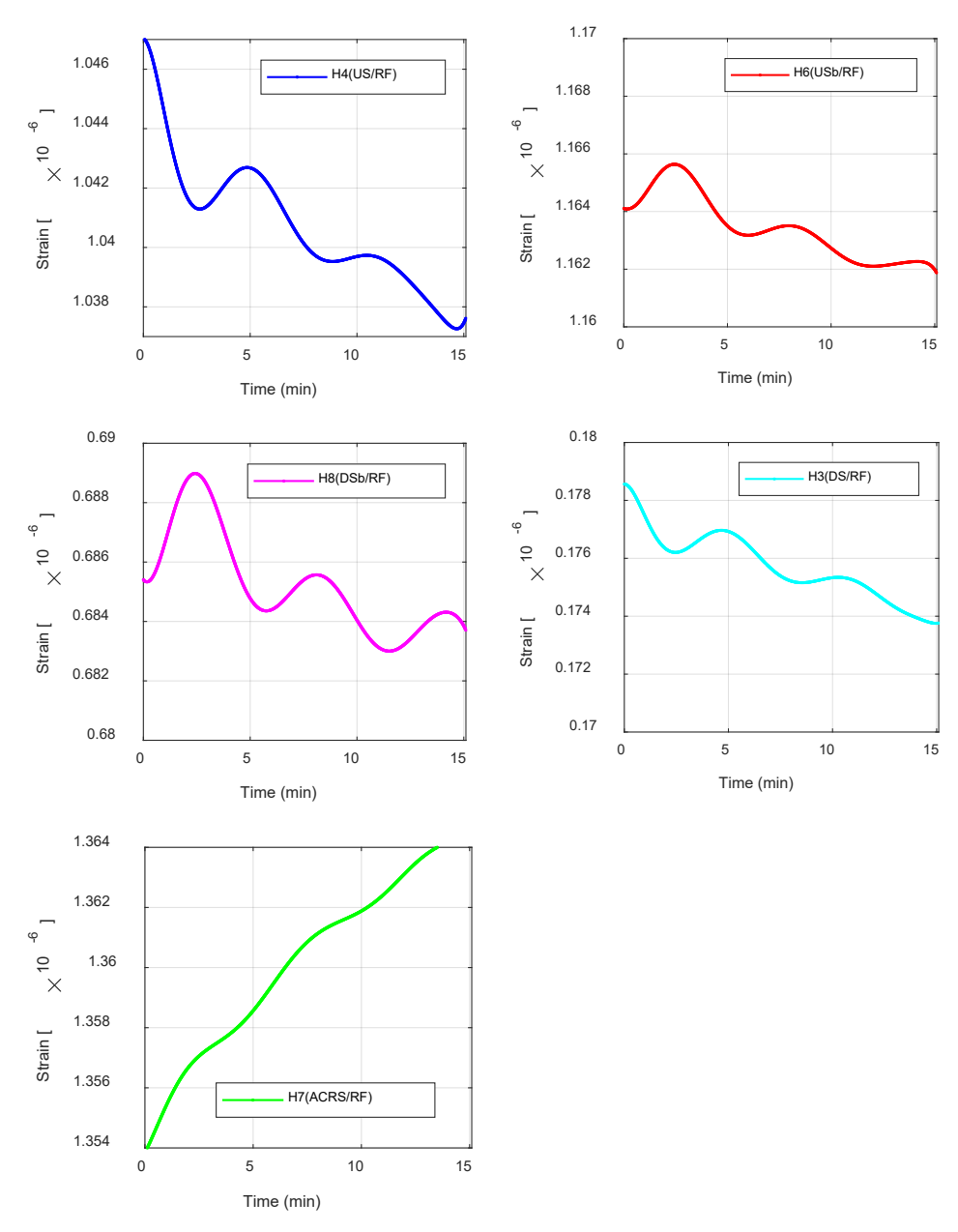


Figure 5.14: Variation of measured strain on the roof in 15 min for normal operation during stop- reducing effect from 75 MW to 0 (2011-01-19 22:51). Y-axis scale is $0.03 \mu strain$.

Figures 5.15-16 shows a variation of measured strain in 15 min for normal operation during start- increasing effect from 25 MW to 110 MW (2011-01-20 06:49) on the wall and roof, respectively. It is seen from figures that except sensor H1 (US/WL) and H9 (DS/RF), all sensors have a small ascending behaviour. All sensors convergence to the value of strain measurement from 1 min readings at time 07:00 when there are 110 MW operations, see **Tables 5.7-5.8**.



Table 5.7: Average measured strain on the wall at time 06.00 and 07:00 from 1 min reading (μstrain).

	H1 (US/WL)	H9 (USb/WL)	H10 (DSb/WL)	H2 (DS/WL)
25 MW (06:00)	0.9464	0.1786	0.3369	0.5158
110 MW (07:00)	0.9383	0.1985	0.3405	0.5306

Table 5.8: Average measured strain on the roof at time 06.00 and 07:00 from 1 min reading (µstrain).

	H4 (US/RF)	H6 (USb/RF)	H8 (DSb/RF)	H3 (DS/RF)	H7 (ACRS/RF)
25 MW (06:00)	1.022	1.147	0.6701	0.5155	1.353
110 MW (07:00)	1.05	1.167	0.6936	0.5164	1.374

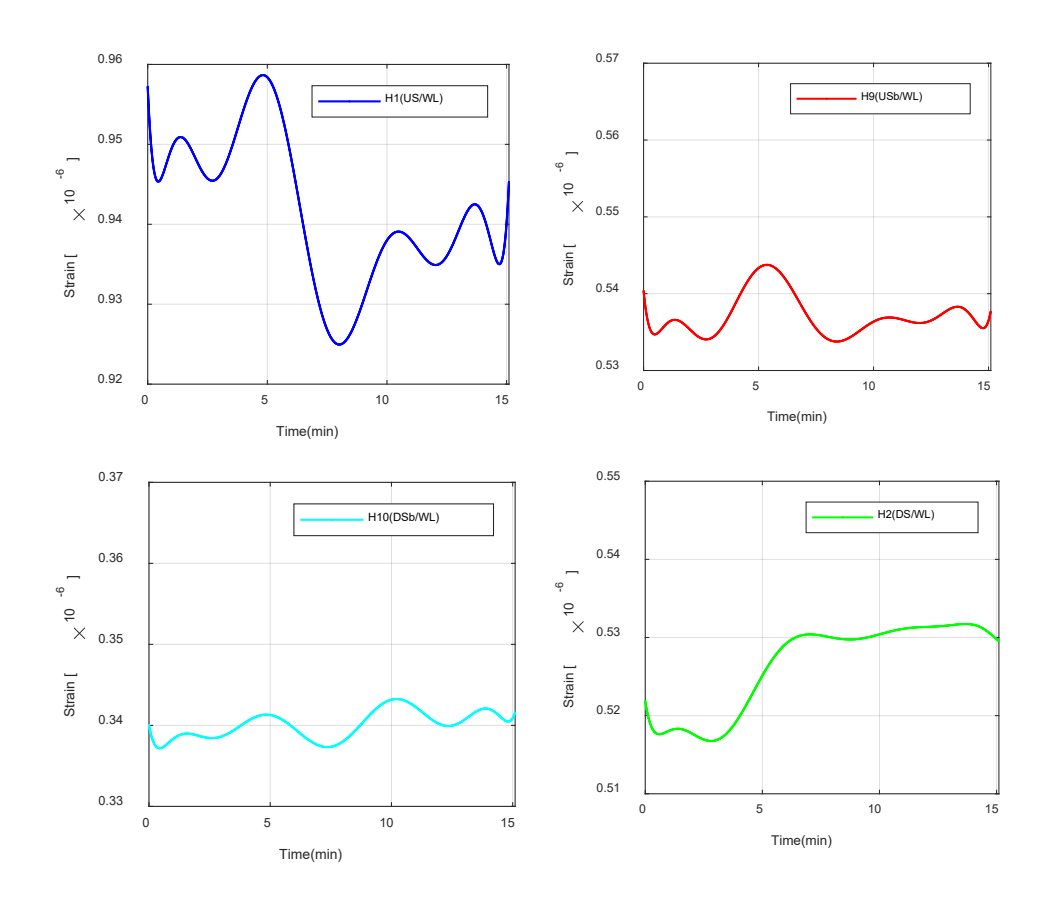


Figure 5.15: Variation of measured strain on the wall in 15 min for normal operation during start- increasing effect from 25 MW to 110 MW (2011-01-20 06:49). Y-axis scale is 0.04 µstrain.



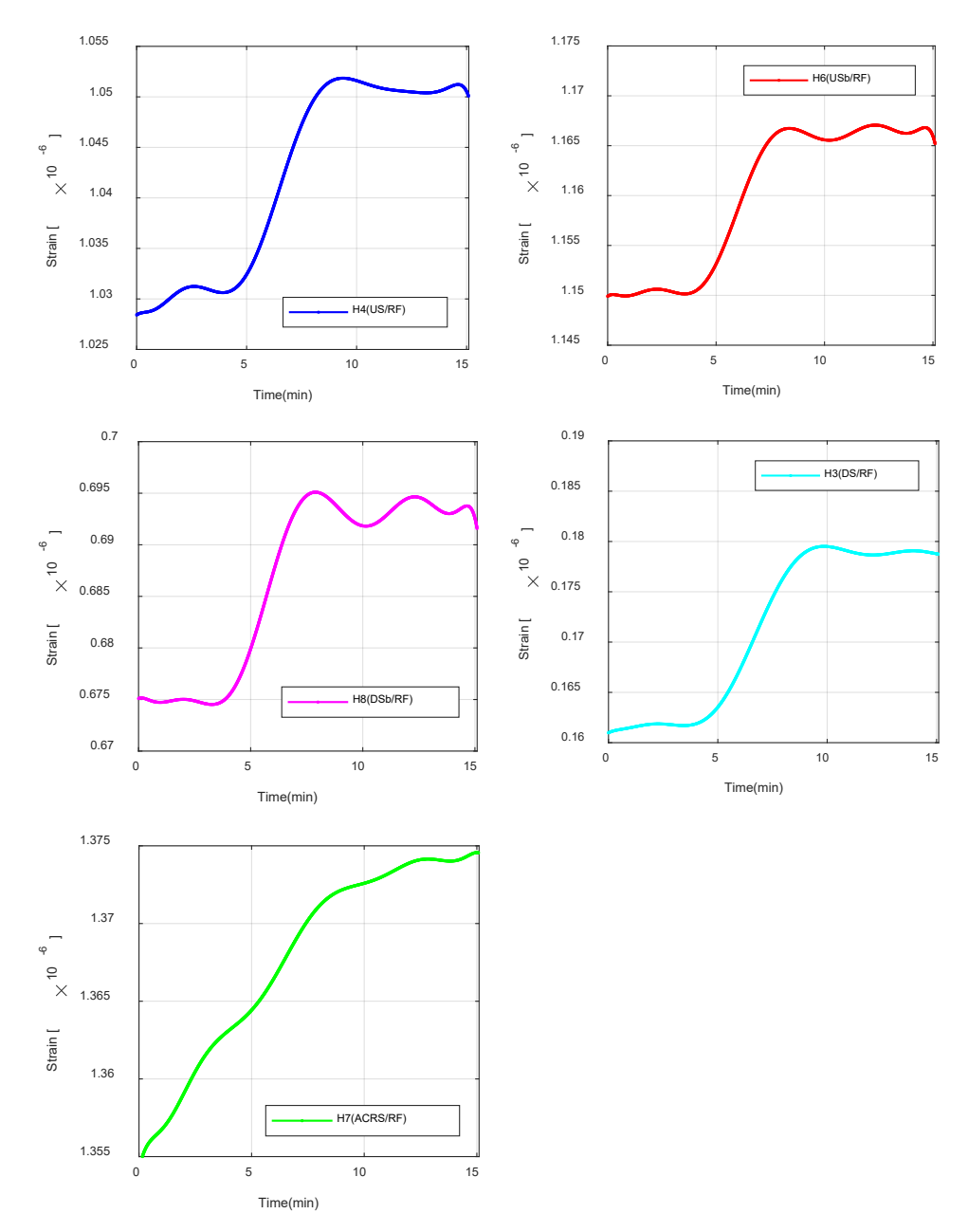


Figure 5.16: Variation of measured strain on the roof in 15 min for normal operation during start- increasing effect from 25 MW to 110 MW (2011-01-20 06:49). Y-axis scale is 0.03 µstrain.

5.2 CONTINUOUS OPERATION WITH NO STOP

In this section strain measurement for continuous operation by producing power between 38-105 MW is described. Figure 5.17 shows a variation of measured strain during one week on the central wall and roof, respectively. A comparison between two figures indicates that the measured strain on the roof is higher than on the wall. The maximum strain on the wall is for sensor H1 at the upstream side of the wall and for the roof is for sensor H7 at across the roof with values of almost 95e-6 and 138e-6, respectively.



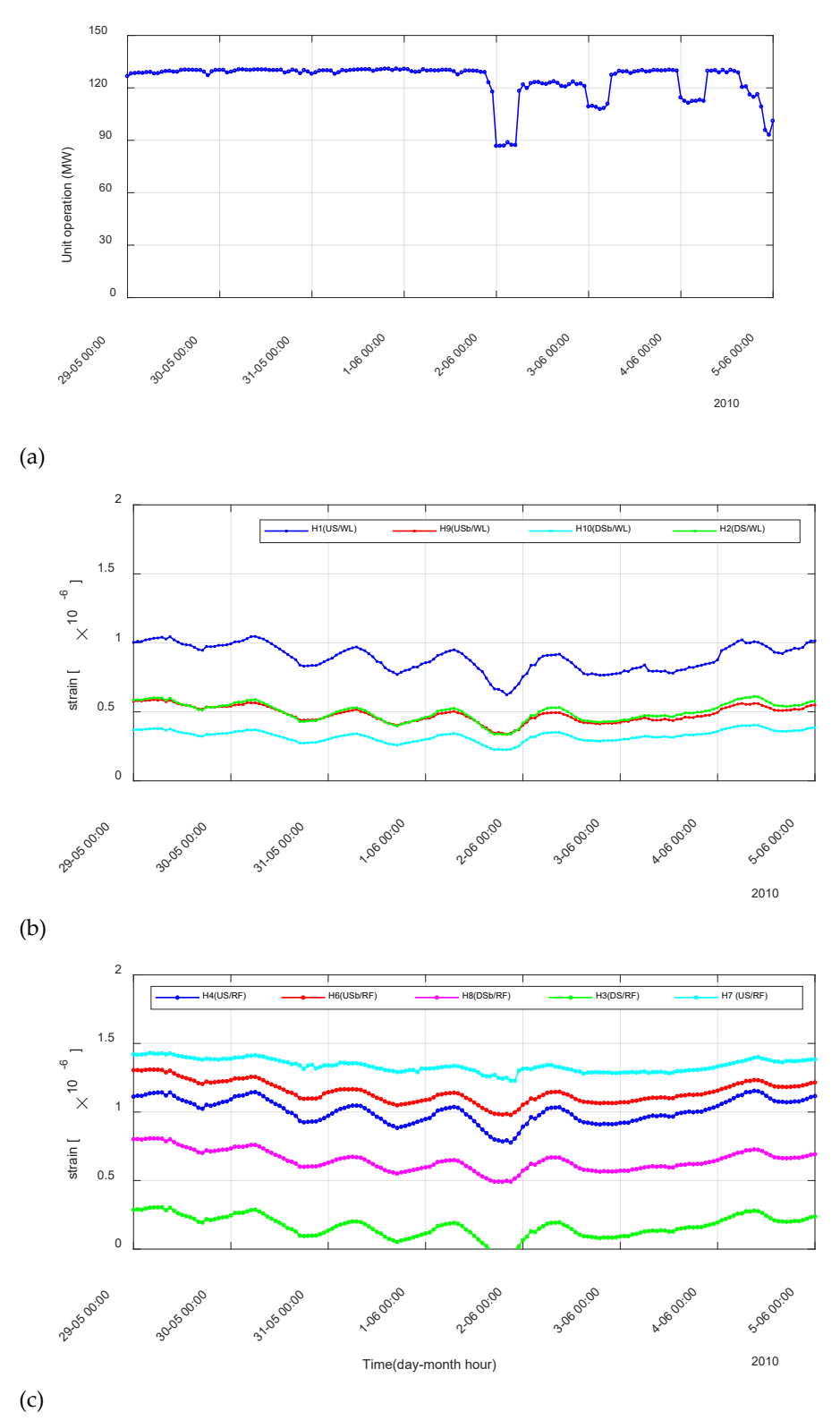


Figure 5.17: Continuous operation with producing the power between 85-130 MW (a) for one week and measured strain on (b) the wall and (c) the roof.

Figures 5.18-5.19 show the variation of strain in 24 hours during power fluctuation between 85-130 MW on the central wall and roof, respectively. As seen from these



figures except for sensors H1 (US/WL), H10 (DSb/WL) and H9 ((DS/RF) with decreasing effect, the strain is decreased. This decreasing for the sensors on the roof is higher than the sensors on the central wall which is about (0.5-1) $\times 10^{-6}$.

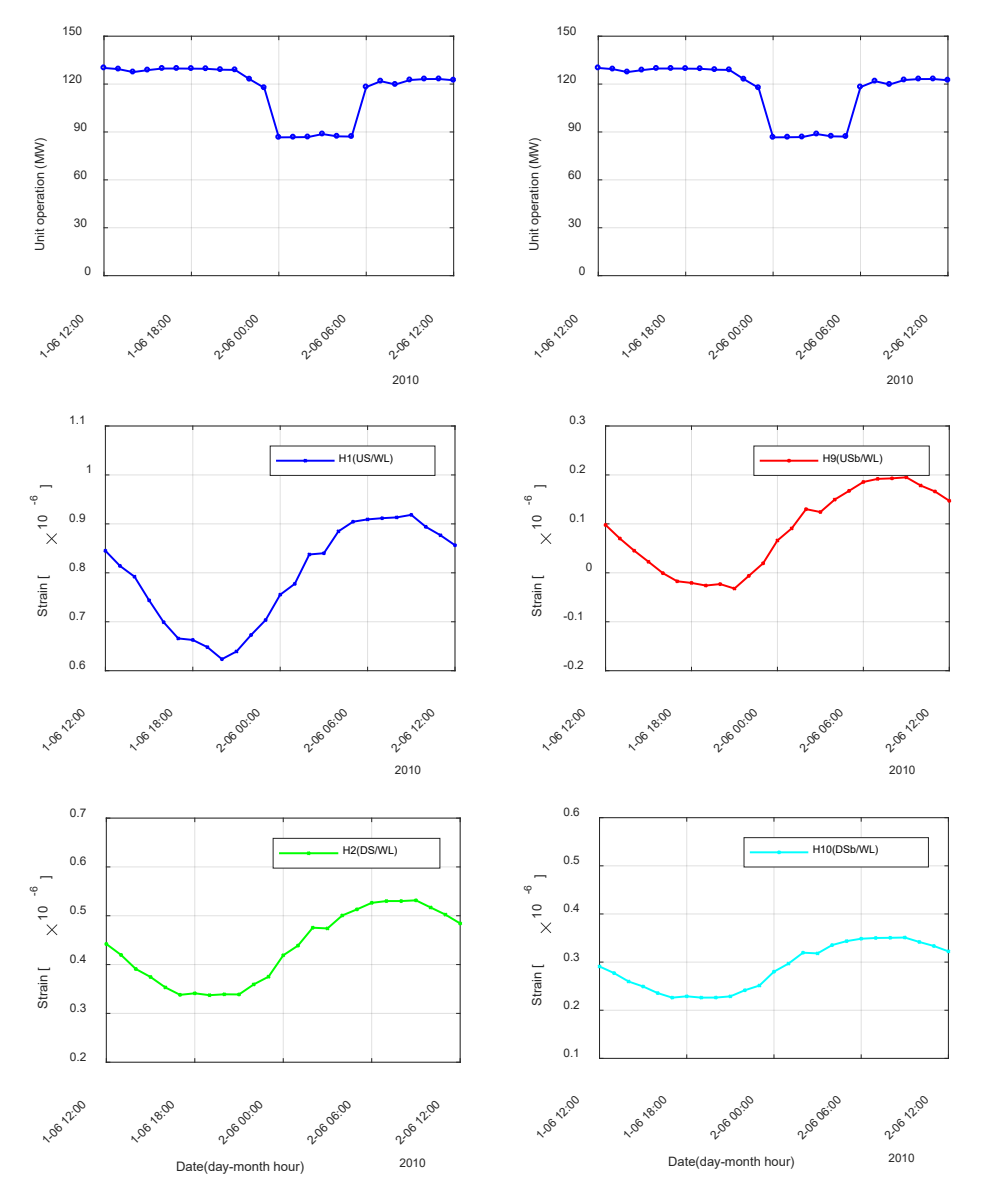


Figure 5.18: Variation of measured strain on the wall in 24 hours for continuous operation with producing power between 85-130 MW. Y-axis scale is $0.05 \mu strain$.



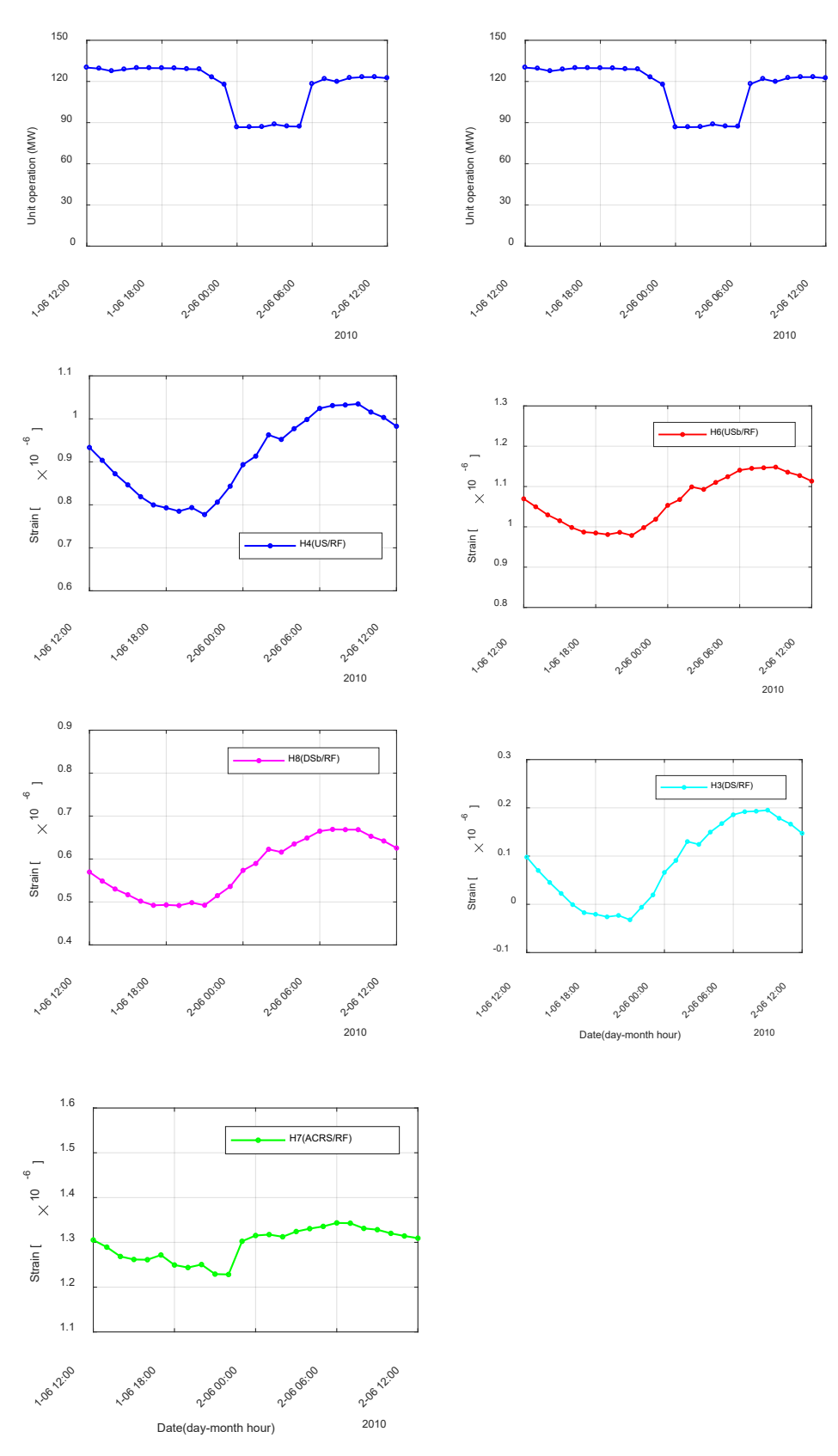


Figure 5.19: Variation of measured strain on the roof in 24 hours for continuous operation with producing power between 85-130 MW. Y-axis scale is $0.05 \mu strain$.



Tables 5.9-5.10 summarize average strain measurement during continuous operation of 105 and 90 MW and fluctuation of 60 and 38 MW for the sensors on the wall and roof, respectively.

Table 5.9: average measured strain on the wall for continuous operation (µstrain).

	H1	Н9	H10	H2
	(US/WL)	(USb/WL)	(DSb/WL)	(DS/WL)
130 MW	0.6629	-0.21	0.2289	0.341
0 MW	0.755	0.066	0.280	0.419
120 MW	0.9133	0.193	0.351	0.530

Table 5.10: Average measured strain on the roof for continuous operation (μstrain).

	H4 (US/RF)	H6 (USb/RF)	H8 (DSb/RF)	H3 (DS/RF)	H7 (ACRS/RF)
130 MW	80.0	98.5	49.3	-2.1	124.9
0 MW	90.0	105.3	57.4	6.6	131.5
120 MW	103.1	114.7	66.8	19.2	133.1

In the following figures the correlation between pressure and strain measurements is shown. For this, the closest strain sensor to pressure gauges has been considered. Figure 5.20 shows the pressure vs. strain measurement on the roof. Figure 5.21 shows the pressure vs. strain measurement on the wall. Figure 5.22 shows pressure across the central wall vs. strain measurement on the wall for continuous operation.

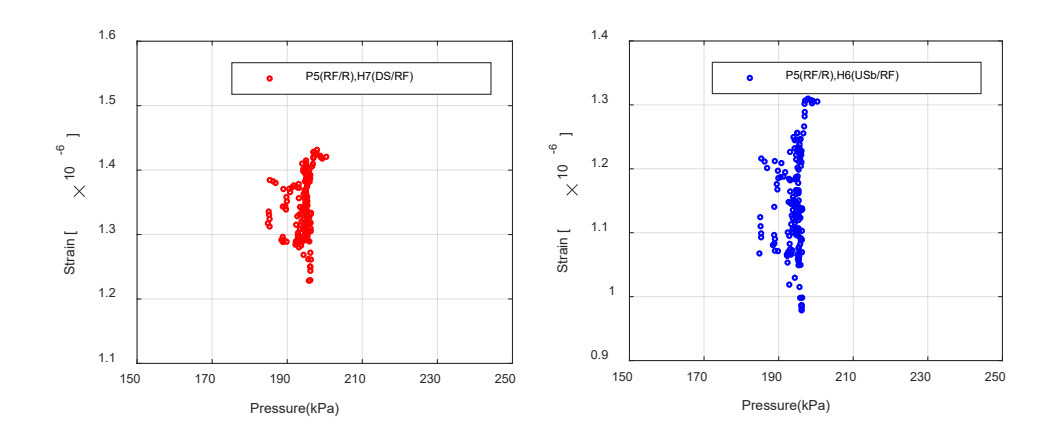


Figure 5.20: Correlation between pressure and strain measurement on the roof for continuous operation by producing power between 38-105 MW in a week



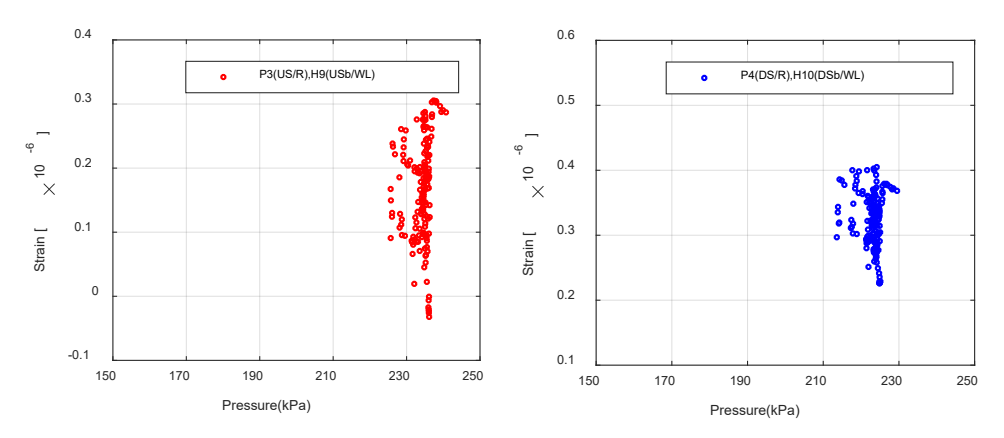


Figure 5.21: Correlation between pressure and strain measurement on the wall for continuous operation by producing power between 38-105 MW in a week

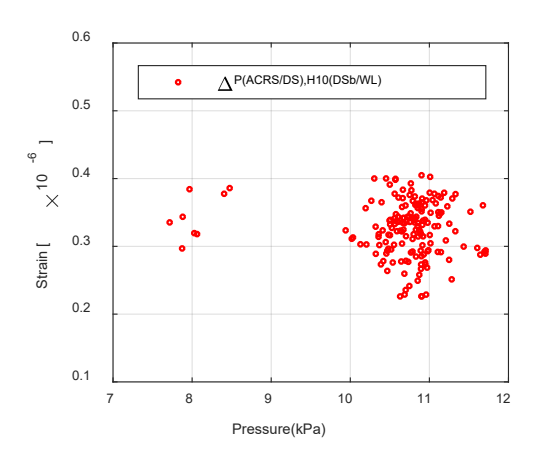
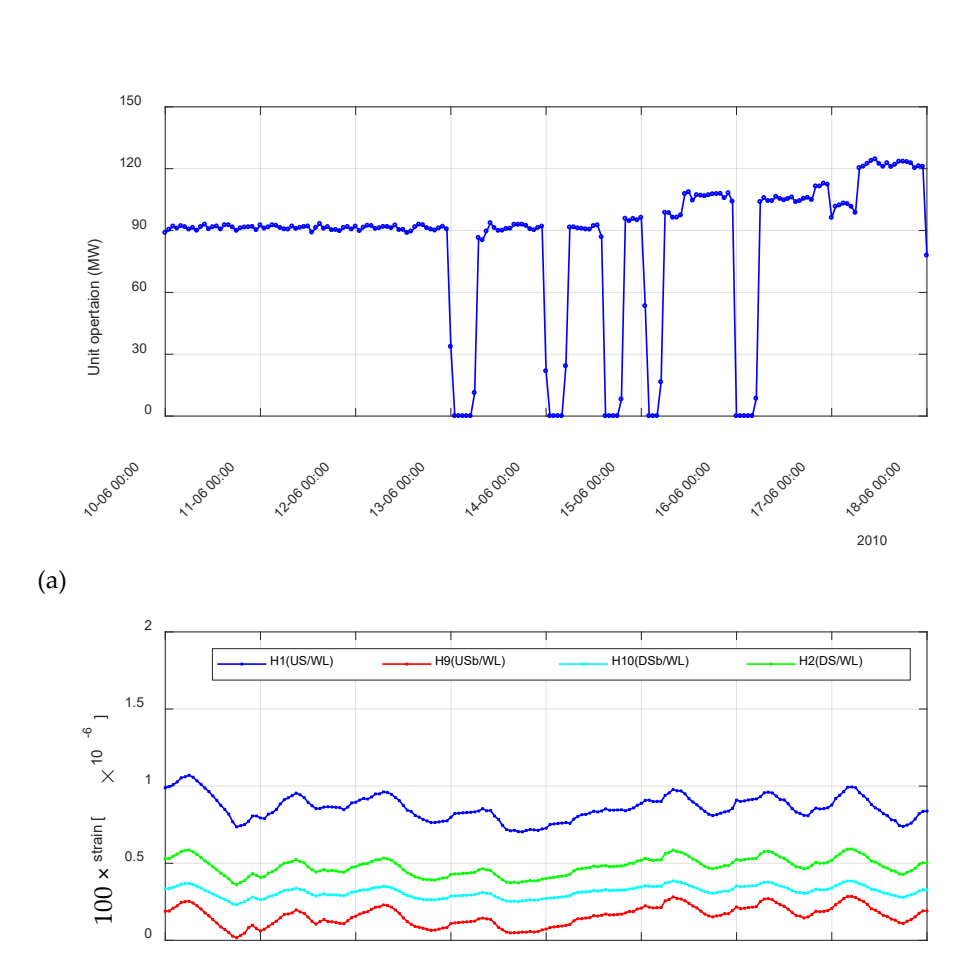


Figure 5.22: Correlation between pressure across the central wall and strain measurement on the wall for continuous operation by producing power between 38-105 MW in a week

5.3 START AND STOP EVENTS

This section describes the variation of strain on the central wall and roof of the straight diffuser during a sequence of start and stops in the daytime. Figure 5.23 illustrates a variation of measured strain on the wall and roof in a week, respectively. As seen from these figures strain on the roof is higher than the central wall. The sequence of start and stop in daytime is seen on 20th of December which in the following is described.





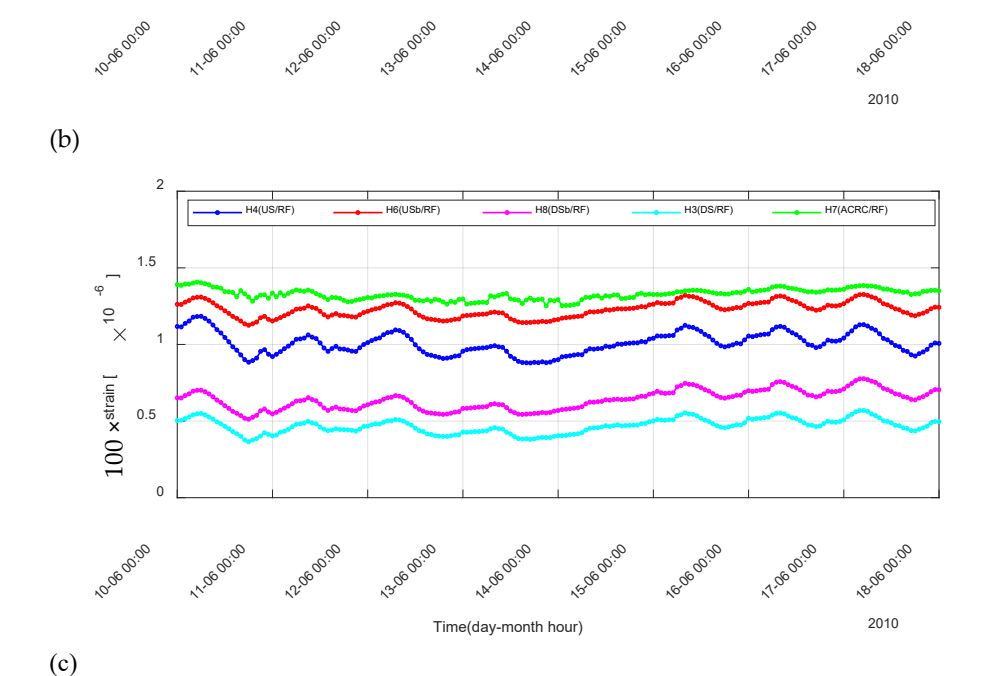


Figure 5.23: Normal and quick start and stops (a) operation for one week and measured strain on (b) the wall and (c) the roof.



Figures 5.24 and 5.25 show variations of strain measurement during a sequence of start and stops on central wall and roof, respectively. Three start/stop events are observed in 12 hours in the morning and afternoon. As seen from these figures for the second start/stop, except sensors H1 (US/WL), H3 (USb/WL) and H7 (ACRS/RF) variation of strain on this time interval are insignificant. While, for all sensors, strain corresponding to the zero MW operation is higher than, other strain measurement corresponding to zero MW operation. This shows the effect of fast stop/start. Table 5.11 and 5.12 summarize measured strain during this time interval for sensors on the central wall and roof, respectively. It should be noted that strain measurement for this time is higher than strain during normal operation of 110 MW, see Tables, 5.3-5.4.

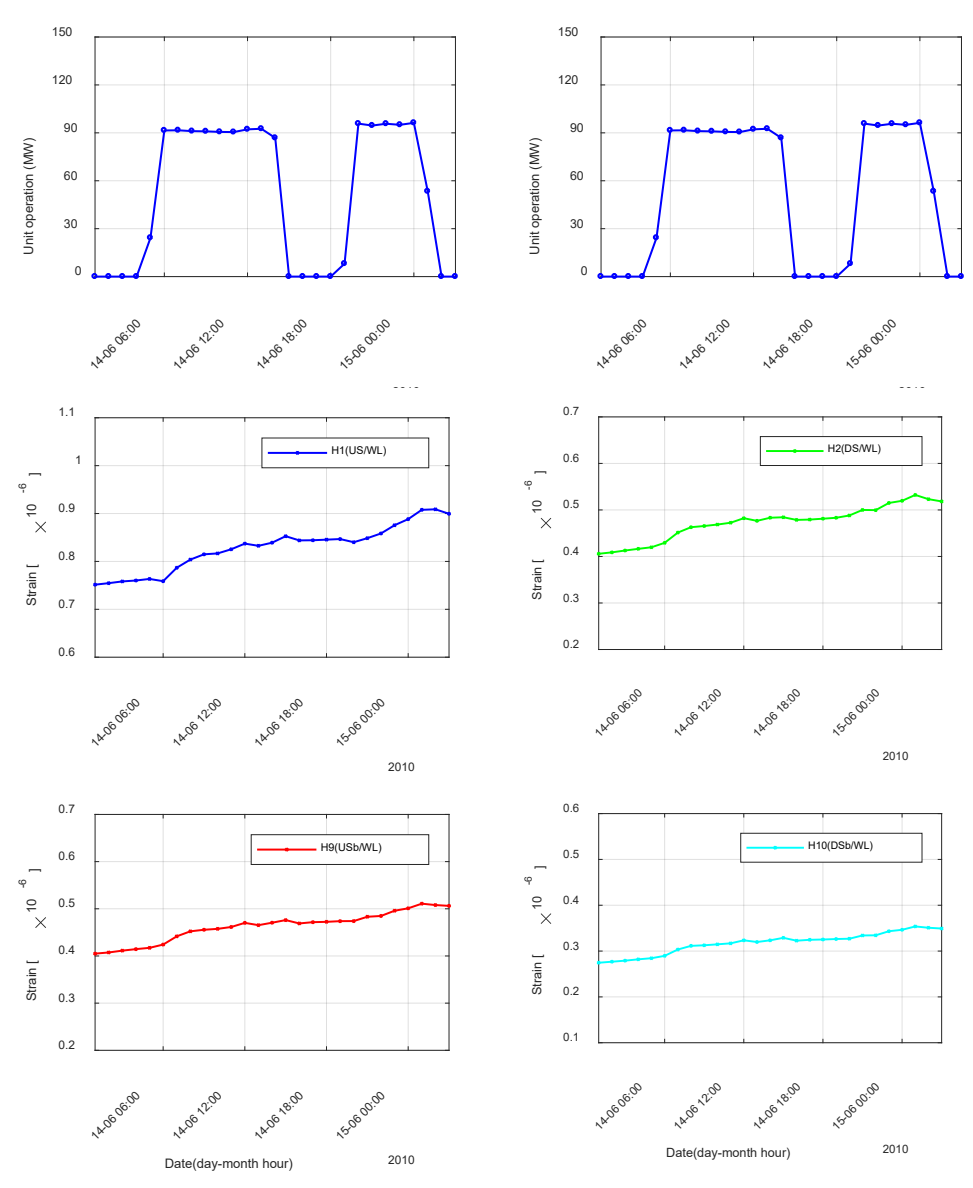


Figure 5.24: Variation of measured strain on the wall in 24 hours for normal and quick start and stops



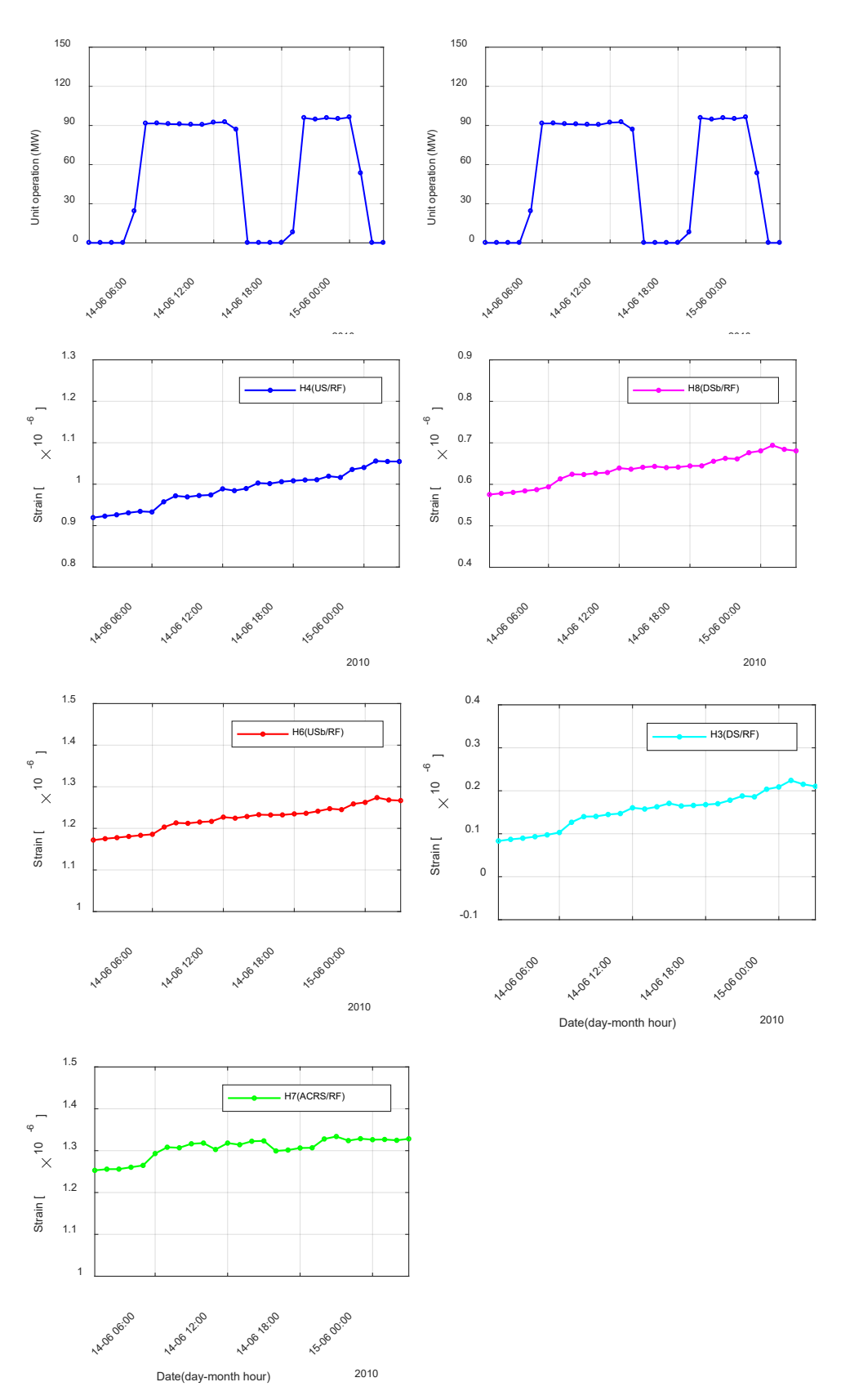


Figure 5.25: Variation of measured strain on the roof in 24 hours for normal and quick start and stops



Table 5.11: average measured strain on the wall from 1 min reading (µstrain).

	H1 (US/WL)	H9 (USb/WL)	H10 (DSb/WL)	H2 (DS/WL)
19.15 MW (12:00)	0.9651	0.1885	0.3439	0.5251
0 MW (13:00)	0.9698	0.1945	0.3447	0.5276

Table 5.12: average measured strain on the roof from 1 min reading (μstrain).

	H4 (US/RF)	H6 (USb/RF)	H8 (DSb/RF)	H3 (DS/RF)	H7 (ACRS/RF)
19.15 MW (12:00)	1.053	1.165	0.6841	0.5247	1.368
0 MW (13:00)	1.056	1.168	0.6873	0.5246	1.38

In the following strain measurement in 15 min while stopping the unit from 8.68 MW and 19.15 MW is shown. It should be noted that strain measurement during the starting unit is not shown due to insignificant variation in strain measurement. Strain measurement indicates lower values compared to the measured value at 10:00 from 1 min readings, see Tables 5.11-12. Furthermore, a variation of strain during 15 min reading for sensors H3, H2, H6, H8 and H9 is insignificant.

Figures 5.26-5.27 show variation of measured strain in 15 min during stop-reducing effect from 19.15 MW to 0 (2010-12-20 12:23) for central wall and roof, respectively. Strain measurements indicate peaks that significantly are higher than the measured value from 1 min reading at time 12:00, see Tables 5.11-12. Compared to Figure 5.29-30, strain measurement during stop-reducing effect from 8.68 MW to 0, Variation of strain significantly is high. This can be due to fast stopping the unit. It should be noted that pressure and strain measurement from time 12:00 to 13:00 was increased while the operation was reducing from 19.15 MW to zero.



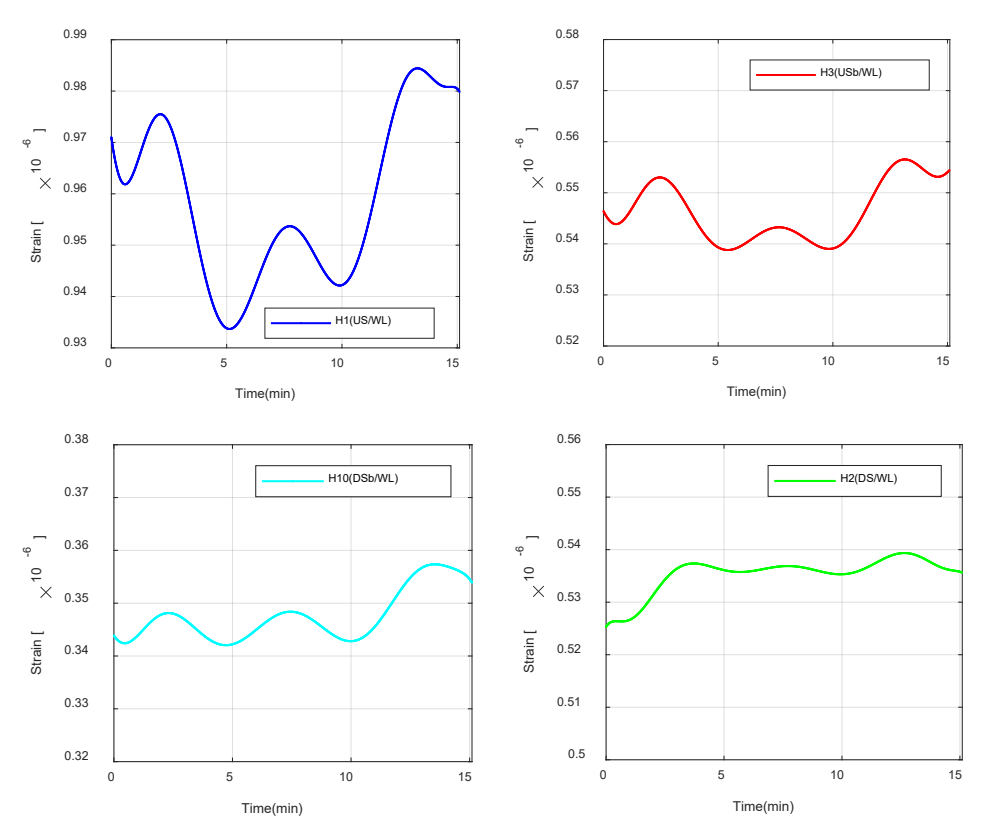


Figure 5.26: Variation of measured strain on the wall in 15 min during stop- reducing effect from 19.15 MW to 0 (2010-12-20 12:23). Y-axis scale is $0.025~\mu strain$.



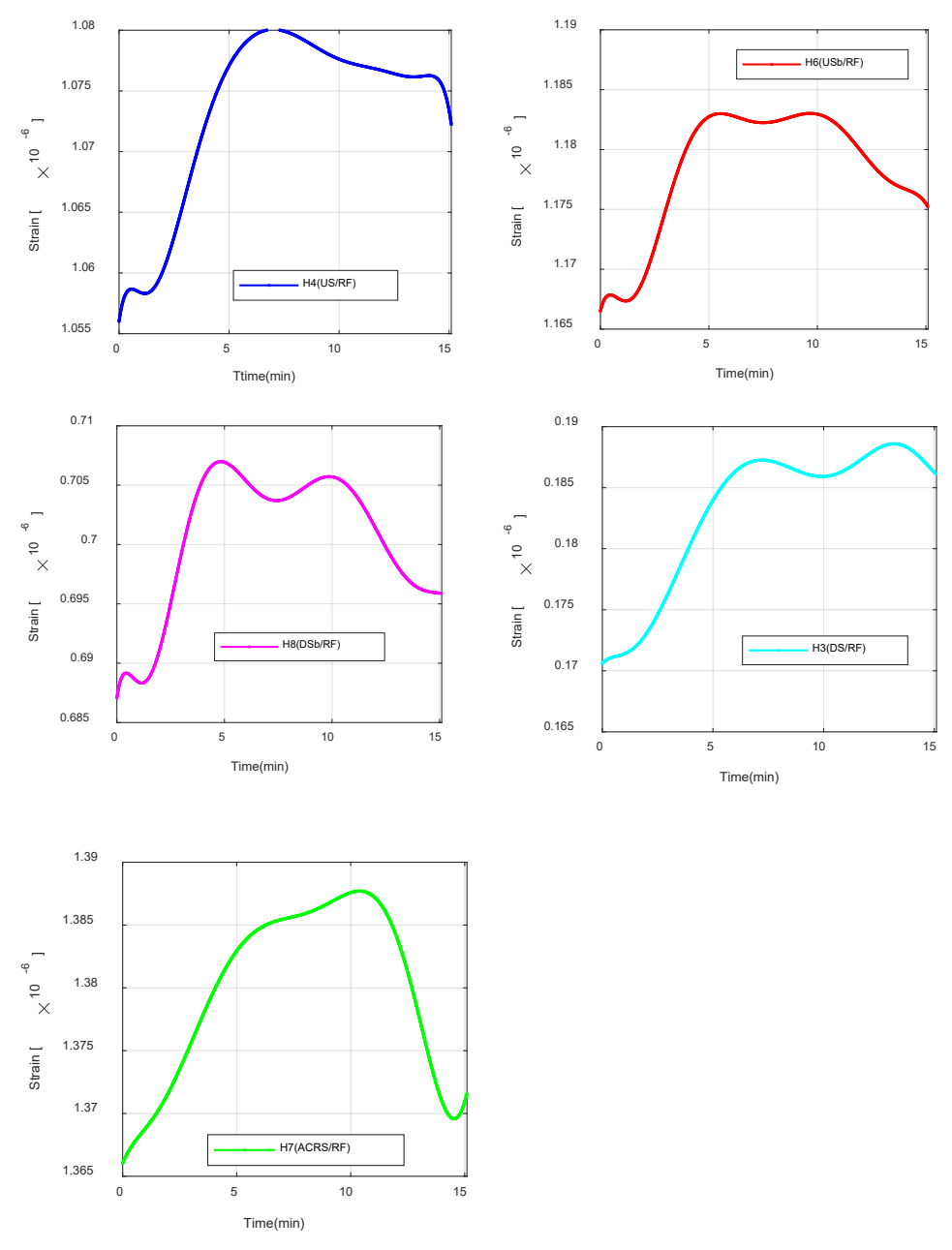


Figure 5.27: Variation of measured strain on the roof in 15 min during stop- reducing effect from 19.15 MW to 0 (2010-12-20 12:23). Y-axis scale is $0.025~\mu strain$.



6 Finite element model

In this chapter, a simplified three-dimensional FE model of the draft tube with the central wall is presented, where FE modelling, boundary conditions, material properties and applied load are described. Furthermore, structure response from FEM is compared with the strain measurements.

6.1 FE MODELLING

Finite element modelling of the draft tube with the central wall has been performed using the ABAQUS/Standard finite element program. As discussed in chapter 1, the important part of the draft tube for this project is a straight diffuser, where there is a central wall and cracking problems. Therefore, the FE model of the draft tube is reduced to this part with considering appropriate boundary conditions for other connecting parts. The simulated straight diffuser is a quadrilateral channel with 13 m length and 16.6 m width with varying height from 4 m to 6.5 m, from the upstream side of the diffuser to downstream side. The draft tube roof has 1.5 m thickness, and an empty space between roof and rock tunnel roof above. The height of the empty space is about 3.5 m. The central wall has 1.08 m thickness and is connected to the floor only by its weight. The lateral wall of the diffuser is replaced by fixed boundary condition at roof lateral boundary. The roof also is restricted to move along the diffuser. The fixed boundary condition is considered for the floor, where the floor is connected to the rock foundation. A surface to surface discretization method (master-slave contact) is assigned to represent tangential and normal contact behaviour between the central wall and floor. Tangential behaviour is described with a rough friction formulation, i.e. no slip will occur once points are in contact and normal behaviour is defined by hard contact. The central wall is a constraint to the roof by tie interaction. The FE model is discretized by 45205 element type C3D8R, an 8-node linear brick element with a maximum nodal interval of 0.5 m, see Figure 6.1. The material properties that have been used for the draft tube are concrete with an elastic modulus of 30 GPa, Poisson's ratio of 0.2, the density of 2400 kg/m³, the compressive strength of 21.5 MPa and tensile strength of 1.6 MPa.



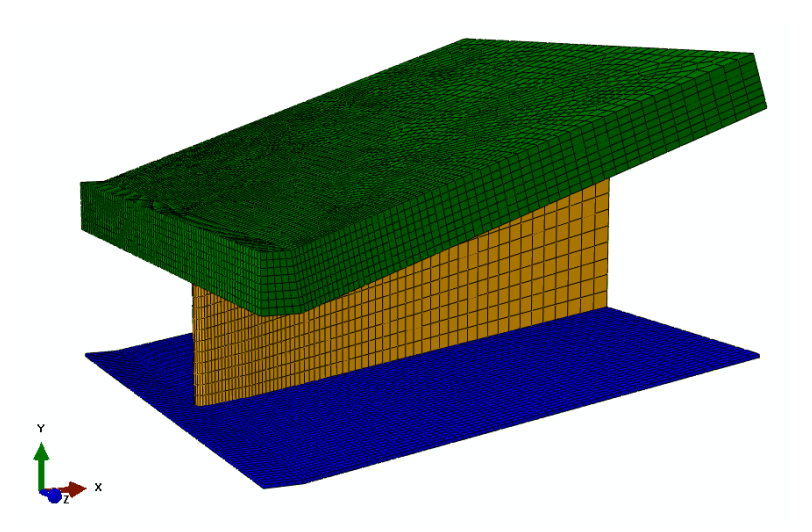


Figure 6.1: Finite element model of draft tube.

6.2 LOAD

Applied loads on the structure are gravity load from the structure and pressure load due to the unit operation. The pressure loads are applied as a static load.

The pressure measurements indicated that pressure on the right side of the diffuser is higher than the left side. The measured pressure difference $\Delta P(ACRS/DS)$ from 18th June to 26th June 2010 is applied as a uniform pressure on the right side of the central wall. Figure 6.1 shows the applied load

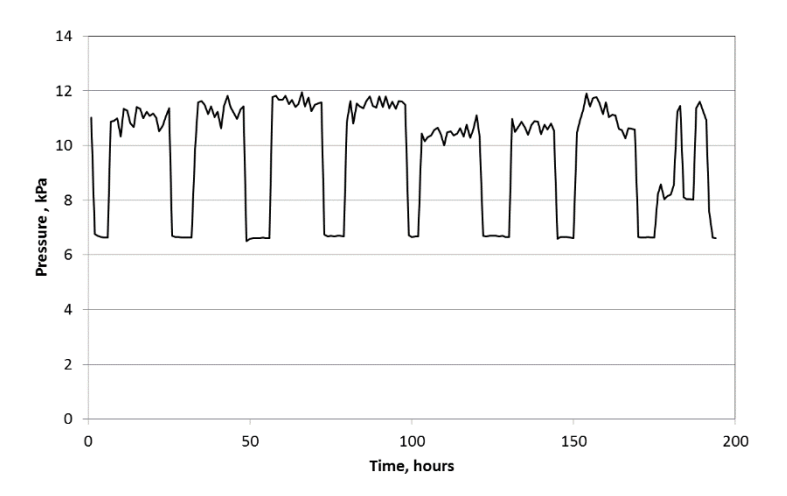


Figure 6.1: The applied load on the central wall.

The pressure acting on the underside of the right section roof is interpolated using the pressure of sensor P5 (RF/R). For simplicity, uniform pressure is applied on the underside of the roof on both sides. Figure 6.2 shows the applied, hydrostatic, downstream and the measured pressure (P5). The applied pressure was calculated by excluding the hydrostatic pressure from the measured pressure (P5). The hydrostatic pressure was calculated by subtracting the elevation of the sensor P5



250

200

Applied roof pressure
Hydrostatic pressure
Downstream pressure
Measured pressure (P5)

100

Time, hours

from the downstream pressure. Pressure from water in empty space on the roof has been considered as a dead load with a value of 35 kPa.

Figure 6.2: The applied pressure on the roof.

50

0

6.3 STRUCTURE RESPONSE

The response of the structure due to applied pressure loads are described by maximum tensile stress which is an important key parameter for concrete structures. In order to compare the behaviour of the structure with strain measurements, strain component that is in the direction of sensor position is implemented. In this regard, strain in direction x (E11), y (E22) and z (E33) have been considered for strain gauges along the roof, on the wall and across the roof, respectively. In the following, the response of structure due to pressure loads that described in section 6.2 is presented.

150

200

Figures 6.3-6.5 show the results from FE modelling of the straight diffuser due to pressure loads from normal operation with a maximum production of 130 MW. Figure 6.3 illustrates the distribution of maximum principal stress on the draft tube. As seen from this figure maximum stress on the right side of the draft tube is higher than the left side. The concentration of maximum tensile stress apart from an area close to the boundary is between the roof and central wall at the upstream side of the straight diffuser where crack propagation had been detected. Figure 6.4 shows the distribution of maximum tensile stress and strain component E22, in the vertical direction of the central wall. This figure shows that under defined pressure loads, the central wall is in tension. Maximum tensile stress on the tip of the central wall-close to the roof exceeds the maximum tensile strength of concrete. Figure 6.5 illustrates the distribution of strain along-E11 and across-E33 the roof.



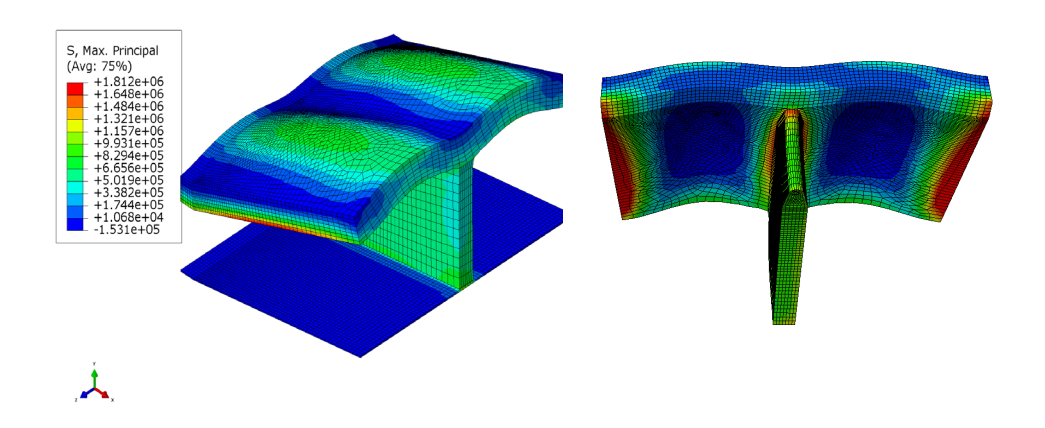


Figure 6.3: Distribution of maximum principal stress on the draft tube.

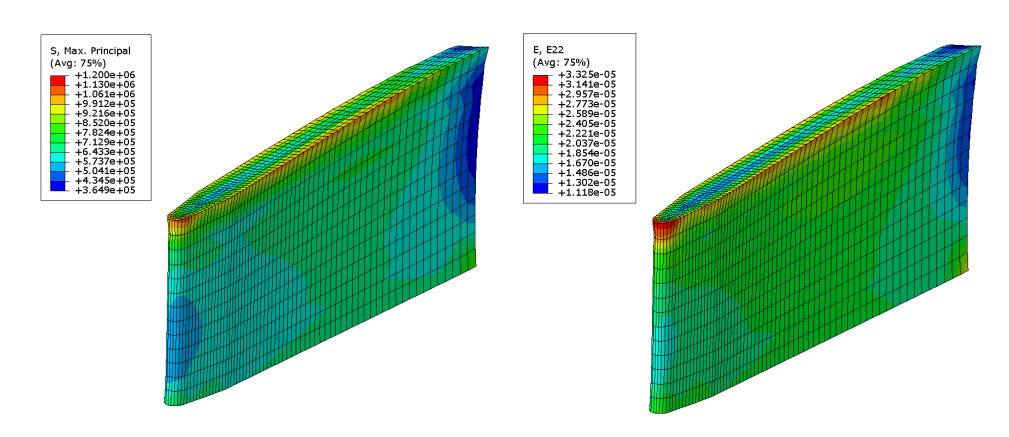


Figure 6.4: Distribution of maximum principal stress and strain in the vertical direction on the central wall.

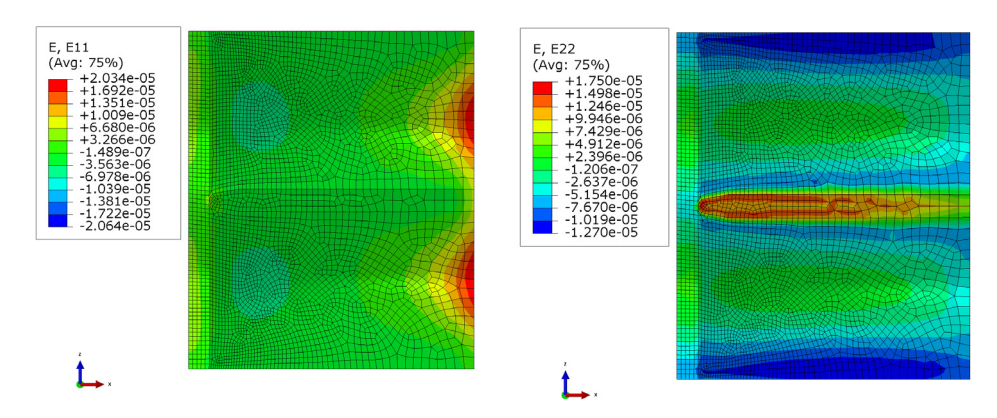


Figure 6.5: distribution of strain along (E11) and across the wall (E33).

Figures 6.6 and 6.7 compare the structure response from FEM and measurement due to normal operation for the central wall and roof, respectively. A comparison of the results on the wall indicates that the results from FEM have the same trend as the measurement but higher values; see Figure 6.6. For the roof, strain values from the measurement are much higher than the results from FEM, see Figure 6.7.



It can also be seen that the structure response along the roof from FEM has the same trend as the measured results.

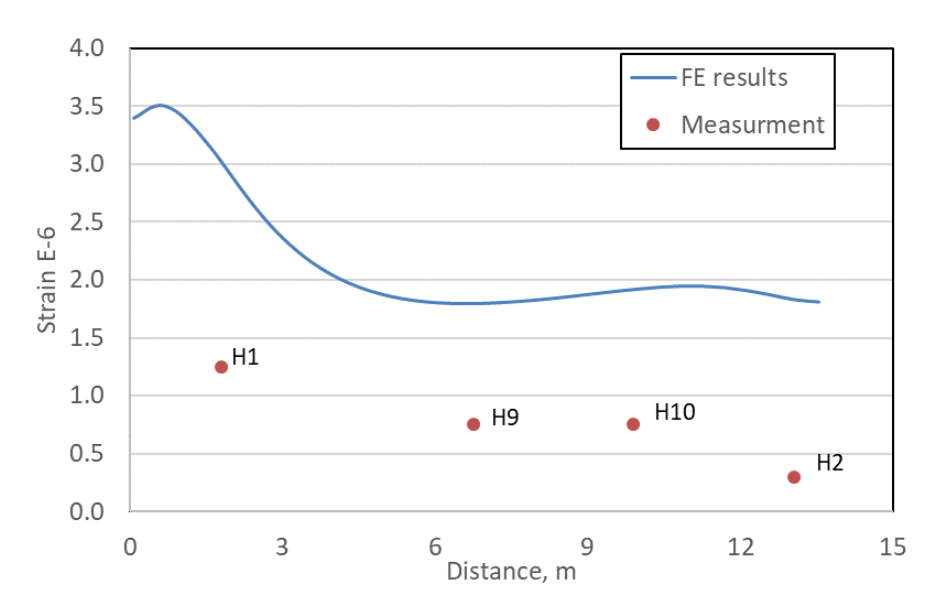


Figure 6.6: Comparison between strain measurement and strain from FEM for the central wall.

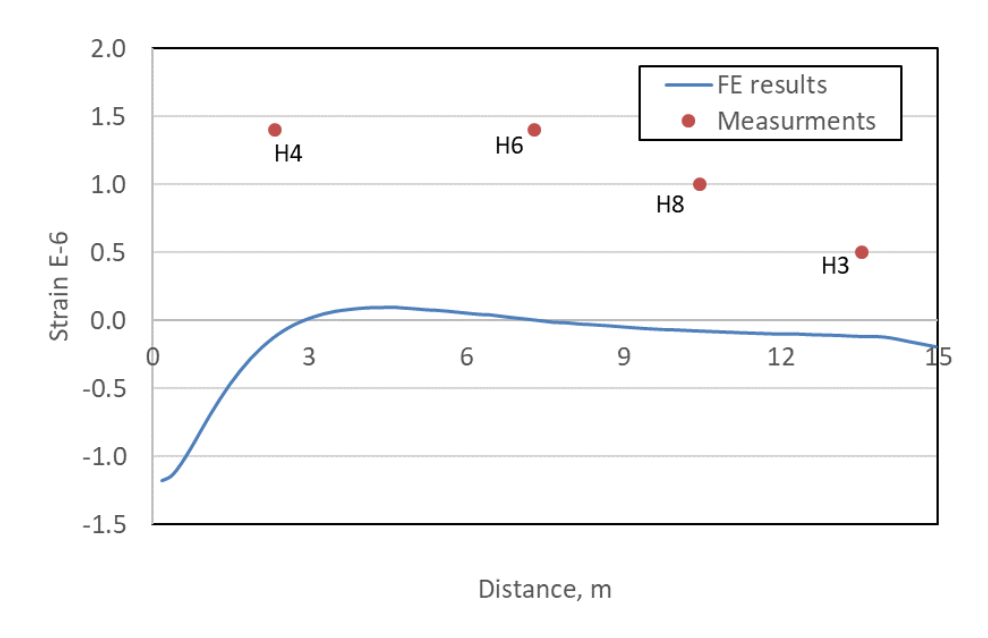


Figure 6.7: Comparison between strain measurement and strain from FEM.



7 Conclusions

In this project, long-term pressure and strain measurements that was done on one of the Swedish draft tubes was analysed. The measurements were classified according to the different operational pattern. A simplified finite element model was then developed to study the theoretical effect of operational pressures on the structure in terms of strains. In this chapter the results from measurements and FE modelling is discussed and compared. Then, general conclusions and future work is presented.

7.1 DISCUSSIONS

One-year measurements of the unit operation indicated that the unit operates over the whole range with many starts/stop with the maximum operation of 130 MW. In some time-intervals, it operates continuously; this can be due to the time of the year. For example, early summer due to ice melting, the unit operates continuously. Furthermore, in winter, the demand for power is higher and the unit works continuously. There are also other factors that generally make the unit operates in a flexible way, such as the number of units at the power station and the type of runner, the geographical location and the effect from wind and solar energy in the system.

Generally, controlled downtime for the units occurred commonly during night 21:00-04:00 when the demand for power is lower, but it can also occur during daytime if power demand is low or if wind farms or other renewable energy sources produce at a high level. There was also seen sharp starts/stops in the morning and afternoon possibly due to a practical problem in the unit. Unit measurements also showed no unit operation in July for 7 days and water was also drained from the draft tube in this period which may show e.g. inspection time in the unit. In this project three major types of operation were considered: **normal operation** (working in the daytime and downtime at night), **continuous operation** with no stop and **start-stop events** with sharp start/stop in the morning and afternoon. In the following the results from pressure and strain measurement corresponding to each operating condition and FE, modelling is discussed.

During normal/daytime and continuous operation, the pressure measurements indicated that the pressure on the right side of the straight diffuser is higher than the left side. This deviation pattern may be related to the effect of runner rotation direction giving an uneven distribution in the two sections. However, the high flow rates in the right side of the draft tubes is because of this highly turbulent and influence from vortex ropes can be part of the explanation The maximum pressure difference across the central wall was around 8-12 kPa when the unit produces power between 110-130 MW. During night-time of normal operation, the pressure difference between the two sides of the straight diffuser was insignificant. It was also seen that during normal/daytime and continuous operation, pressure along straight diffuser at downstream was higher than upstream side. This may show the function of the straight diffuser, increasing pressure difference along the central wall was around 1-4 kPa for unit operation between 105-130 MW. The pressure



measurement on the roof was lower than the pressure on the wall due to lower elevation difference with downstream tailrace water. Maximum measured pressure on the roof was between 190-200 kPa for unit operation between 110-130 MW. It was observed an increase in measured pressure due to a significant reduction in unit production during continuous operation (i.e. reduction of power from 90 MW to 38 MW). Pressure measurements from a sequence of start/stop during daytime showed insignificant pressure difference across the wall. The pressure measurement on the roof was about 173 kPa, close to the value of no operation unit, see **Table 7.1**.

The pressure measurement from 15 min compared to 1 min reading showed more fluctuation of pressure which indicates that the flow in draft tube is turbulent and probably affected by surge. During normal start/stop event, the measured pressure from 15 min reading is close to the 1 min reading while during sequence start/stop event 15 min readings demonstrated high-pressure fluctuation across the central wall and on the roof during stopping the unit. For example, during stopping the unit from 19 MW, the maximum pressure across the central wall and on the roof was almost 4 kPa and 200 kPa, respectively.

Table 7.1: Average measured pressure from 1 min reading

Effect		$\Delta P(ACRS / DS)$	$\Delta P(ALG/R)$	P5 (RF/R)	
Normal	110 MW (daytime)		4.1	-3.522	190.48
	0 MW (night time)		0.193	-1.19	172
126-130 MW		.30 MW	3.4-4.6	-1.6-3.6	193-200
	105 MW		3.44	-3.2	187.88
	90 MW		1.76	-2.58	184.94
Continuous	fluctuation	60 MW	0.1039	-1.148	171
		38 MW	2.019	-	186
Start/stop	8.68 MW (10:00)		-0.1435	-	163.6
	0 MW (11:00)		-0.1358	=	173.6
	19.15 MW (12:00)		-0.1477	-	172.9
	0 MW (13:00)		-0.184	-	173

Generally, the strain measurements give very uncertain values due to the drifting of the gauges. It has also been very difficult to correlate the behaviour to any of the other measured parameters like operational patterns or pressure as a result from this. The strain measurements indicated that strain on the roof is higher than the central wall. Furthermore, strains across the roof is higher than strain along the roof. For both central wall and roof strain at upstream is higher than downstream side. High strain value on the upstream of the straight diffuser may be due to the high speed of water that comes from the elbow of the draft tube and hits the roof and central wall. Table 7.2 and 7.3 summarizes strain measurement values from 1 min readings for different operation type on the central wall and roof, respectively. For normal operation, all sensors except sensor H1 and H9 followed the operation,



i.e. decrease in measured strain from daytime to nighttime. During continuous operation and fluctuation from 90 MW to 60 MW, except sensors H1, H10 and H9, with decreasing effect strain are decreased. While during fluctuation from 90 MW to 38 MW, changes in strain measurement are insignificant. This can be due to increasements in measured pressure during reducing unit operation from 90 MW to 38 MW. Strain measurement during a sequence of start/stop showed high values compared to the low level of operation in the unit. This is due to the high-pressure fluctuation that observed during analysis of pressure measurement from 15 min readings.

Table 7.2: Average measured strain on the central wall from 1 min reading (µstrain)

Effect		H1 (US/WL)	H3 (USb/WL)	H10 (DSb/WL)	H2 (DS/WL)
			, , ,	, , ,	, , ,
al ition	110 MW (daytime)	0.9455	0.1987	0.34	0.53.26
Normal	0 MW (night time)	0.9574	0.183	0.3387	0.5212
	105 MW	0.946	0.21	0.342	0.546
nous	90 MW	0.950	0.208	0.343	0.542
Continuous	60 MW	0.954	0.206	0.343	0.539
	38 MW	0.948	0.209	0.342	0.542
	8.68 MW (10:00)	0.9864	0.1983	0.3566	0.5398
top	0 MW (11:00)	0.9693	0.1842	0.3448	0.5268
Start/stop event	19.15 MW (12:00)	0.9651	0.1885	0.3439	0.5251
Sta eve	0 MW (13:00)	0.9698	0.1945	0.3447	0.5276

Table 7.3: Average measured strain on the roof from 1 min reading

Effect		H4 (US/RF)	H6 (USb/RF)	H8 (DSb/RF)	H9 (DS/RF)	H7 (ACRS/RF)
Normal operation	110 MW (daytime)	1.0522	1.161	0.6948	0.5185	1.3774
	0 MW (night time)	1.028	1.144	0.6754	0.5207	1.359
	105 MW	1.08	1.24	0.687	0.508	1.38
uo	90 MW	1.08	1.24	0.682	0.509	1.38
Continuous	60 MW	1.07	1.23	0.677	0.508	1.37
	38 MW	1.08	1.24	0.684	0.509	1.38
Start/stop event	8.68 MW (10:00)	1.078	1.18	0.7004	0.5364	1.376
	0 MW (11:00)	1.056	1.167	0.6865	0.5261	1.376
	19.15 MW (12:00)	1.053	1.165	0.6841	0.5247	1.368
Sta	0 MW (13:00)	1.056	1.168	0.6873	0.5246	1.38

To better understanding the behaviour of central wall and roof due to operational load, a simplified FE model was developed. The response of model due to loads from pressure measurement during normal operation, i.e. Figure 6.1 and 6.2 was



investigated. The concentration of maximum tensile stress in the FE model was in the contact between the roof and central wall at the upstream side of the straight diffuser where crack propagation had been detected also in the real structure, see Figure 6.4 and 6.5. Although that the measurements and the FE results have the same trend, the variation of strain values obtained from FEM differs from the measurements. This may be because of the simplification of the model's boundary conditions. In addition, it may be due to the effect of the pressure load in FE model, which was applied as a static load but in reality, the flood in draft tube is turbulent and like an impact, load hits the central wall and roof.

One important factor that makes interpretation of the results and behaviour of the structure complicated and difficult is related to the measurement report. There was insufficient information about measurement, potential errors in given sensor positions, accuracy of the system and potential source of noticed errors in data. This forced the authors to make assumptions during analysis of data. Some sensors also failed with time. Another major uncertainty is the real water load on the upside of the roof and the corresponding water pressure in the empty space at different operational situations.

7.2 GENERAL CONCLUSIONS AND FUTURE WORK

In this project, long-term measurement on the large draft tube was analysed and the simplified FE model was developed. The objective of the project was to get a better understanding of the behaviour of the roof and centre wall during different operational events by evaluating measurements from the draft tube. The goal was to clarify if there are any load cases apart from quick refill of the draft tube after drainage that can create continued crack propagation during operation.

The analysis of pressure measurement indicated that the fluid motion in the straight diffuser is turbulent. A pressure difference of up to 12 kPa was seen across the central wall during normal and continuous operation. The pressure on right side of the central wall was higher than the left side. During changes of the unit operation no higher levels on differential pressure were reached but instead the total pressure on both sides fluctuated in line with the change.

The analysis of strain measurement indicated higher strain values at the upstream side of the central wall and roof. Furthermore, the strain on the roof was higher than the central wall. This can show a risk from uplift pressure for draft tubes with empty space. Sudden fluctuation during continuous operation and sequence of start/stop were the cases that structure experienced high strain compared to the low level of operation in the unit. It seems that load patterns in long term may cause damage to the structure due to fatigue problems. The results from finite element model indicated high tensile strength at the upstream side of the straight diffuser, between the roof and the central wall where the crack had been detected.

In this project, the analysis of data and implementing them in the FE model was complicated and difficult, due to the limitation that caused by insufficient information from measurement report and also failing of some sensors. However, for future work, it is recommended for improving applied pressure load on FE model by defining it as a dynamic load/impact load. Because of the limitation in



project time the FE analysis has been done for normal operation. It is motivated to investigate the behaviour of FE model for the sequence of start/stop event and fluctuation during continuous operation with considering pressure load as a dynamic load. Furthermore, the effect of the rock around the structure and other parts of draft tube in FE model can be investigated.



8 References

Marjavaara, **D.** (2006). CFD Driven optimization of hydraulic turbine draft tubes using surrogate Models, Doctoral thesis, Luleå University of Technology.

Andersson, U. (2009). An Experimental Study of the Flow in a Sharp-Heel Kaplan Draft Tube, Doctoral thesis, Luleå University of Technology.

Som, S.K., and Biswas, G. (2008). Introduction to fluid mechanics and fluid machines, Revised second edition, Tata McGraw-Hill.

Gubin, M.F. (1973). Draft tubes of Hydro-Electric Stations, Amerind Publishing Co, New Dehli.

Amiri, K., Mulu, B., Raisee, M. and Cervantes, M.J. (2016). Experimental study on flow asymmetry after the draft tube bend of a Kaplan turbine, Advances and Applications in Fluid Mechanics, 19:2, 441-472

Andersson, U., Jungstedt, J., and Cervantes, M.J. (2008). Model experiments of dynamic loads on a draft tube pier, 24th Symposium on Hydraulic Machinery and Systems, Foz Do Iguaçú, Brazil.

Mauri, S. (2002). Numerical Investigation and Flow Analysis in an Elbow Diffuser, EPFL Thesis No 2527.

ARPE, J. (2003). Experimental Investigation of Unsteady Pressure and Velocity Field in a draft tube of Francis Turbine, EPFL Thesis No 2779.

Björnström, **J.** (2005). FE- Analys av Akkats sugrör, Vattenfall Utveckling AB, Rapportnummer U 05:08. (in Swedish)

Abbas, A. and Kumar, A. (2015). Development of draft tube in hydro-turbine: a review, International Journal of Ambient Energy, 38:3, 323-330.

Holmström, M. (2010). Mätningar sugrör vid vattenfyllning. Vattenfall Power Consultant report 3045500-001. (in Swedish)

Nakayama, Y. and Boucher, R.F. (1999). Introduction to fluid mechanics, Arnold, London, pp. 308

Holmström, M. (2010). Akkats G1, Mätningar sugrör vid vattenfyllning, Vattenfall AB Vattenkraft, Rapport nummer 3045500. (in Swedish)

Kwan, AKH., Zheng, W. and Lee, PKK. (2002). Shock vibration test of concrete, ACI Material Journal, 99, 361-370.



ANALYSIS OF LOAD AND RESPONSE ON LARGE HYDROPOWER DRAFT TUBE STRUCTURES

De här resultaten bidrar till en bättre förståelse av beteendet hos tak och vägg i sugrör under olika driftfall genom mätningar och undersökningar om det finns lastfall som kan ge upphov till propagerande uppsprickning.

Skador och sprickor har framför allt rapporterats i kontakten mellan sugrörstaket och den stödjande mellanväggen vilket troligen har uppkommit vid för snabb återfyllning efter att sugröret tömts för inspektion.

Rapporten redovisar mätningar från ett års drift över hela effektregistret och med periodvis många start och stopp. Resultaten tyder på att strömningen i den raka diffusorn är turbulent och möjligen påverkade av virvelrep som bildas under löphjulet. Därav är trycket på höger sida av väggen högre än på vänster sida.

Resultaten från den numeriska modellen indikerar höga dragspänningar i uppströmsdelen av den raka diffusorn i kontakten mellan taket och mellanväggen på samma ställe som där det finns en spricka i den verkliga konstruktionen.

Energiforsk is the Swedish Energy Research Centre – an industrially owned body dedicated to meeting the common energy challenges faced by industries, authorities and society. Our vision is to be hub of Swedish energy research and our mission is to make the world of energy smarter!

